An Efficient Mesh-Free Particle Method for Modeling of Free Surface and Multiphase Flows

by Mohammad Amin Nabian

B.Sc. in Civil Engineering, July 2013, Sharif University of Technology

A Thesis submitted to

The Faculty of
The School of Engineering and Applied Science
of The George Washington University
in partial fulfillment of the requirements
for the degree of Master of Science

May 17, 2015

Thesis directed by

Leila Farhadi
Assistant Professor of Engineering and Applied Science

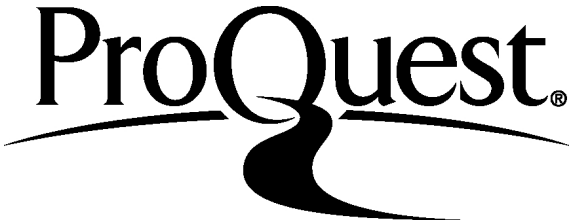

Dedication

I dedicate this thesis to my family; to Dad and Mom for instilling the importance of hard work and higher education; to my brothers Ali and Omid, for being inspirations to me.

Acknowledgments

I would like to express my sincere gratitude to my very respectful advisor Prof. Leila Farhadi for the continuous unfailing support of my study and research, for her patience, affection, motivation, enthusiasm, and immense knowledge. Her professional guidance helped me in all the time of this research. Her dedication and enthusiasm for scientific research is unsurpassed, and her vast knowledge and incisive insight have been inspiring. Her frequent insights and patience with me are always appreciated. I am very proud of what we have achieved together, thank you Prof. Farhadi. I can never pay you back for all the help you have provided me, the experience you have helped me gain by working with you, and the precious time you spent making sure my research is always on track. What I owe you cannot be written down.

I especially thank my dad, mom, and brothers, for their endless love, devotion and encouragement. My hard-working parents have sacrificed their lives for my brothers and myself and provided unconditional love and care. I love them so much, and I would not have made it this far without them. My brothers have been my best friends all my life and I love their dearly and thank them for all their advice and support. I know I always have my family to count on when times are rough.

I also thank my friends for providing support and friendship that I needed. I would like to thank a very nice lady in our water resources group, Mrs. Abedeh Abdolghafoorian, for being supportive throughout my time here.

Abstract of Thesis

An Efficient Mesh-Free Particle Method for Modeling of Free Surface and Multiphase Flows

Numerical methods have been used extensively in modeling of free surface flows. These methods are generally classified into two categories; grid methods, and particles methods. In recent years, particle methods are gaining further attentions among numerical model developers for simulation of free surface flows. Computer simulation using particles has the capacity to analyze more complex geometry and physics than grid methods. Particularly, topological deformation of the fluid can be analyzed efficiently by particles, while it is hard and sometimes not possible to fit and move a grid continuously in such domains. Also, convection is directly calculated by the motion of particles without numerical diffusion. In addition, grid generation which recently seems to be used to analyze complex domains is not necessary, eliminating a significant portion of computational time. Although it is necessary to initialize configurations of particles in particle methods, this is much easier than grid generation as there is no need to set up topological relations among the particles. Problems with severe and sharp changes of free water surface can be simulated successfully with numerical methods based on the Lagrangian approach.

In this research the development of a numerical method based on the Lagrangian formulation to solve the Navier-Stokes equations is reported. Navier-Stokes equations are the governing equations of the fluids; a set of coupled partial differential equations that describe how the density, pressure, and velocity of a moving fluid are related. The Navier-

Stokes equations are solved by the Moving Particle Semi Implicit (MPS) method, a mesh-free particle method. A fractional step method is applied which consists of splitting each time step in two steps. The fluid is represented with particles, and the motion of each particle is calculated based on the interactions with the neighboring particles covered by a kernel function.

In general, the contributions of this research can be categorized into three distinct parts:

1. Application of the MPS method is shown through the successful simulation of two sample complex free surface flows. Compared to the similar former studies focused on the application of this method, this research implements a newly-introduced kernel function. It is shown that by utilizing this new kernel function the stability of the simulations is significantly enhanced.
2. A multiphase MPS method is proposed for incompressible flows. The multiphase system is treated as a multi-density multi-viscosity fluid. A single set of governing equations is solved on the whole computational domain, and high-order accurate density and viscosity schemes are applied to stabilize the fluid pressure and shear stress fields. The proposed method is utilized for modeling of granular flows and sediment transport.
3. An algorithm is introduced to enhance the efficiency of the mesh-free particle methods. This algorithm enables the implementation of sets of particles with different sizes in one computational domain.

Table of Contents

Dedication iii

Acknowledgments iv

Abstract of Thesis v

Chapter 1 : Introduction 1

1.1. Computational fluid dynamics 1

1.2. Free surface flow 3

1.3. Eulerian and Lagrangian viewpoints 4

1.4. Mesh-free particle methods 5

1.5. Research Objective 9

1.6. Organization of thesis 10

Chapter 2 : Fundamentals of the MPS Method 11

2.1. Governing Equations 11

2.2. MPS Interpolations 12

2.3. Solution Method 17

2.3.1. Time splitting 17

2.3.2. Prediction step 18

2.3.3. Pressure Poisson equation 18

2.3.4. Correction step 19

2.4. Weakly compressible model 20

2.5. Boundary Treatment 21

Chapter 3 : Landslide-Induced Water Waves 23

3.1. Vertical Landslide Simulation 24

3.1.1. Problem definition.....24

3.1.2. Results and Analysis 26

3.1.3. Stability of the model.....36

3.2. Submarine Landslide Simulation.....38

3.2.1. Introduction to the Problem 38

3.2.2. Results and Analysis 39

3.2.3. Results of the WC-MPS simulation 46

3.3. Introduction to multiple-size particle technique.....52

3.4. Summary.....55

Chapter 4 : Multiphase MPS Method for Granular Flows.....57

4.1. Multiphase MPS Formulation.....58

4.2. Granular Media Rheology.....60

4.3. Boundary Treatment.....62

4.4. Deformable Submarine Landslide 62

4.5. Dam-Break over an Erodible Bed.....72

4.6. Summary.....85

Chapter 5 : Multiple-Size Particle Algorithm for Mesh-Free Methods 87

5.1. Problem Definition.....87

5.2. Mechanism of fine-region coarse-region interaction 89

5.3. Calculation of the particle number density.....93

5.4. Dam-break induced water waves.....96

5.5. Landslide-induced water waves 104

5.6. Summary 109

Chapter 6 : Conclusion and Recommendation 111

6.1. Major contributions 111

6.2. Recommendations for future work 113

6.2.1. Efficiency 113

6.2.2. Accuracy and Stability 114

6.2.3. Applicability 116

References 1118

Apendix 11130

List of Figures

Figure 1- Shape of the different kernel functions 14

Figure 2- Definition of particle spacing and kernel size.....15

Figure 3- Calculation algorithm of the MPS method.....21

Figure 4- Ghost particle recognition.....22

Figure 5- Scope and dimensions of the vertical landslide problem.....25

Figure 6- Vertical landslide mass velocity at different heights. 25

Figure 7- Particle Configuration at different times for the vertical landslide simulation. 27

Figure 8- Velocity field at different times for the vertical landslide simulation.....31

Figure 9- Pressure field at different times computed by the present model.....32

Figure 10- Solitary wave profile comparison between the MPS results and the experimental data the vertical landslide problem. 33

Figure 11- Comparison between analytical solution and solution by the present model for the horizontal velocity of particles on the free surface. 34

Figure 12- Definition of the parameters used in reverse plunging wave measurements in the vertical landslide problem. 35

Figure 13- Number of particles on free surface in the vertical landslide simulation, (a) up to 2.5s, (b) up to 40s.....37

Figure 14- Scope and dimensions of the submarine landslide problem.....38

Figure 15 - Particle configuration at different times for submarine landslide simulation.....40

Figure 16- Velocity field at different times for the submarine landslide simulation. 41

Figure 17- Pressure field at different times for the submarine landslide simulation. 43

Figure 18- Water surface profile comparison between the MPS results and the experimental data for the submarine landslide problem. 45

Figure 19- WC-MPS results for particle configuration at different times for the submarine landslide. 47

Figure 20- WC- MPS results for pressure field at different times for the submarine landslide. 49

Figure 21- A comparison for the water surface profile between the MPS, WC-MPS, and experimental results. 51

Figure 22- Tracking the motion of the marked particles (white particles) in the computational domain. 54

Figure 23- A schematic of the pseudo particles carrying a number of attached grains. 61

Figure 24- Experimental setup for the deformable underwater landslide experiment performed by Rzadkiewics et al. (1997). 64

Figure 25- Particle configuration for the deformable submarine landslide at t=0.4s and 0.8s. The landslide mass is considered as an ideal fluid. x to y ratio is 1. 65

Figure 26- A comparison for the water surface profile at t=0.4s (top) and t=0.8s (bottom) between the MPS and experimental results. The mass is considered as an ideal fluid. x to y ratio is 0.2. 66

Figure 27- Particle configuration for the deformable submarine landslide problem at different times. 67

Figure 28- Velocity field for the deformable submarine landslide problem at t=0.4s and 0.8s. The landslide mass is considered as a non-Newtonian fluid. x to y ratio is 1.....69

Figure 29- A comparison for the water surface profile at t=0.4s (top) and t=0.8s (bottom) between the MPS, SPH and experimental results. The mass is considered as a Non-Newtonian fluid. x to y ratio is 0.2. 70

Figure 30- A comparison for the landslide mass profile at t=0.4s (top) and t=0.8s (bottom) between the MPS, SPH and VOF results. x to y ratio is 1.....71

Figure 31- Experimental setup for the mobile bed dam-break experiment performed by Spinewine and Zech (2005). 73

Figure 32- Particle configuration for the mobile-bed dam break problem at different times. The sediment material is PVC. x to y ratio is 0.5. 75

Figure 33- Pressure field for the mobile-bed dam break problem at different times. The sediment material is PVC. x to y ratio is 0.5. 77

Figure 34- Velocity field for the mobile-bed dam break problem at different times. The sediment material is PVC. x to y ratio is 0.5. 78

Figure 35- A comparison between the experimental data, MPS results, and the WC-MPS results for the water surface and sediment profiles at 0.25s (top), 0.50s (middle), and 0.75s (bottom). The sediment material is PVC. x to y ratio is 0.3.....81

Figure 36- Particle configuration for the mobile-bed dam break problem at different times. The sediment material is sand. x to y ratio is 0.5.....83

Figure 37- A comparison between the experimental data, MPS results, and the WC-MPS results for the water surface and sediment profiles at 0.25s (top), 0.50s (middle), and 0.75s (bottom). The sediment material is sand. x to y ratio is 0.3. 84

Figure 38- Schematic of a sample two-scale computational domain. 89

Figure 39- Definition of the four distinct scenarios of particle interaction. 90

Figure 40- The particle interaction mechanism in each of the four scenarios. 93

Figure 41- Calculation of the kernel function for inner particle interaction. 94

Figure 42- Geometry of the dam-break experiment. 97

Figure 43- Particle configuration for dam-break problem computed by the WC-MPS method. 98

Figure 44- configuration of the coarse and fine regions in computational domain of the dam-break problem. 100

Figure 45- Particle configuration for dam-break problem computed by the proposed MS-WC-MPS method. 101

Figure 46- Comparison for the dam-break wave front position between the experimental, MPS, WC-MPS, and MS-WC-MPS results. 103

Figure 47- Particle configuration at different times for the submarine landslide problem using the multiple-size particle algorithm. 106

Figure 48- A comparison for the water surface profile between the MS-WC-MPS, WC-MPS, and experimental results. 108

List of Tables

Table 1: Formulation of the different kernel functions.....13

Table 2- A comparison between the present MPS model, I-SPH, SPH, and experimental results for the reverse plunging wave measurements.....35

Table 3- Information on water surface elevation at different times obtained by MPS, WC-MPS and I-SPH methods 48

Nomenclature

1.	D	water depth
2.	H	solitary wave amplitude derived from analytical solution
3.	N	number of particles in a unit volume
4.	P	pressure
5.	V	velocity of the vertical landslide mass
6.	$\mathbf{f}$	gravity acceleration vector
7.	g	acceleration gravity
8.	m	mass of a fluid particle
9.	n	particle number density
10.	r	distance between two fluid particles
11.	$\mathbf{r}$	Particle position vector
12.	t	time
13.	$\mathbf{u}$	velocity vector
14.	v	vertical velocity of the submarine landslide mass
15.	β	free surface parameter
16.	η	water surface elevation derived from analytical solution
17.	λ	a parameter to keep same variance increase as that of the analytical solution
18.	ν	kinematic viscosity of fluid
19.	ρ	fluid density
20.	φ	a scalar quantity
21.	C_n	Courant number

22. C_w solitary wave celerity

23. c_1, c_2 constant values in the equation of vertical velocity of landslide mass

24. l_0 initial particle spacing

25. Ll a label for large particles

26. Ls a label for small particles

27. Lf_n a label for fictitious small particles corresponded to a neighboring particle

28. Lf_r a label for fictitious small particles corresponded to a reference particle

29. n^0 constant particle number density

30. $n*$ particle number density at the prediction step

31. r_e kernel size

32. $\mathbf{u}^*$ velocity at the prediction step

33. $\Delta\mathbf{u}'$ velocity correction

34. ρ^* density at fictitious time step

35. $\Delta\rho'$ density correction

36. μ_{eff} effective dynamic viscosity

37. μ_B Bingham plastic dynamic viscosity

38. τ_B Bingham yield stress

39. $\dot{\gamma}$ shear rate

Chapter 1 : Introduction

Incompressible fluid motion is governed by the so called *Navier-Stokes* equations, a set of coupled and nonlinear partial differential equations derived from the basic laws of the conservation of mass, momentum, and energy. In this set of equations, the unknowns are usually the velocity, density, pressure, and temperature. The analytical solution of these equations is practically impossible due to the nonlinearity of the governing equations. Thus, in the past, scientists had to provide simplifications and approximations to the equations until they had a set of equations that was analytically solvable, or they had to resort to laboratory experiments. However, the experimental results might be qualitatively different as it is difficult to enforce the dynamical and geometric similitude simultaneously between the prototype and the experiment. An example is the Reynolds' number similarity which can turn a turbulent flow to a laminar flow if violated. There are also some phenomena that cannot be reproduced experimentally, such as ocean, weather, etc. Moreover, the construction and design of the laboratory experiments can be costly or difficult.

1.1. Computational fluid dynamics

Computational fluid dynamics, abbreviated as CFD, is an additional tool for simulation of the fluid flow. CFD is a computational technology that enables the scientists to study the dynamics of fluids. Using CFD, scientists can build a computational model that is representing the device or system they want to study. Then, by applying the physics of the

fluid flow to this virtual prototype, the software will output a prediction of the fluid dynamics. The benefits of using CFD in simulation of fluid flow include the following:

- Insight: There are numerous systems that are difficult to prototype. Often, CFD can represent features of the phenomena happening within the system that cannot be visible or captured by any other means. CFD gives the scientists a means of visualizing and an enhanced understanding of their design or the system under their study.
- Foresight: As the CFD is a tool for the modeling and prediction of what will happen under a set of given conditions, it can quickly and efficiently answer many "what if" questions. Given the variables, it gives the outputs. Within a short time, scientists can predict how their design will perform, and test many variations until they arrive at an optimal result. All of this is done prior to physical prototyping and testing. The foresight gained from CFD helps for faster and better design.
- Efficiency: Faster and better analysis or design leads to shorter design cycles. Time is saved, and costs are reduced.

The central process in CFD is the discretization process. Within this process, the governing differential equations with infinite number of degrees of freedom are reduced to a system of finite degrees of freedom. Therefore, instead of determining the solution for all times in everywhere in the computation domain, calculations are performed at specified time intervals and at a finite number of locations in the domain. The partial differential equations are then reduced to a system of algebraic equations that can be solved on a computer.

Errors creep in during the discretization process. The nature and characteristics of the errors must be controlled, ensuring that we are solving the correct equations (consistency property), and that the error can be reduced as we increase the number of degrees of freedom (stability and convergence). Once these two criteria are established, the power of computing machines can be leveraged to solve the problem in a numerically reliable fashion.

1.2. Free surface flow

In fluids, a free surface is the surface that is subject to zero parallel shear stress and zero perpendicular normal stress. Free surface flows are common in nature and in man-made structures. Examples of this type of flows include water waves in ocean and coastal zones, flow in rivers and estuaries, and flow around the hydraulic structures such as dams.

Analysis of the free surface flow is significantly more complex than the closed conduit flows. The contributing forces causing and resisting motion and the inertia must form a balance such that the free surface is a streamline along which the pressure is constant and equal to the atmospheric pressure. This extra degree of freedom in free surface flow means that the flow boundaries are no longer fixed by the conduit geometry, as in closed conduit flow, but rather the free surface adjusts itself to accommodate the given flow conditions (Sturm 2010). Another characteristic of the free surface flow is the extreme variability in the free surface profile and in the cross-sectional shape and roughness. In free surface flow, often large deformation and fragmentation of the free surface exists.

The limitation of the experimental study of flow is more significant in case of the flow associated with free surface. The detailed measurements of the fluid flow features such as

free surface profile, velocity distribution, and pressure in very difficult in experimental studies. Alternatively, CFD is a strong tool for analysis of such flows. The capability to computationally model these types of flows is attractive if such computations are done accurately, with reasonable computational resources.

Many computer programs can solve the partial differential equations describing the dynamics of fluids. However, not many programs are capable of including free surfaces in their simulations. The difficulty is a classical mathematical one often referred to as the free-boundary problem. A free boundary poses the difficulty that on the one hand the solution region changes when its surface moves, and on the other hand, the motion of the surface is in turn determined by the solution. Changes in the solution region include not only changes in size and shape, but in some cases, may also include the coalescence and break up of regions (i.e., the loss and gain of free surfaces) (Hirt and Nichols 1981).

1.3. Eulerian and Lagrangian viewpoints

The Eulerian description of the fluid motion records the evolution of the fluid flow properties at every point in space as the time proceeds. It describes the flow using quantities as a function of the spatial location and time. This viewpoint has us watch a fixed point in space with specified coordinates as the time varies. The Eulerian viewpoint can be visualized as sitting on a river bank and watching the flow passing from a fixed point.

In Lagrangian viewpoint of fluid mechanics, the attention is focused on material particles as they move through the fluid flow. Each fluid particle (parcel) carries its own properties such as velocity, density, momentum, etc. The properties may change in time as

the particles advance. This viewpoint can be visualized by sitting in a boat and drifting down a river.

1.4. Mesh-free particle methods

Numerical methods are generally classified into grid methods and particle (mesh-less/mesh-free) methods. Particle methods, in comparison with the grid-based methods, have the advantage of tracking the free surfaces and multi-interfaces naturally without extra complicated algorithms. Unlike the grid-based methods, mesh-free discretization techniques are based only on a set of independent points which eliminate the cost of mesh generation. Moving boundaries and interfaces can be analyzed by particle methods much easier than by finite element methods as it is hard to fit and move a mesh continuously (Idelsohn et al. 2002). Moreover, in particle methods the convection term is calculated by the motion of particles and thus, numerical diffusion, which is a problem in finite difference methods, does not take place. For a comprehensive review on mesh-free methods readers are referred to (Liu 2010; Liu and Gu 2005; Nguyen et al. 2008; Li and Liu 2002).

The Smoothed Particle Hydrodynamics (SPH) method is one of the earliest mesh-free methods. It was initially developed to solve problems in astrophysics that involve fluid masses moving arbitrary in three dimensions in absence of boundaries (e.g. Lucy 1977; Gingold and Monaghan 1977; Monaghan 1988). Later this method was generalized to solve fluid mechanic problems (e.g. Monaghan 1994; 2005; Dalrymple and Rogers 2006). The SPH method is capable of dealing with free surface flow, multiphase flow, deformable

boundary, moving interface as well as problems which consist of extremely large deformation.

Diffuse Element Method (DEM) is the first weak-form meshless method introduced by Nayroles et al. (1992). Weak-form methods solve an integral function instead of solving a differential equation of the underlying problem. In the DEM method, the governing equations are discretized by a Galerkin weak-form over the problem domain. Shape functions are created using the Moving Least Square (MLS) method (Lancaster and Salkauskas 1986). However, in order to compute the integrals derived from the Galerkin approach, a set of background mesh is necessary.

Belytshko et al. (1994) proposed the Element-Free Galerkin (EFG) method as the improved version of the DEM method. Using Galerkin approach to discretize the governing equations, the stiffness matrices are symmetric. Essential boundary conditions are implemented efficiently by penalty method. EFG is an accurate and efficient method as the rate of convergence is higher compared to the Finite Element Method (FEM) (Shobeyri and Afshar 2010). The EFG can be implemented accurately for both regular and irregular special discretization. Since the integrals are calculated on a background cell structure, this method is not a completely mesh-free method. The EFG method has been applied to a variety of engineering applications such as unsteady nonlinear heat transfer (Singh et al. 2007), 2D elastic analysis (Liu et al. 2008), and 3D structural analysis (Chen and Guo 2001).

The Meshless Local Petrov–Galerkin (MLPG) is a mesh-free method proposed by Atluri and Zhu (1998). No background mesh is necessary for interpolations and integrations in this method. To implement the numerical integrations, a local quadrature

domain with a regular and simple shape is defined for each field node. Similar to the EFG method, shape functions are created by the MLS approximation. The efficiency of the MLPG is adversely affected by asymmetric coefficient matrix. The MLPG also encounters some difficulties when numerical integrations are carried out for nodes on and around the boundaries. The MLPG has been implemented in simulation of a wide range of engineering problems such as fluid dynamic and heat transfer problems (Lin and Atluri 2001; Arefmanesh et al. 2005) and solid mechanic problems (Atluri et al. 2006).

The Finite Point (FP) method proposed by Onate et al. (1996) combines a weighted least square approximation of the unknowns over each local interpolation domain with a stabilized point collocations procedure which eliminates any numerical instability (Löhner et al. 2002). Examples of applications of the finite point method have been shown in successful simulation of advection diffusion (Onate and Idelsohn 1998) and incompressible flow (Onate et al. 2000) problems.

A mesh-free numerical method, called the moving particle semi implicit (MPS) method, was proposed by Koshizuka and Oka (1996) and Koshizuka et al. (1998) for simulation of free surface flows. In this method, Navier-Stokes equations are solved in a fully Lagrangian form using a fractional step method which consists of splitting each time step in two steps. The fluid is represented with particles. The motion of each particle is calculated through interactions with neighboring particles by means of a kernel function. Stability of the simulations, efficiency and ease of free surface tracking using Lagrangian particles, straightforward boundary treatment and ease of coding are the advantages of using this method in modeling of free surface flows.

The MPS and SPH methods are similar in that they both provide approximations to the strong form of partial differential equations on the basis of integral interpolants. The major difference between the two methods is that unlike the SPH, the MPS method applies a simplified differential operator model which is only based on a local weighted averaging process without taking the gradient of a kernel function (Koshizuka and Oka 1996; Koshizuka et al. 1998). Additionally, the semi-implicit prediction-correction process of the MPS has shown better stability compared to the fully explicit conventional SPH method (Koshizuka and Oka 1996; Koshizuka et al. 1998).

The MPS method has gained a lot of interest among numerical modelers in the past decade and has been successfully applied to a variety of complex hydraulic problems such as dam break in 2D (Ataie-Ashtiani and Farhadi 2006; Khayyer and Gotoh 2009) and 3D (Shakibaeinia 2011), hydraulic jump formation (Shakibaeinia and Jin 2010; Shakibaeinia and Jin 2011), breaking waves on slopes (Koshizuka et al 1998), and landslide-induced water waves (Nabian and Farhadi 2014a,b,c). In addition, the MPS method has been applied to a wide range of engineering applications including ocean engineering (e.g. Shibata and Koshizuka 2007), coastal engineering (e.g. Nabian and Farhadi 2014b,c; Gotoh et al 2005), mechanical engineering (e.g. Heo et al. 2002), structural engineering (e.g. Chikazawa et al 2001), chemical engineering (e.g. Sun et al. 2009) and bioengineering (e.g. Tsubota et al. 2006).

1.5. Research Objective

The main objectives of this research are:

a) Showing the application of the MPS method in modeling of complex free surface flows: Application of the MPS method is shown through the successful simulation of rockslide-induced and landslide-induced water waves. The stability of this method is improved by utilizing a newly-introduced kernel function (Ataie-Ashtiani and Farhadi 2006). It is shown that compared to other common kernel functions in the mesh-free methods, the utilized kernel function will provide significantly better stability.

b) Developing a multiphase MPS algorithm: The applicability of the MPS method is enhanced by introducing a new algorithm, extending the MPS method for simulation of multiphase flows and granular flows.

c) Developing an algorithm for improving the efficiency of the MPS method: Efficiency of the MPS method is improved by proposing a new algorithm allowing the numerical models to utilize sets of particles with different sizes in one computational domain, enabling allocation of reasonable computational resources to those parts of the computational domain with relatively low complexity in fluid flow.

Each of the proposed improvements is followed by a number of verification tests to show the accuracy and stability of the numerical models. In these sets of simulations, fluid is considered incompressible and viscid. Only low Reynolds number flows are considered in this research and thus, no turbulence model is applied to the simulations.

1.6. Organization of thesis

The thesis is organized in the following way: Chapter 2 provides an introduction to the MPS method and how this method treats the boundaries and interfaces. Chapter 3 presents the results for the simulation of rockslide-induced and landslide-induced water waves to show the application of the MPS method in simulation of complex free surface flows. This application section is then followed by a discussion on the effect of different kernel functions on the stability of the MPS method and how the kernel function utilized in this research will contribute to stability of the MPS method. There is also a comparison between the MPS method and another simplified form of this method, the explicit form, from the accuracy and performance point of view.

In Chapter 4, a new algorithm for the simulation of multiphase flows is introduced based on the MPS formulation. This algorithm is further extended for simulation of granular flows and sediment transport. Results for the deformable landslide-induced water waves and sediment transport via dam–break are presented and compared with the available experimental data for the sake of model verification. Chapter 5 presents a new formulation on how to use particles with different sizes in a computational domain to enhance the efficiency of the simulations. Dam-break induced water waves and landslide-induced water waves are simulated to verify the improvements in efficiency of the method while keeping the accuracy at almost the same level. Chapter 6 presents a conclusion and a number of suggestions for future work in this area of research. A thorough literature review on each of the simulations performed in this research is presented at the beginning of each chapter.

Chapter 2 : Fundamentals of the MPS Method

2.1. Governing Equations

In fluid mechanics, the conservation of mass equation and the conservation of momentum equation with Newton's viscosity law are commonly known as the Navier-Stokes equations; a set of coupled nonlinear partial differential equations. These equations describe how the velocity, density, pressure, and other quantities of a moving fluid are related. The Navier-Stokes equations are extensions of the Euler equations (conservation of mass and momentum for inviscid flow) by considering the effects of fluid viscosity. For incompressible fluid, and in Lagrangian form of fluid description, the Navier-Stokes equations are expressed as

$$\begin{cases} \dfrac{1}{\rho}\dfrac{D\rho}{Dt} + \nabla . \mathbf{u} = 0 \\ \dfrac{D\mathbf{u}}{Dt} = -\dfrac{1}{\rho}\nabla P + \upsilon \nabla^2 \mathbf{u} + \mathbf{f} \end{cases} \tag{2.1}$$

in which ρ is the fluid density, t is time, $\mathbf{u}$ is the velocity vector, P is pressure, υ is kinematic viscosity of fluid and $\mathbf{f}$ is the gravity acceleration. Note that there is no convective acceleration term in momentum conservation equation in the Lagrangian system. Therefore, one of the sources of error resulting from discretization of governing equations is eliminated.

The derivative with respect to a variable, i.e. the time herein, is called the *material derivative*:

$$\frac{D(\,)}{Dt} \equiv \frac{\partial(\,)}{\partial t} + (\mathbf{u}.\nabla)(\,) \tag{2.2}$$

In Lagrangian description, the *material* is referred to fluid parcels. Equation (2.2) means that the amount of change of a variable (in time) in Lagrangian coordinates consists of a temporal change plus a spatial change. The temporal change is observed in Eulerian coordinate and the spatial change is due to the change in moving coordinate (Chen 2014).

2.2. MPS Interpolations

In the MPS method, the motion of each particle is calculated based on the interactions with neighboring particles covered with a kernel (weight) function. Table 1 and Figure 1 show 6 commonly used kernel functions in mesh-free methods. KF1 is the most common kernel function in the MPS method, suggested by Koshizuka et al. (1998) for simulating incompressible, inviscid flows. Belytschko et al. (1996) proposed an exponential (KF2), a quartic spline (KF3) and a cubic spline (KF4) kernel function. KF5 is introduced by Koshizuka and Oka (1996) for simulating incompressible, viscid flows by MPS method. Shao and Lo (2003) proposed KF6, which is the commonly used kernel function in the SPH method. This kernel function is introduced to simulate Newtonian and non-Newtonian flows with a free surface using incompressible SPH method.

Table 1: Formulation of the different kernel functions

KF1 (Koshizuka et al. 1998)	$w(r)=\frac{r_e}{r}-1$
KF2 (Belytschko et al. 1996)	$w(r)=e^{-(\frac{r}{\alpha r_e})^2}$
KF3 (Belytschko et al. 1996)	$w(r)=1-6\left(\frac{r}{r_e}\right)^2+8\left(\frac{r}{r_e}\right)^3-3\left(\frac{r}{r_e}\right)^4$
KF4 (Belytschko et al. 1996)	$w(r)=\begin{cases}\frac{2}{3}-4\left(\frac{r}{r_e}\right)^2+4\left(\frac{r}{r_e}\right)^3 & 0\le r\le \frac{r_e}{2}\\ \frac{4}{3}-4\left(\frac{r}{r_e}\right)+4\left(\frac{r}{r_e}\right)^2-\frac{4}{3}\left(\frac{r}{r_e}\right)^3 & \frac{r_e}{2}\le r\le r_e\end{cases}$
KF5 (Koshizuka and Oka 1996)	$w(r)=\begin{cases}2-\left(2\frac{r}{r_e}\right)^2 & 0\le r\le \frac{r_e}{2}\\ \left(2\frac{r}{r_e}-2\right)^2 & \frac{r_e}{2}\le r\le r_e\end{cases}$
KF6 (Lee et al. 1982)	$w(r)=\begin{cases}\frac{40}{7\pi r_e^2}\left(1-6\left(\frac{r}{r_e}\right)^2+6\left(\frac{r}{r_e}\right)^3\right) & 0\le r\le \frac{r_e}{2}\\ \frac{10}{7\pi r_e^2}\left(2-2\frac{r}{r_e}\right)^3 & \frac{r_e}{2}\le r\le r_e\end{cases}$

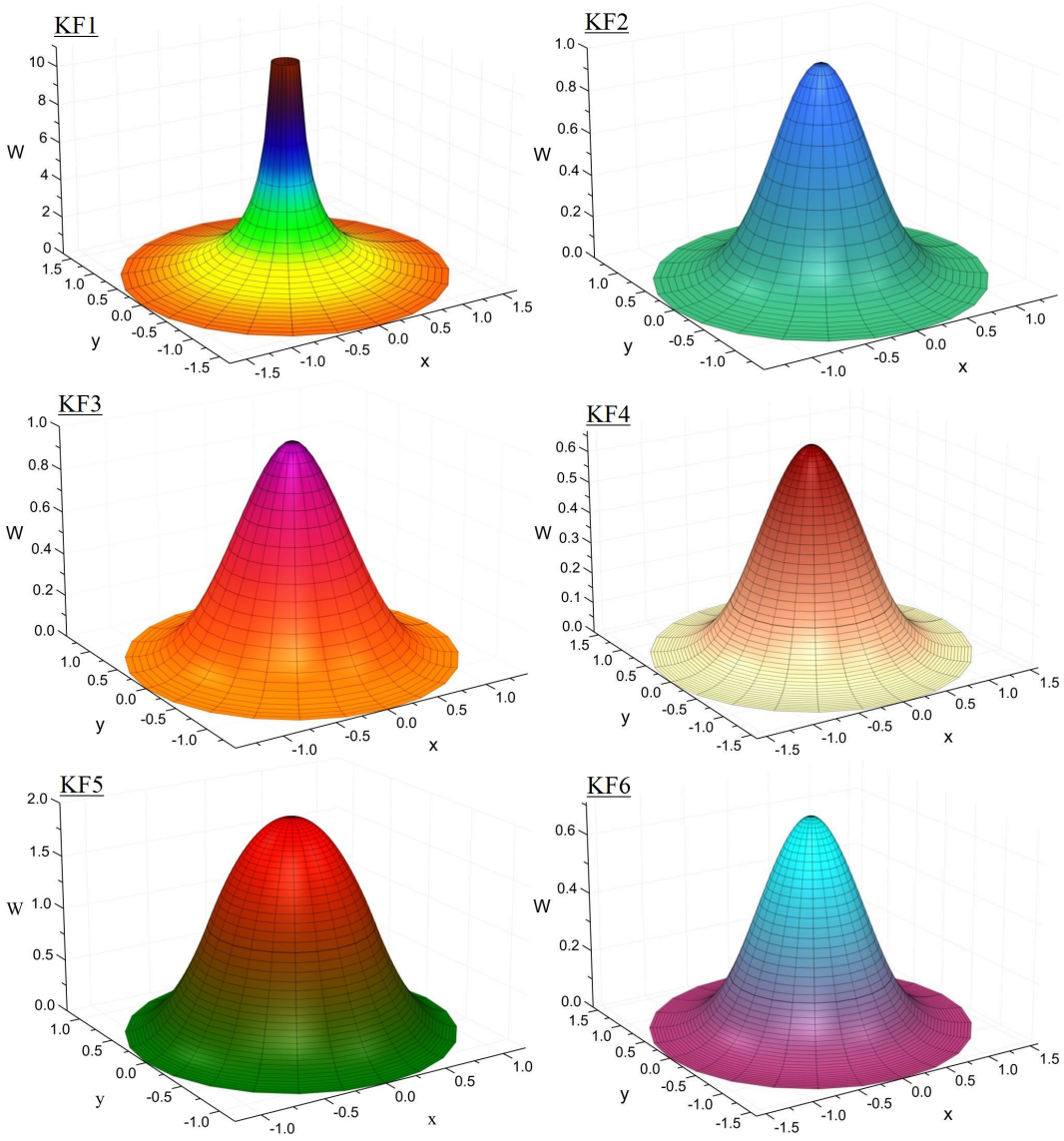

Figure 1- Shape of the different kernel functions

$w(r)$ is a kernel function. r is the distance between two fluid particles and r_e is the kernel size (see Figure 2). The value of the kernel functions out of the kernel size ($r > r_e$) is zero. There are stability issues with the MPS method as some of the common kernel functions in this method do not realistically model the particle interactions (Ataie-Ashtiani and Farhadi 2006). Ataie-Ashtiani and Farhadi (2006) performed a study on the effect of the kernel

functions introduced in Table 1 on the stability of dam-break simulation using the MPS method. Based on their study, the cubic spline kernel function (KF6) formulated by Shao and Lo (2003) is shown to improve the stability of the MPS. This kernel function is used herein in this research to improve the stability of the simulations.

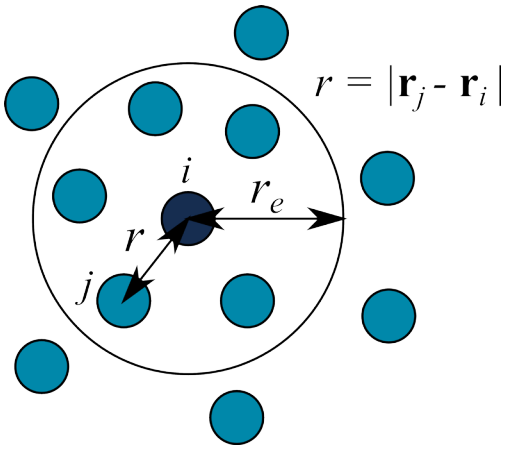

Figure 2- Definition of particle spacing and kernel size.

In the MPS method, particle number density is defined as

$$\langle n \rangle_i = \sum_{i \neq j} w(|\mathbf{r}_j - \mathbf{r}_i|) \tag{2.3}$$

$\mathbf{r}$ is the position vector. The subscripts denote a specific particle. In this equation, the contribution of particles to themselves does not take part in the summation. Once the particle number density is divided by the volume occupied by neighboring particles of the reference particle i, the number of particles in a unit volume, denoted by N_i, is calculated as

$$\langle N \rangle_i = \frac{\langle n \rangle_i}{\int_V w(r)dv} \tag{2.4}$$

Assuming all the fluid particles have the same mass, m, the fluid density, ρ, is expressed as

$$\langle \rho \rangle_i = m \langle N \rangle_i = \frac{m \langle n \rangle_i}{\int_V w(r) dv} \tag{2.5}$$

Equation (2.5) shows that the fluid density is proportional to particle number density. Accordingly, in incompressible flows, far from the free surface, particle number density should be constant. This constant value is denoted by n^0.

Koshizuka and Oka (1996) expressed particle interaction models for differential operators. The gradient operator is given as

$$\langle \nabla \phi \rangle_i = \frac{d}{n^0} \sum_{i \neq j} \frac{\phi_j - \phi_i}{| \mathbf{r}_j - \mathbf{r}_i |^2} (\mathbf{r}_j - \mathbf{r}_i) \; w(| \mathbf{r}_j - \mathbf{r}_i |) \tag{2.6}$$

where φ is an arbitrary scalar, $\hat{\varphi}$ is the minimum value of that scalar among the neighboring particles of the reference particle i, and d is the number of space dimensions. The term $\varphi_j - \hat{\varphi}_i$ always remains positive which keeps repulsive forces between the particles.

The Laplacian operator is modeled in a transient diffusion problem and expressed as

$$\langle \nabla^2 \phi \rangle_i = \frac{2d}{\lambda n^0} \sum_{i \neq j} [(\phi_j - \phi_i) \; w(| \mathbf{r}_j - \mathbf{r}_i |)] \tag{2.7}$$

The role of parameter λ is to keep the variance increase equal to the analytical solution and is given by

$$\lambda = \frac{\int_v w(r) r^2 dv}{\int_v w(r) dv} \tag{2.8}$$

2.3. Solution Method

2.3.1. Time splitting

Following the approach of Zienkiewicz and Codina (1995), the time differentiation of the particle densities can be split as

$$\frac{D\rho}{Dt} = \frac{\rho^{n+1} - \rho^n}{\Delta t} = \frac{\rho^{n+1} - \rho^* + \rho^* - \rho^n}{\Delta t} = \frac{\Delta\rho' + \Delta\rho^*}{\Delta t} \tag{2.9}$$

Likewise, the particle acceleration term in the momentum conservation equation can be expressed as

$$\frac{D\mathbf{u}}{Dt} = \frac{\mathbf{u}^{n+1} - \mathbf{u}^n}{\Delta t} = \frac{\mathbf{u}^{n+1} - \mathbf{u}^* + \mathbf{u}^* - \mathbf{u}^n}{\Delta t} = \frac{\Delta\mathbf{u}' + \Delta\mathbf{u}^*}{\Delta t} \tag{2.10}$$

Using the presented time differentiation of the particle densities and velocities, the mass and momentum conservation equations can be respectively written as

$$\frac{1}{\rho}\frac{\Delta\rho' + \Delta\rho^*}{\Delta t} = -\nabla.(\mathbf{u}^{n+1} - \mathbf{u}^* + \mathbf{u}^*) \tag{2.11}$$

$$\frac{\Delta\mathbf{u}' + \Delta\mathbf{u}^*}{\Delta t} = -\frac{1}{\rho}\nabla P + \upsilon\nabla^2\mathbf{u} + \mathbf{f} \tag{2.12}$$

To apply the semi-implicit prediction-correction scheme, the mass conservation equation is written in two steps as

$$\frac{1}{\rho}\frac{\Delta\rho^*}{\Delta t} = -\nabla.\,\mathbf{u}^* \tag{2.13}$$

$$\frac{1}{\rho}\frac{\Delta\rho'}{\Delta t} = -\nabla.\,\Delta\mathbf{u}' \tag{2.14}$$

In a similar way, the conservation of linear momentum equation is written in two steps as

$$\frac{\Delta\mathbf{u}^*}{\Delta t} = \upsilon^n\nabla^2\mathbf{u}^n + \mathbf{f}^n \tag{2.15}$$

$$\frac{\Delta\mathbf{u}'}{\Delta t} = -\frac{1}{\rho}\nabla P^{n+1} \tag{2.16}$$

2.3.2. Prediction step

At the prediction step, the viscous and gravitational forces are explicitly calculated without enforcing the incompressibility to the fluid and an intermediate velocity and position is obtained for each particle as

$$\begin{cases} \Delta\mathbf{u}_i^* = \upsilon_i^n\nabla^2\mathbf{u}_i^n\Delta t + \mathbf{f}_i^n\Delta t \\ \mathbf{r}_i^* = \mathbf{r}_i^n + \Delta\mathbf{u}_i^*\Delta t \end{cases} \tag{2.17}$$

2.3.3. Pressure Poisson equation

At the prediction step, fluid incompressibility is not enforced. Accordingly, the fluid density at the intermediate time step, ρ^*, has deviated from the initial fluid density, ρ^0. As it is previously shown, there is a direct relation between the particle number density and the

fluid density. Hence, to satisfy the incompressibility, the particle number density is implicitly corrected to n^0 by

$$n^* + \Delta n' = n^0 \tag{2.18}$$

$\Delta n'$ is the difference between constant particle number density and the particle number density at the intermediate time step.

Using the particle number density as the representative of density, Equation (2.14) can be expressed as

$$\frac{1}{n^0}\frac{\Delta n'}{\Delta t} = -\nabla.\Delta \mathbf{u}' \tag{2.19}$$

By simply combining the equations (2.16), (2.18), and (2.19), a Poisson equation of pressure is obtained

$$\left\langle \nabla^2 P^{n+1} \right\rangle_i = -\frac{\rho}{dt^2}\frac{\left\langle n^* \right\rangle_i - n^0}{n^0} \tag{2.20}$$

2.3.4. Correction step

The Poisson equation of pressure (equation (2.20)) can be turned to a system of linear equations by replacing the left side of the equation by the Laplacian model expressed in equation (2.7). Once the system is solved and the pressure is calculated, it is replaced into the gradient model (equation (2.6)) to calculate the pressure gradient. The pressure gradient is then replaced in equation (2.16) and accordingly, the velocity correction is calculated.

Finally, the velocity and position of the particles at the end of each time step are calculated as

$$\begin{cases} \mathbf{u}^{n+1} = \mathbf{u}^{*} + \Delta\mathbf{u}' \\ \mathbf{r}^{n+1} = \mathbf{r}^{n} + \mathbf{u}^{n+1}\Delta t \end{cases} \tag{2.21}$$

The step by step calculation algorithm of the MPS method is shown in Figure 3.

2.4. Weakly compressible model

Monaghan (1994) modified the equation of state given by Batchelor (1973) to simulate the free surface flows with the SPH method. This equation of state has the form of

$$P = \frac{\rho_0 C^2}{\gamma}\left(\left(\frac{\rho}{\rho_0}\right)^{\gamma} - 1\right) \tag{2.22}$$

with γ=7. C is the numerical sound speed. It is shown by Shakibaeinia (2011) that in order to keep the fluid density variation less than 1% of the reference density, the Mach number (Ma) should be smaller than 0.1, meaning that the numerical sound speed should be ten times higher than the maximum fluid particle velocity.

Using the aforementioned equation of state in the MPS formulation, the pressure can be obtained explicitly without solving the Poisson equation of pressure. This explicit method is known as weakly–compressible MPS (WC-MPS) method.

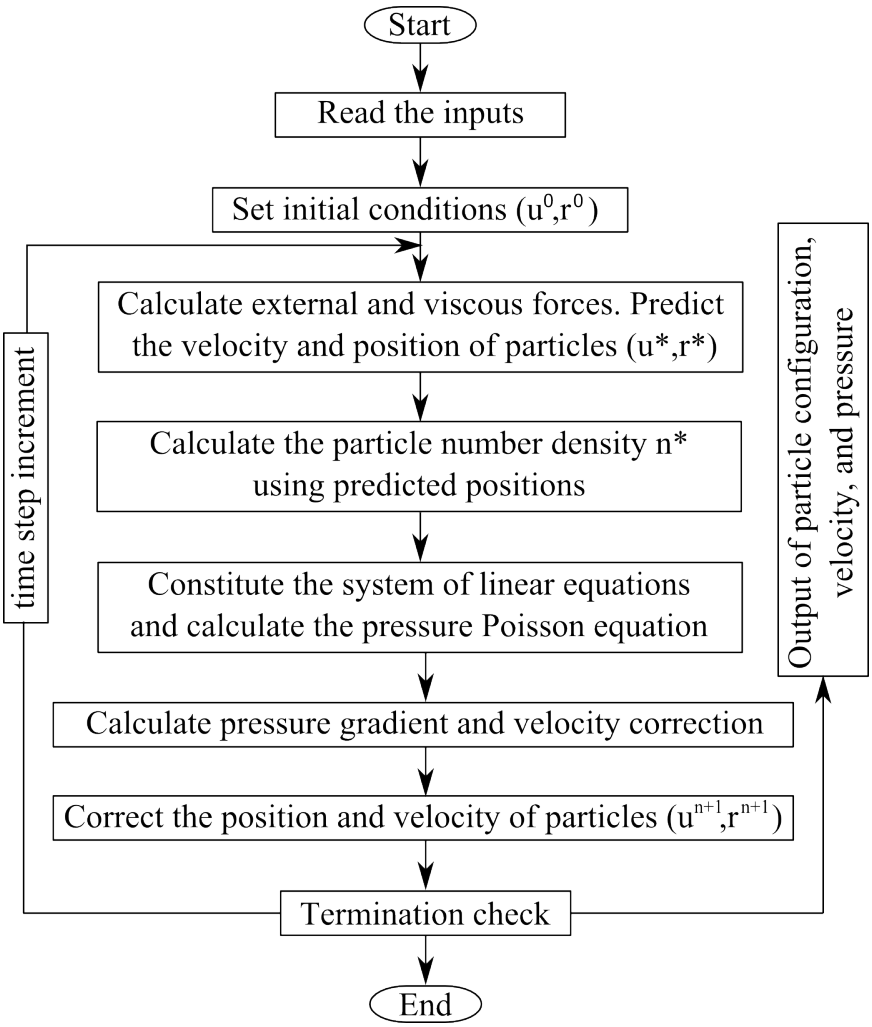

Figure 3- Calculation algorithm of the MPS method.

2.5. Boundary Treatment

In the MPS method, a fluid particle is considered to be on free surface if it meets the following condition

$$\left\langle n^* \right\rangle_i < \beta n^0 \tag{2.23}$$

Parameter β is called the free surface parameter. The reference pressure is applied to free surface particles as a boundary condition. Approaching solid boundaries, the density of particles will decrease and accordingly, they may satisfy the free surface boundary condition and be considered on the free surface. To avoid this issue, few layers of so-called *ghost particles* are simulated outside the solid boundaries to take part in particle number density calculations (Figure 4).

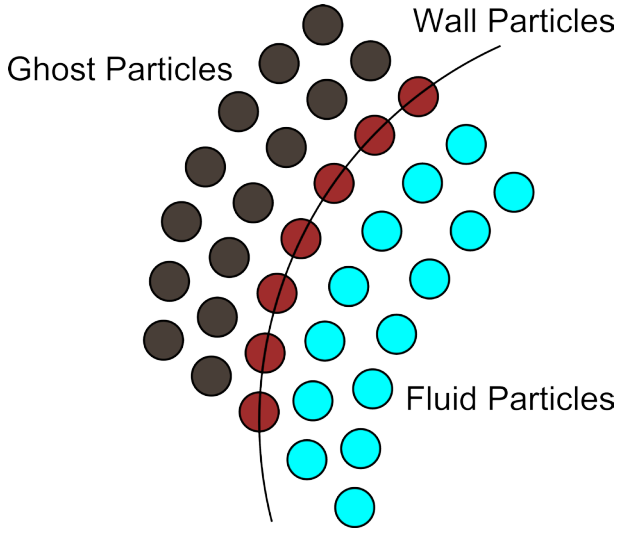

Figure 4- Ghost particle recognition.

The first layer of solid boundaries will take part in pressure Poisson equation calculations. As a result, there is always a repulsive force between fluid particles and solid boundary particles to avoid sticking of fluid particles to the solid boundaries.

Chapter 3 : Landslide-Induced Water Waves

Landslides, usually caused by slope failures or liquefaction of sediments, can generate water waves and small-scale tsunamis in coastal areas. Once the landslide-induced water waves reach the coast or structures, they are able to produce disasters including loss of life and collapse of facilities and infrastructures. Therefore, it is of importance to predict the damage of landslide-generated water waves in flood hazard assessment of coastal zones.

Due to the importance of water waves generated by landslides, researchers have conducted empirical, analytical and numerical studies on this phenomenon. Most of these studies are focusing on the rigid underwater landslides. For instance, Wiegel (1955), Iwasaki (1982), Heinrich (1992) and Watts (1997) performed experimental studies on the characteristics of the water waves generated by the motion of solid blocks or boundaries along inclined planes into a channel. Enet and Grilli (2007) conducted large scale, three-dimensional laboratory experiments to study tsunami generation by rigid underwater landslides. Grilli and Watts (1999) developed a boundary element model to simulate water waves due to the motion of a submerged body. Iwasaki (1997) performed several numerical studies on water waves generated by rigid submarine landslides, based on the linear shallow water wave equations. Heinrich (1992) conducted similar studies using the VOF (Volume of Fluid) method. Ataie-Ashtiani and Najafi-Jilani (2006; 2007) provides a comprehensive review on numerical and experimental studies on the landslide-generated water waves.

Modeling surface waves generated by landslides is difficult due to the complex motion of the submerged bodies with arbitrary shapes and the wave interaction with the shore line which results in non-linearity of governing equations. Therefore, numerical methods have been used to overcome such difficulties. In this chapter, the water waves generated by rigid vertical landslides and rigid underwater landslides along an inclined plane are simulated by the MPS method. Particles configuration, velocity fields, and pressure fields are presented at different times. Results are compared with the available experimental data and analytical solutions.

3.1. Vertical Landslide Simulation

3.1.1. Problem definition

In this section, the water waves generated by vertical rigid landslide (rockslide) are simulated using MPS method. A box, modeling the landslide, descends into an open channel partially filled with water, and then generates a solitary wave and a reverse plunging wave. Scope and dimensions of this problem are depicted in Figure 5.

Monaghan and Kos (2000) described an experimental relation for the velocity of the descending box (equation (3.1)). In their experiment, the weight of box was 38.2 kg, which is sufficient to ensure that the box sinks rapidly.

$$\frac{V}{\sqrt{gD}} = 1.03\frac{h}{D}\left(1-\frac{h}{D}\right)^{0.5} \tag{3.1}$$

V is the box velocity, D is the depth of water and h is the height of box. At each time step, the velocity of box is known so the position of box is calculated. The variation of box velocity with respect to its height is sketched in Figure 6.

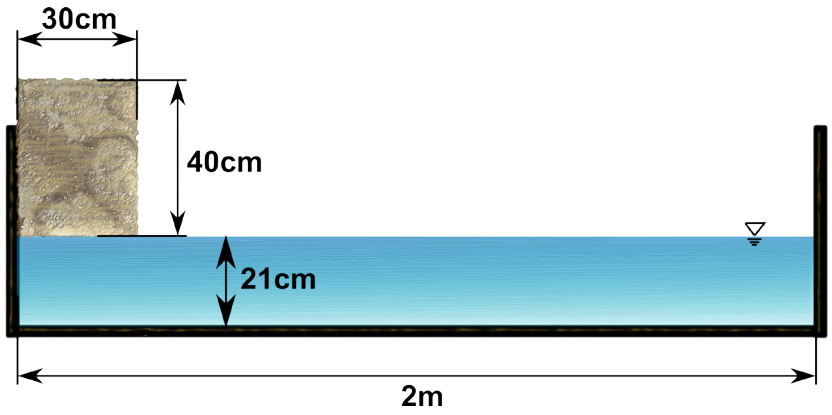

Figure 5- Scope and dimensions of the vertical landslide problem.

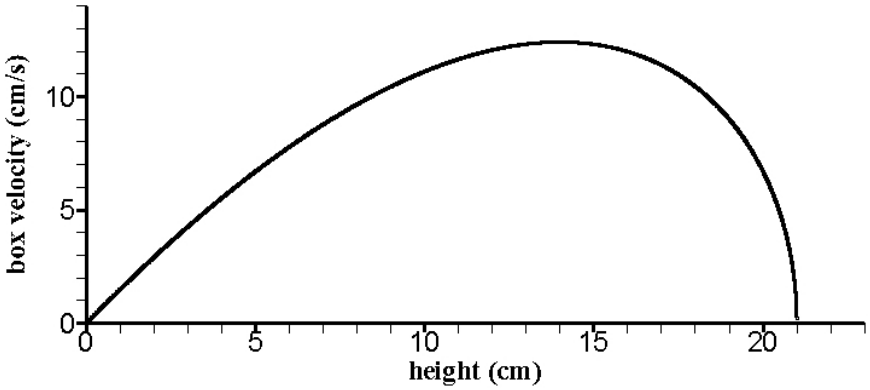

Figure 6- Vertical landslide mass velocity at different heights.

Equation (3.2) shows an analytical solution for the profile of a solitary wave (Lee et al. 1982)

$$\eta = H\left[sec\,h\sqrt{\frac{3H}{4D}}\frac{X}{D}\right]^2 \tag{3.2}$$

where η is the water surface elevation, H is the amplitude of wave, D is water depth and $X = (x - C_w t)$. C_w is the solitary wave celerity which is expressed by

$$C_w = \sqrt{g(D+H)} \tag{3.3}$$

3.1.2. Results and Analysis

In the present model, the initial particle spacing and the free surface parameter are set to 0.8 cm, 0.97, respectively. The kernel size is set to twice the initial particle spacing, as suggested by Ataie-Ashtiani and Farhadi (2006) in case of using the cubic spline kernel function (KF6). The fluid is considered non-viscid. The solution domain is represented by 8126 particles. Initial time step is set to 0.001s, constrained by the CFL stability condition (Courant et al. 1967) and the Courant number is adjusted to 0.4. In addition to one layer of solid boundary particles, two layers of ghost particles are considered.

Figure 7 shows the water surface profile at different times. The box sinks into the channel and as a result water is heaved up to form a solitary wave and a reverse plunging wave that forms a vortex. This vortex follows the solitary wave to the right side of the channel. Around t=1.25s, t=3.4s, t=5.6s, t=7.9s and t=10.5s, the solitary wave strikes the right vertical wall and accordingly, the direction of wave propagation is changed. Around t=2.2s, t=4.4s, t=6.7s, t=9s and t=11.5s, the solitary wave impinges on the right side of box and its direction is changed. At t=17s, the water surface profile is approximately horizontal.

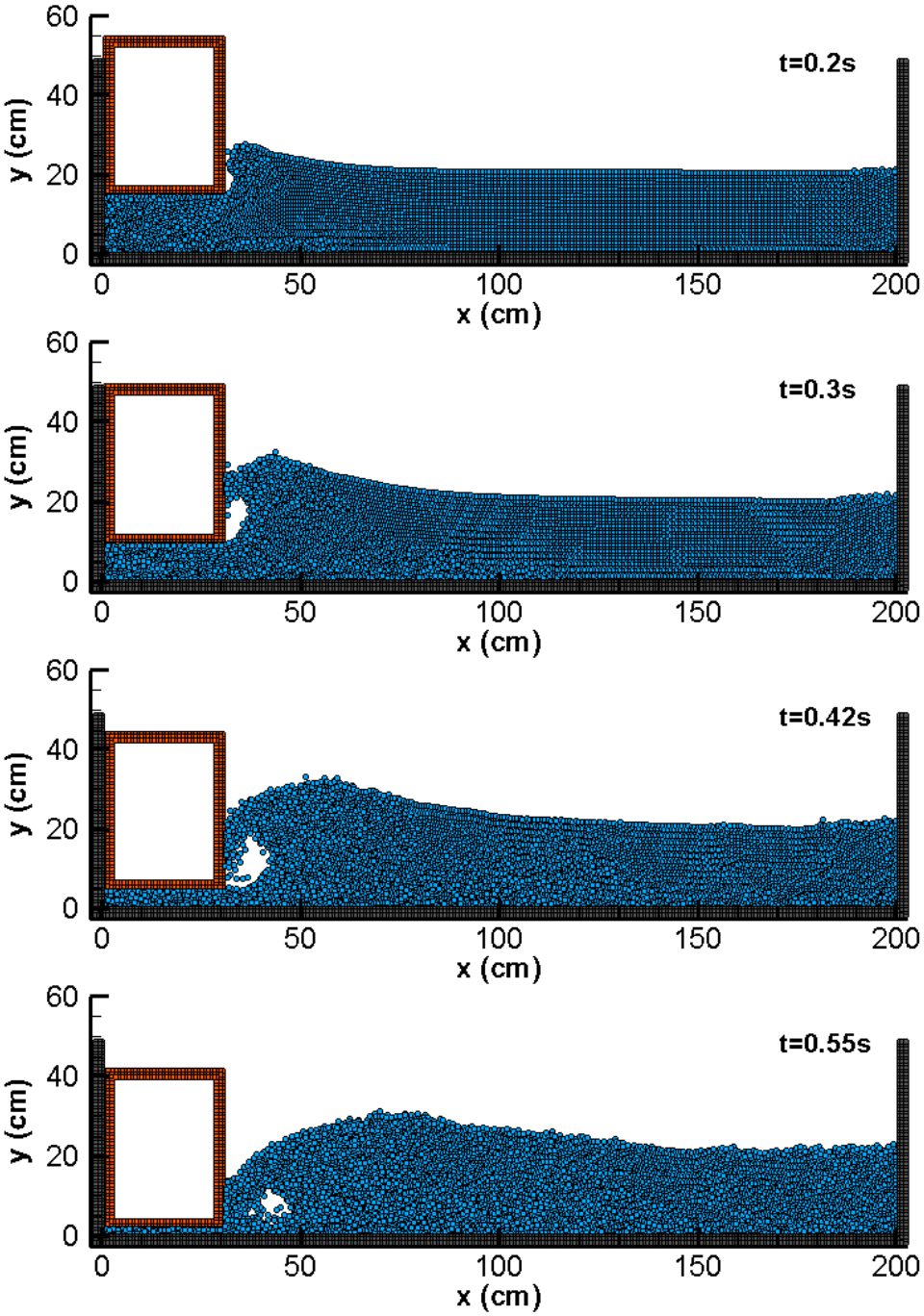

Figure 7- Particle Configuration at different times for the vertical landslide simulation.

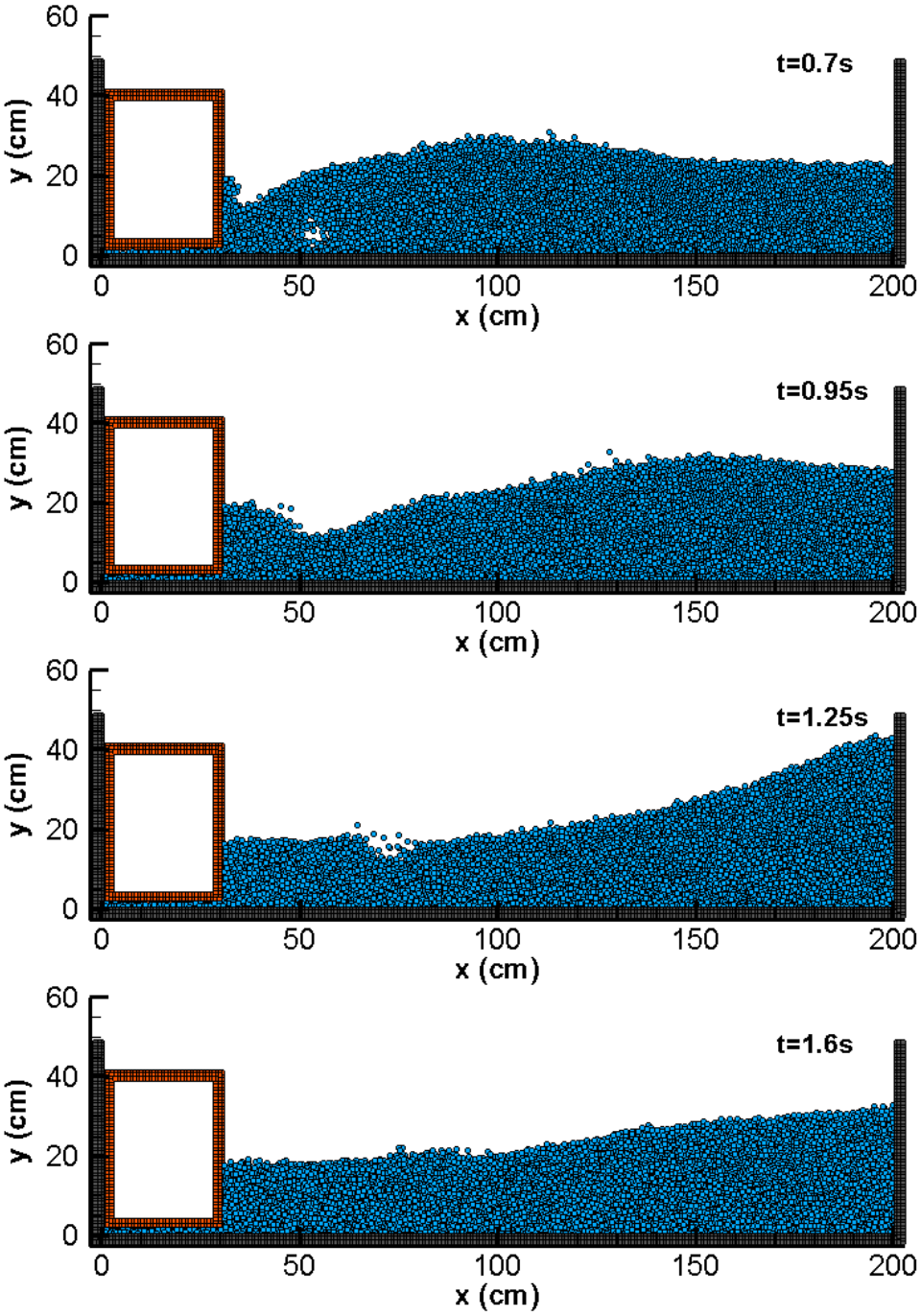

Particle Configuration at different times for the vertical landslide simulation (continued).

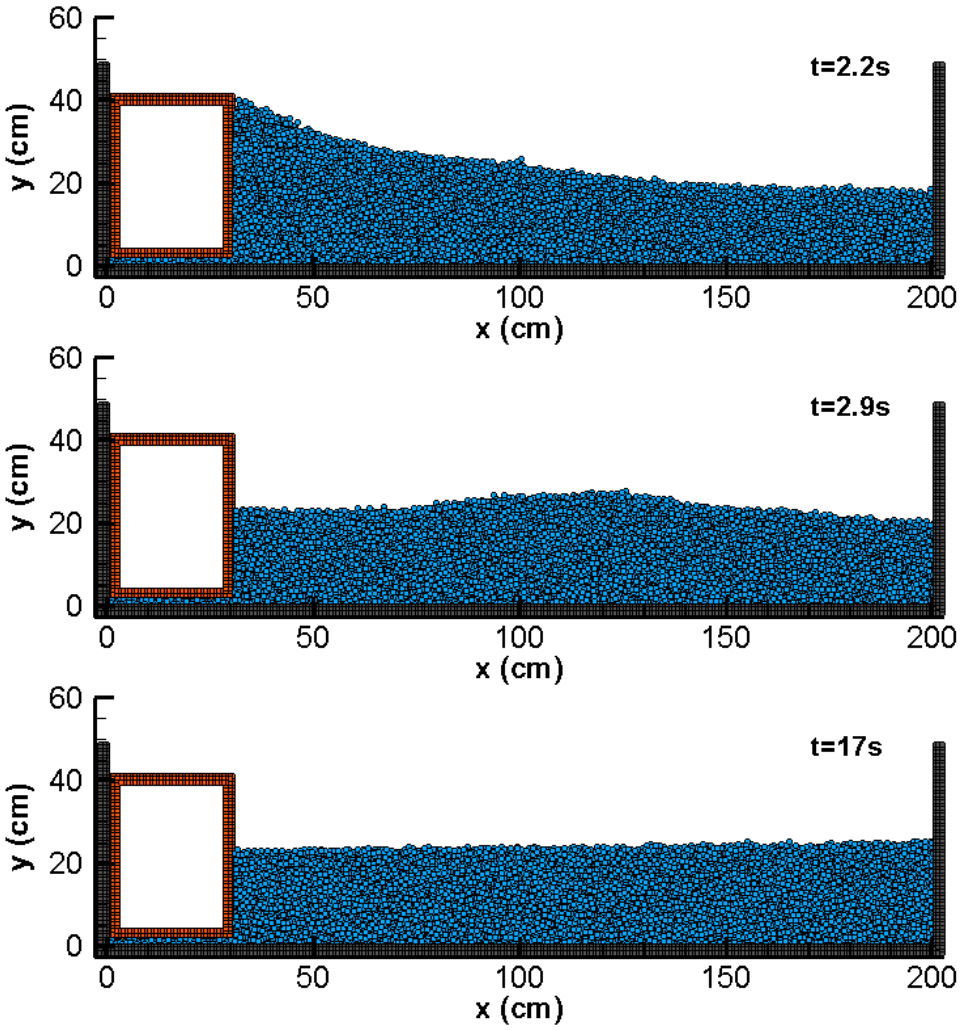

Particle Configuration at different times for the vertical landslide simulation (continued).

The wave amplitude is 11.03 cm, measured by the present model. Ataie-Ashtiani and Shobeyri (2008) computed almost the same value (11 cm) using I-SPH simulation with a Courant number which is 75% less than the value used in this study. Monaghan and Kos (2000) obtained 10.8 cm by their SPH simulation and 9.2 cm by experiment for the amplitude of solitary wave. However, as there was a gap between the box and left vertical wall in the experiment, a narrow stream is moved up the gap. As a result, there was an error in measuring the solitary wave amplitude by experiment. To evaluate the value of this

error, they performed another similar SPH simulation with presence of the gap. They concluded that when the gap opened up in the simulation, about 12% of the wave amplitude is reduced. This accounts for the difference between experimental and numerical results.

Figure 8 shows the velocity field at t=0.4s and t=0.8s. At t=0.4s, the fluid particles on the right side of box are circuiting in a vortex, created by the reverse plunging wave. The velocity magnitude of particles at the right end side of box is high, as the particles tend to escape from that high-pressure region. At t=0.8s, the circulation strength is significantly decreased, but still some fluid particles are circuiting around a small circuit. The particles which escaped from the high pressure region under the box are still moving with high velocity to the right side of the channel.

Figure 9 shows the pressure field at different times computed by the present model. Pressure at the region below the box has a significant deviation from hydrostatic pressure. This is due to the dynamic pressure exerted by the box. Far from the box, as the dynamic pressure disappears, the pressure distribution is hydrostatic. Later, as the particles below the box escape due to significant pressure gradient, a high pressure current starts to form from below of the box and moves toward the right side of water tank. As this current moves, it dissipates due to the pressure gradient between this region and the adjacent area.

Although scientists proposed some modification to pressure model, still MPS method suffers from unphysical pressure fluctuation. Khayyer and Gotoh (2009) proposed a modified formulation for the calculation of pressure gradient for exact conservation of linear momentum. However, as shown by Shakibaeinia (2011), although this modified pressure gradient formulation will result is relatively accurate calculation of pressure field,

it may not yield exact calculation of the pressure gradient between two particles, which is necessary for the accurate estimation of instantaneous motion of the fluid particles.

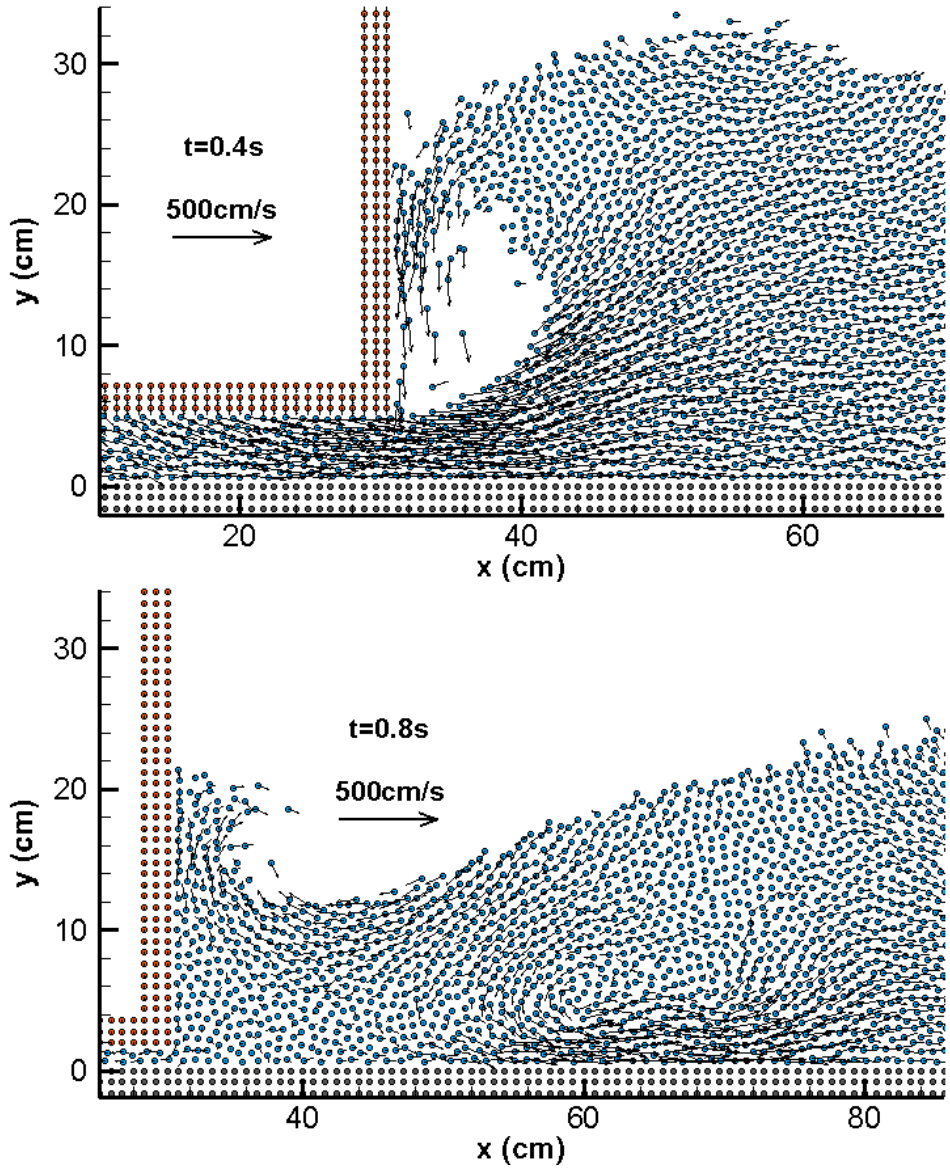

Figure 8- Velocity field at different times for the vertical landslide simulation.

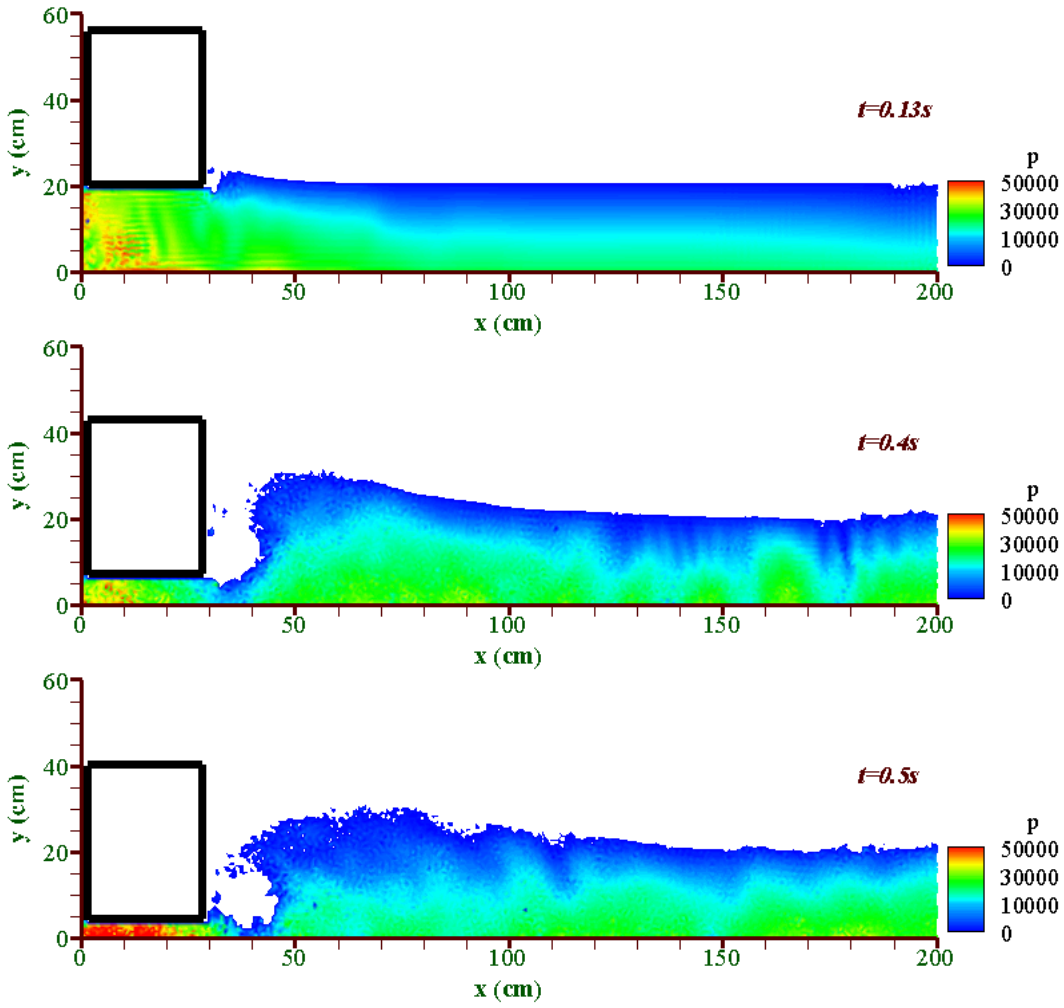

Figure 9- Pressure field at different times computed by the present model.

Figure 10 shows a comparison between the present MPS results and the analytical solution for the solitary wave profile. To make the analytical solution comparable with the simulated solitary wave, the crest of analytical wave profile is adjusted to the crest of simulated solitary wave. Note that the two solutions are not expected to fit where the plunging wave and vortex are affecting the flow. This is the reason that the x-axis range of these plots is limited for the comparison of results. Results show that the predicted solitary wave profile by the present model is in good agreement with the analytical solution.

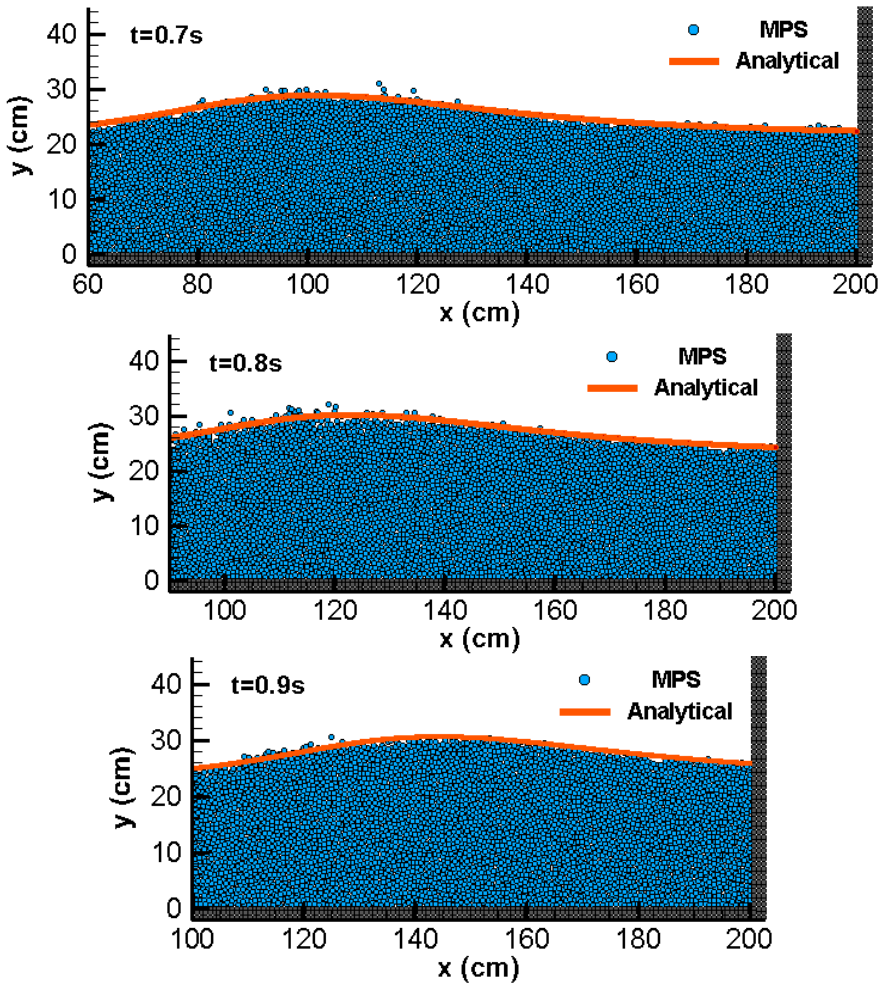

Figure 10- Solitary wave profile comparison between the MPS results and the experimental data the vertical landslide problem.

Figure 11 shows a comparison between analytical solution and solution by the present model for the horizontal velocity of particles on free surface. The data is smoothed by a Laplacian smoothing algorithm to reduce the noise associated with discrete data (Wahba 1979). The agreement between analytical solution and solution by the present model is acceptable.

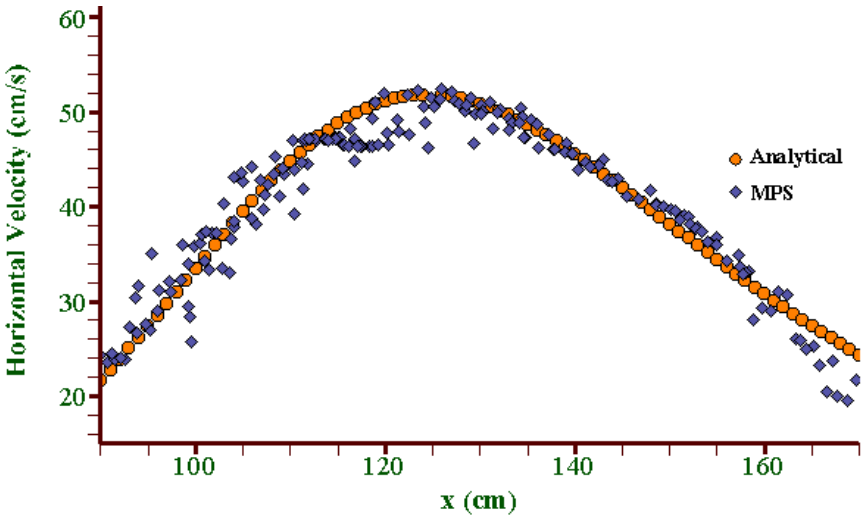

Figure 11- Comparison between analytical solution and solution by the present model for the horizontal velocity of particles on the free surface.

A comparison between the reverse plunging wave measurements by the present model, I-SPH (Ataie-Ashtiani and Shobeyri 2008), SPH (Monaghan and Kos 2000), and Experimental results (Monaghan and Kos 2000) is tabulated in Table 2. The definition of parameters used in these measurements is sketched in Figure 12. The agreement between the measurements obtained by the present model, I-SPH simulation and experiment are satisfactory. However, the SPH measurements do not match appropriately to the experimental results.

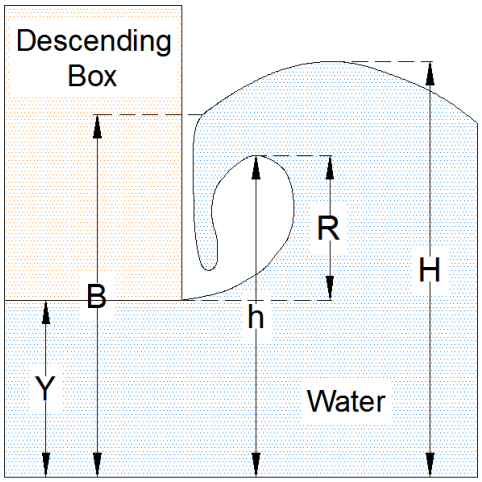

Figure 12- Definition of the parameters used in reverse plunging wave measurements in the vertical landslide problem.

Table 2- A comparison between the present MPS model, I-SPH, SPH, and experimental results for the reverse plunging wave measurements.

l_0 *(cm)*	*Method*	*H (cm)*	*R (m)*	*h (m)*	*B (m)*
0.8	MPS	32.60	12.93	22.43	27.07
1	I-SPH	33.01	14.6	23.4	26.8
1.5	I-SPH	32.9	13	21.8	25.5
0.42	SPH	30.86	11.4	20.8	27.2
0.525	SPH	30.9	10.9	20.3	27.3
0.7	SPH	30.8	9.9	19.3	26.1
10.5	SPH	30.8	7.5	16.9	27.3
---	Experimental	33.3	13.33	22.73	30.3

3.1.3. Stability of the model

The number of free surface particles is used as an indicator of stability of the model. Figure 13 shows two sketches for the number of particles on free surface, one up to 2.5s and the other up to 40s. Until t=2.5s, the solitary wave has hit the right vertical wall and right side of box. From t=0.1s to t=0.5s, the solitary wave, reverse plunging wave and vortex start to form and thus, the number of particles on free surface will significantly increase. From t=0.5s to t=0.85s, the reverse plunging wave accumulates on the right side of box, increasing the number of free surface particles. Meanwhile, the circulation strength starts to decrease after t=0.5s, reducing the number of free surface particles. As a result, there is a considerable fluctuation on the number of free surface particles between t=0.5s and t=0.85s. Around t=0.85s, the plunging wave starts to follow the solitary wave and it gradually mixes with the solitary wave. This makes the water surface profile more uniform, and thus the number of particles on free surface will start to decrease gradually from t=0.85s until it reaches an approximately stable range at around 1.6 s. As there is no unphysical variation or fluctuation in the number of particles on free surface and the simulation is performed without instability occurrence for a long period (40s), it can be concluded that the present model is stable. Despite the SPH (Monaghan and Kos 2000) and I-SPH (Ataie-Ashtiani and Shobeyri 2008) which represent the results only up to 0.7s, the MPS simulates the problem until 17s, when the water surface profile becomes almost horizontal, without any instability occurrence.

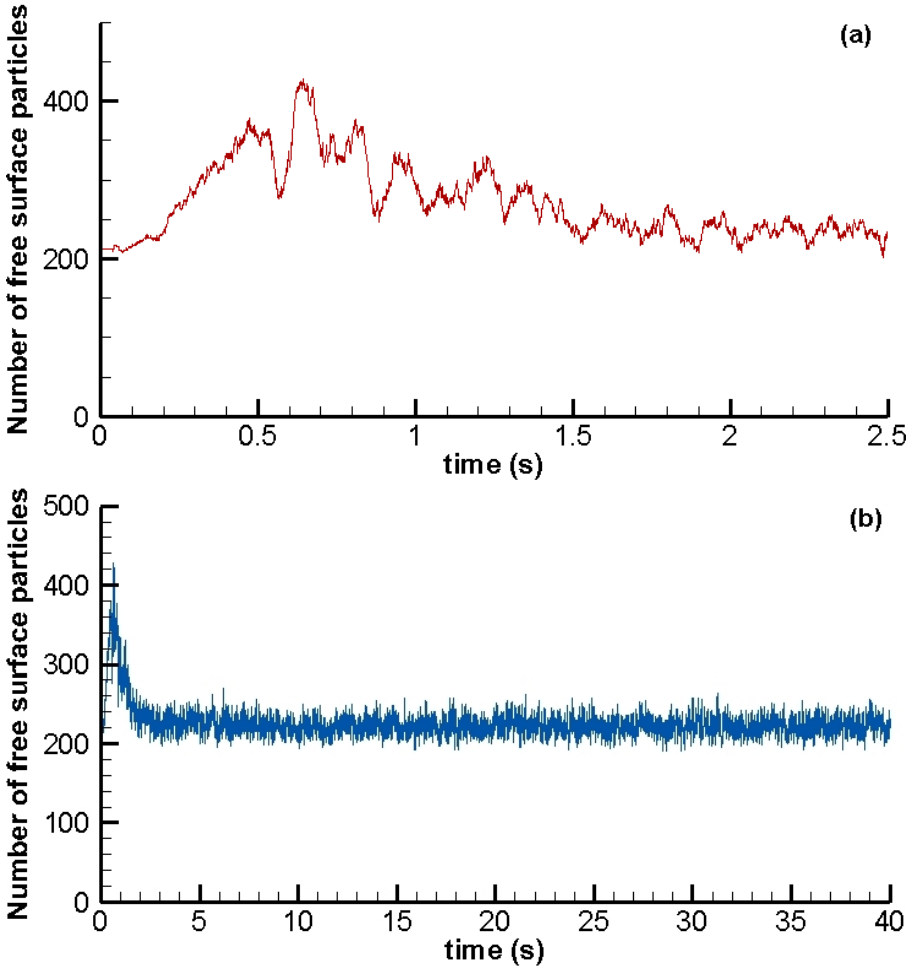

Figure 13- Number of particles on free surface in the vertical landslide simulation, (a) up to 2.5s, (b) up to 40s.

3.2. Submarine Landslide Simulation

3.2.1. Introduction to the Problem

In this section, the water waves generated by submarine landslides are simulated using the MPS method. Landslides herein are modeled by a submerged triangle rigid box sliding along an inclined plane into an open channel filled with water. Scope and dimensions of the present problem are depicted in Figure 14.

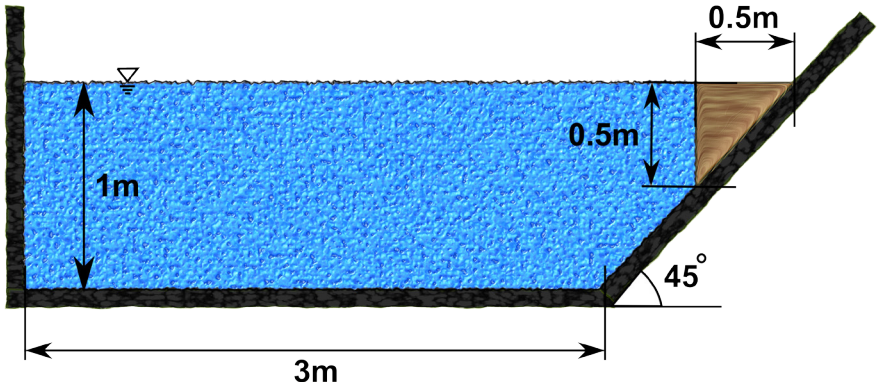

Figure 14- Scope and dimensions of the submarine landslide problem.

Grilli and Watts (1999) have described the vertical velocity of the landslide mass. During the acceleration phase which lasts for 0.4 seconds, the vertical velocity of the rigid landslide mass is described as

$$v(t) = c_1 \tanh(c_2 t) \qquad t \le 0.4s \tag{3.4}$$

Where $v(t)$ is the vertical velocity of box at time t. c_1 and c_2 are constant values. Ataie-Ashtiani and Shobeyri (2008) set 86 cm/s and 0.0175 s^{-1} for the values of c_1 and c_2

in their I-SPH computation, respectively. The same values are used in the current simulation. After the acceleration phase, the vertical velocity of the sliding mass reaches a terminal value of $0.6\ m/s$. At each time step the velocity of the sliding mass is known; thus, its position is calculated.

3.2.2. Results and Analysis

In the present model, free surface parameter and the kernel size are set to 0.99 and 5cm, respectively. The fluid is considered non-viscid. The solution domain is represented by 6242 particles, in which the initial distance between particles is 2.5 cm. Initial time step is 0.001s. The Courant number is set to 0.4. Two layers of ghost particles are modeled near the actual particle layer of solid boundaries.

Particle configuration at different times is presented in Figure 15. As the box slides along the inclined wall, the water is heaved up and a wave is formed. At t=0.6s, water strikes the right inclined wall. The wave moves toward the left vertical wall and around t=1.5s, it reflects from the wall. The maximum height of the water at t=0.8s is about 107.2 cm, which is the same as the value calculated by I-SPH simulation (Ataie-Ashtiani and Shobeyri 2008). The water elevation at t=1.5s adjacent to the left vertical wall is 107.6 cm, 1 cm higher than the value predicted by I-SPH method (Ataie-Ashtiani and Shobeyri 2008).

Figure 16 shows the computed velocity field at different times. As the box slides along the inclined wall, a vortex is gradually generated. At t=1s, the formation of the vortex above the box is clear. The intensity of velocity field is decreased once the box is stopped.

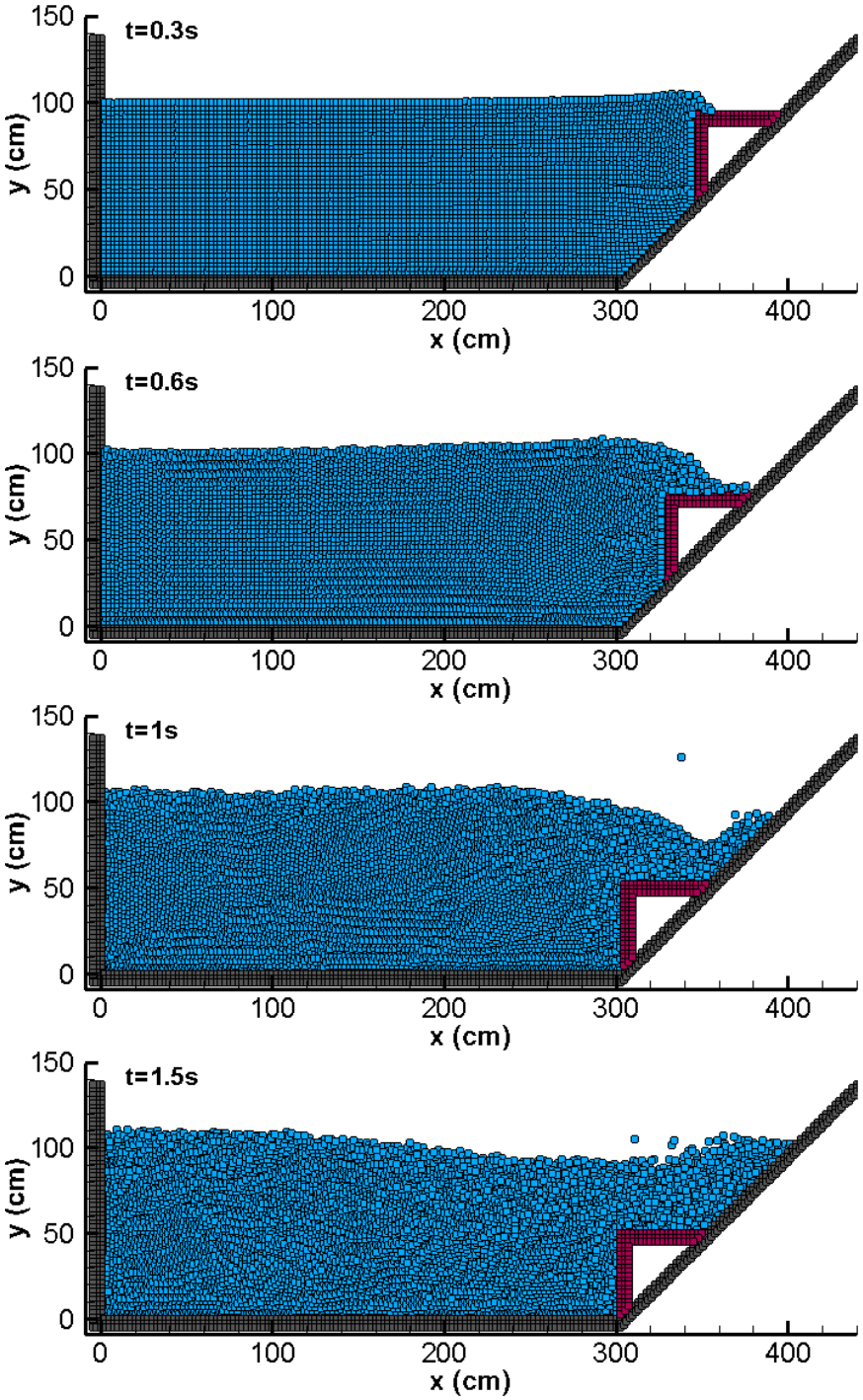

Figure 15 - Particle configuration at different times for submarine landslide simulation.

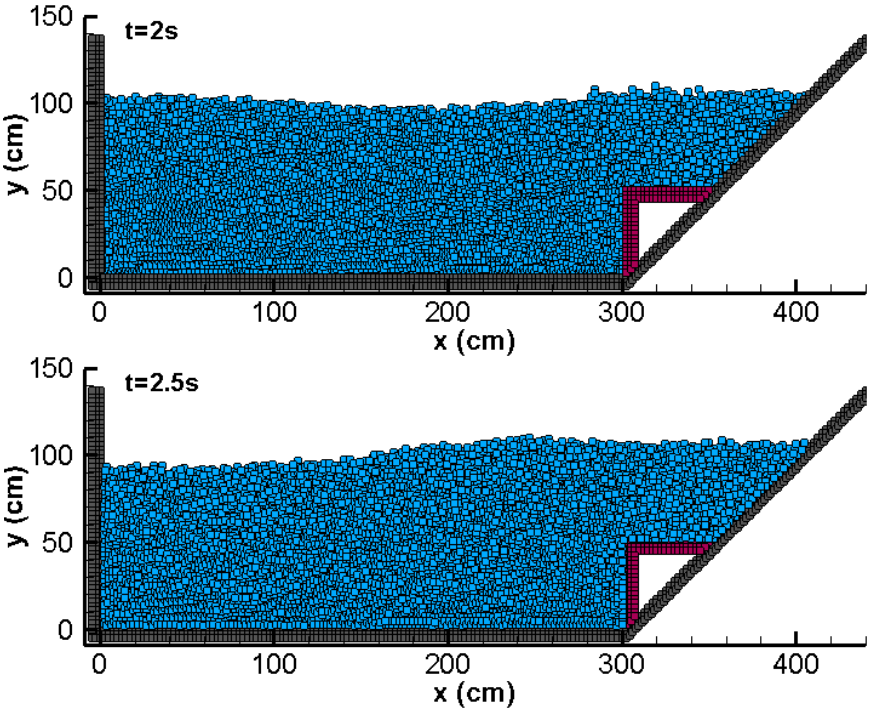

Particle configuration at different times for the submarine landslide simulation

(continued).

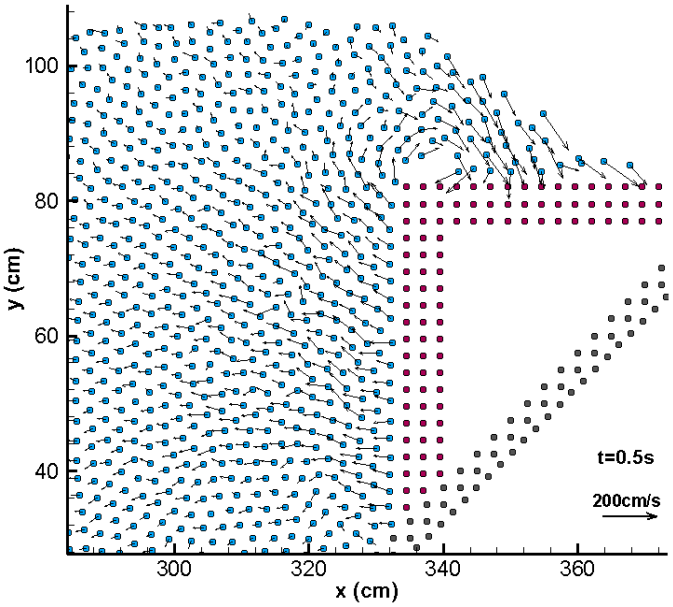

Figure 16- Velocity field at different times for the submarine landslide simulation.

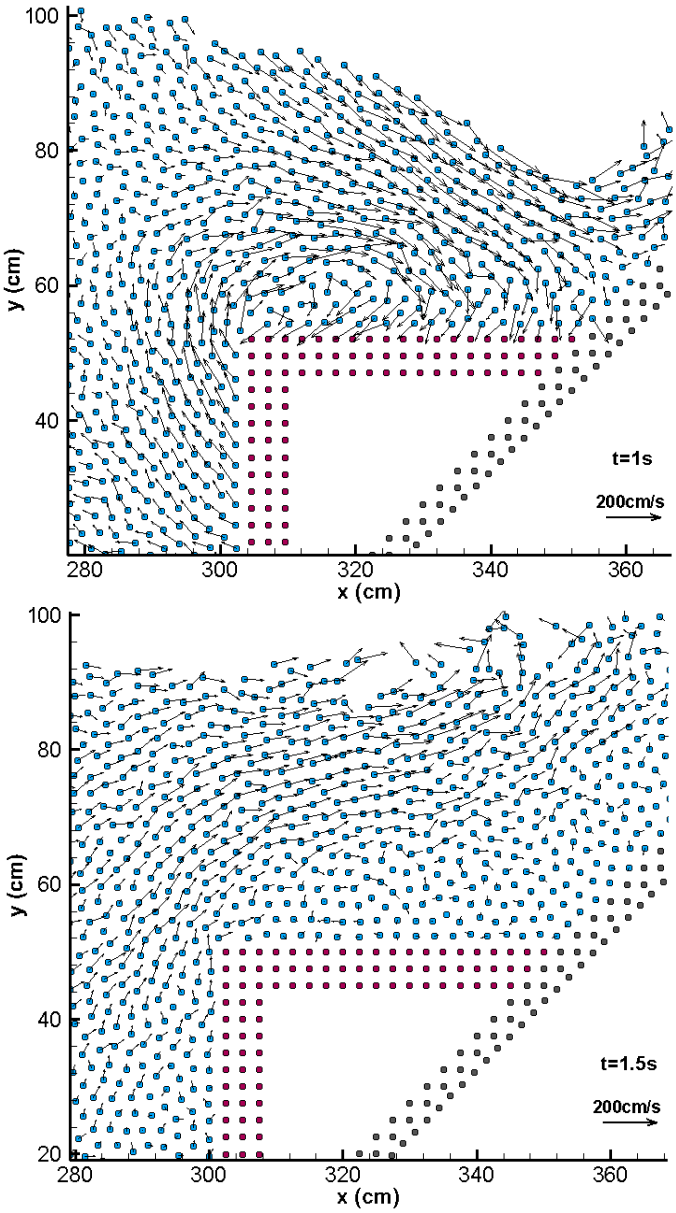

Velocity field at different times for the submarine landslide simulation (continued).

The pressure field at different times is presented in Figure 17. Up to t=0.5s, far from the box, the pressure distribution is nearly hydrostatic. As the wedge moves, it exerts dynamic pressure on the water body and as a result, the hydrostatic pressure distribution near the wedge is disturbed and the pressure is increased.

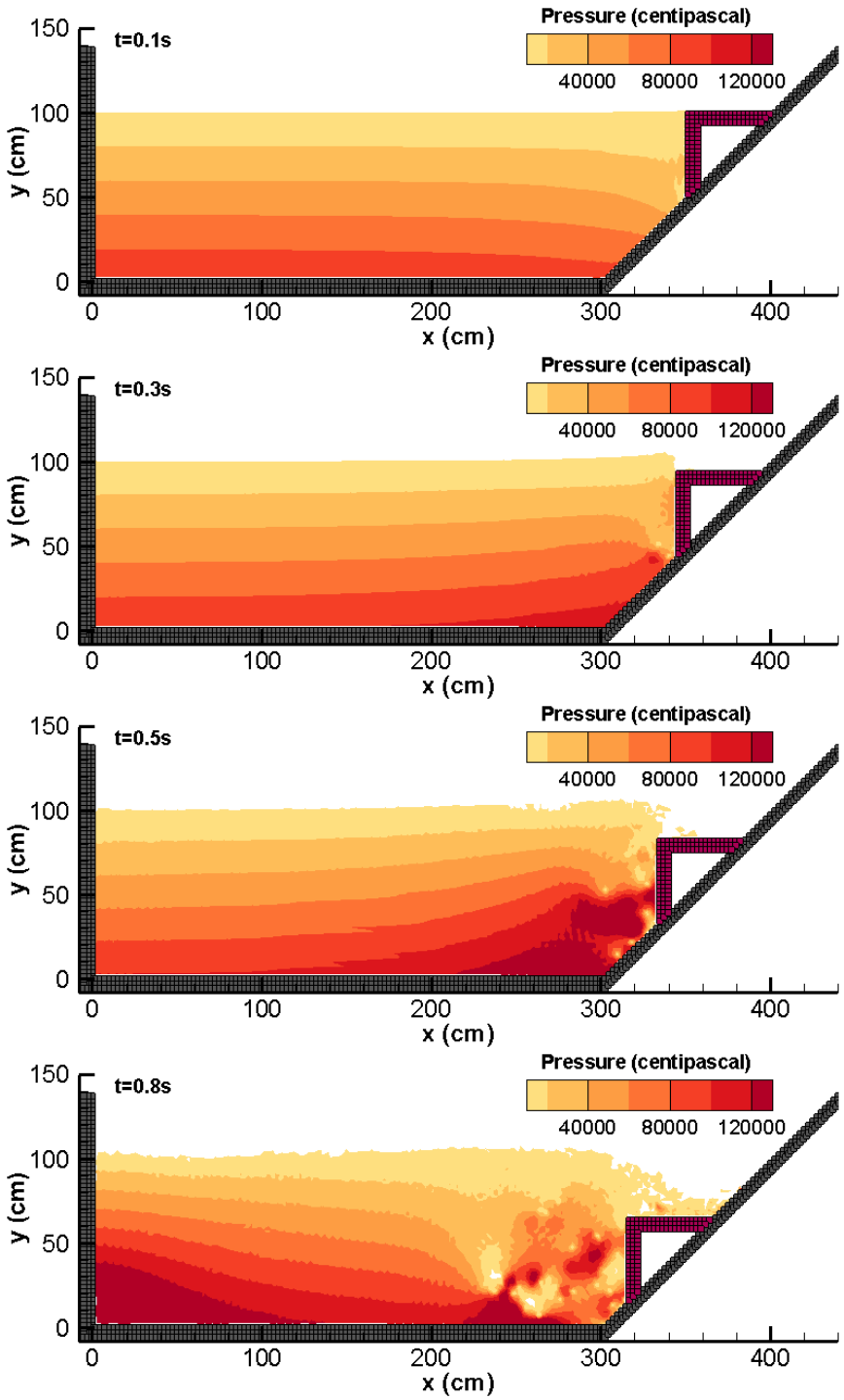

Figure 17- Pressure field at different times for the submarine landslide simulation.

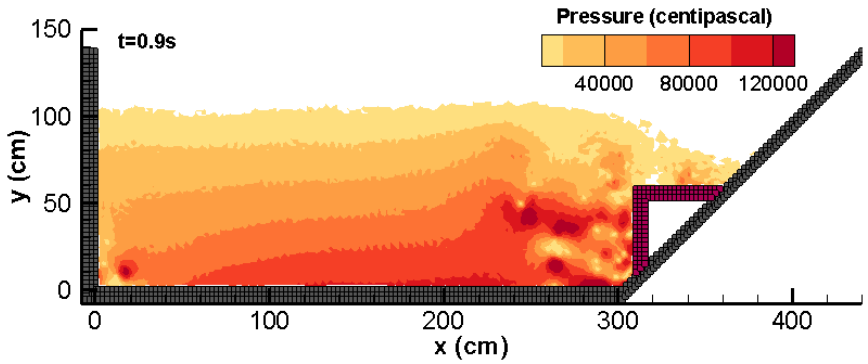

Pressure field at different times for the submarine landslide simulation (continued).

Figure 18 shows a comparison between the present MPS results and the experimental data (Heinrich 1992) for the water surface profile at t=0.5s and t=1s. The overall agreement is satisfactory and demonstrates the accuracy of the model. However, few discrepancies are observed above the box at t=1s. The same issue exists for the simulations performed by the VOF method (Heinrich 1992; Rzadkiewicz et al. 1997) and the I-SPH method (Ataie-Ashtiani and Shobeyri 2008). As noted by Heinrich (1992), part of these differences is explained by the highly turbulent motion of fluid at this region. As no turbulence model is implemented in the code, the present MPS model cannot simulate the free surface turbulence. Additionally, above the box, the experimental wave elevation is recorded on the film with an error of some centimeters (Heinrich 1992).

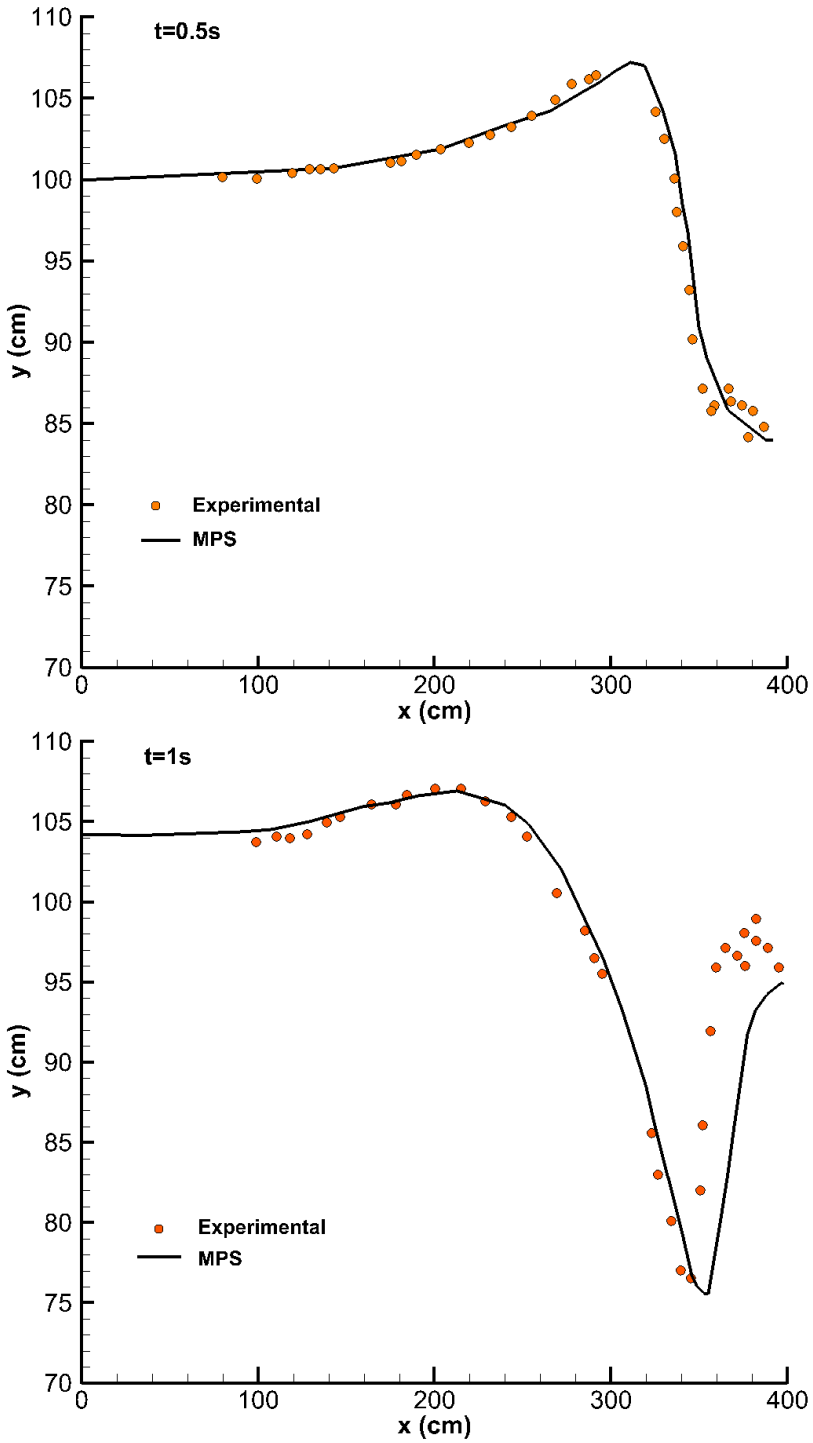

Figure 18- Water surface profile comparison between the MPS results and the experimental data for the submarine landslide problem.

3.2.3. Results of the WC-MPS simulation

As explained earlier in chapter 2, the WC-MPS method is a simplified form of the MPS method which allows a slight compressibility to the fluid. By considering a numerical sound speed in the fluid, an equation of state is introduced to explicitly calculate the pressure without dealing with the Poisson equation of pressure and large systems of equations to implicitly calculate the pressure. In this part, results for the simulation of water waves generated by rigid underwater landslide using the WC-MPS method are presented and compared with the results for the simulation of the same problem using the MPS method.

Particle configuration at different times obtained by the WC-MPS simulation is presented in Figure 19. The overall shape of the water surface profile calculated by the MPS and WC-MPS models are almost the same. At t=0.5s, near the left vertical wall, a slight turbulence on free surface is visible in results of the WC-MPS simulation, which is not physically expected. . Table 3 shows information on water elevation at different times obtained by the MPS, WC-MPS and I-SPH (Ataie-Ashtiani and Shobeyri 2008) methods.

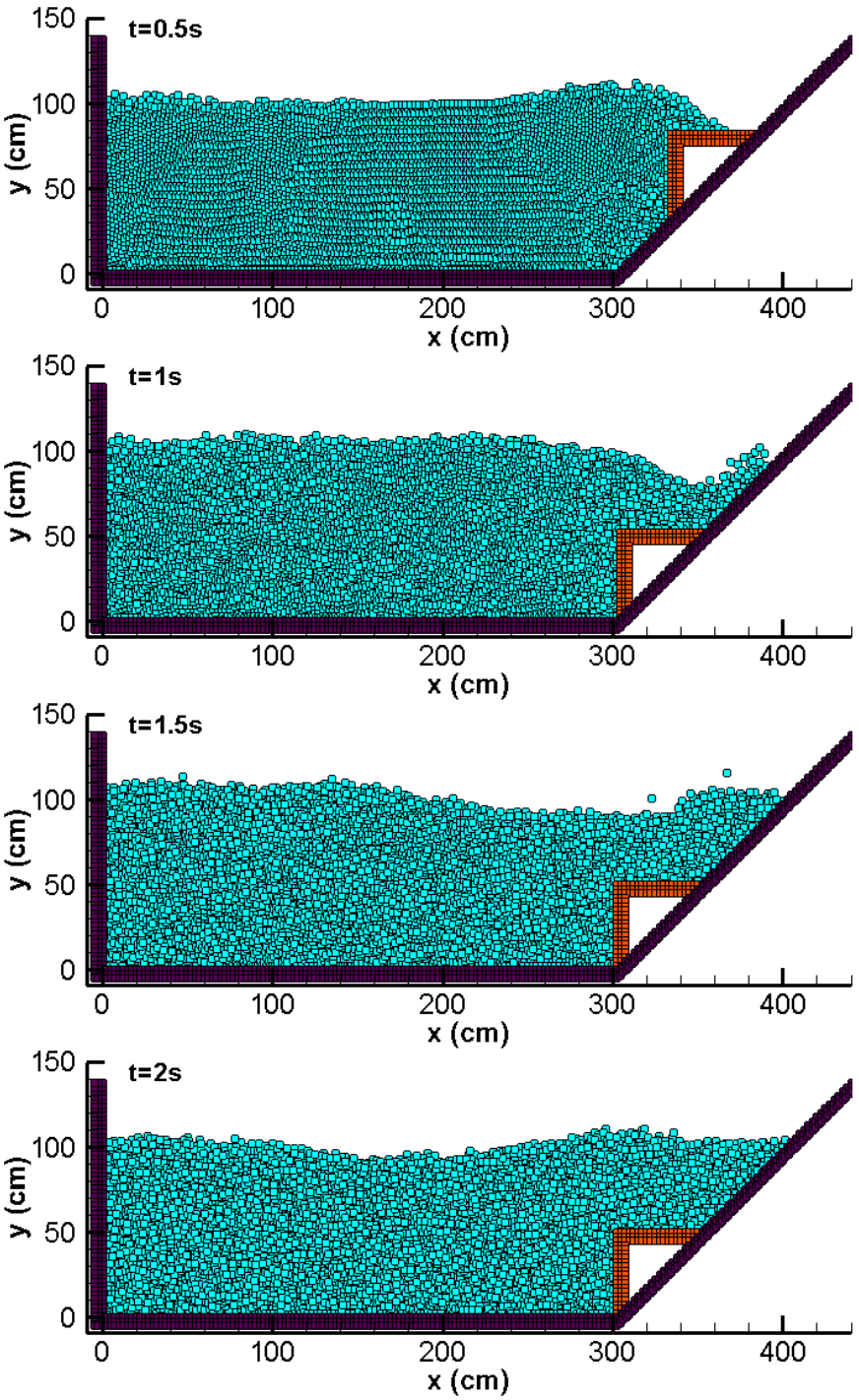

Figure 19- WC-MPS results for particle configuration at different times for the submarine landslide.

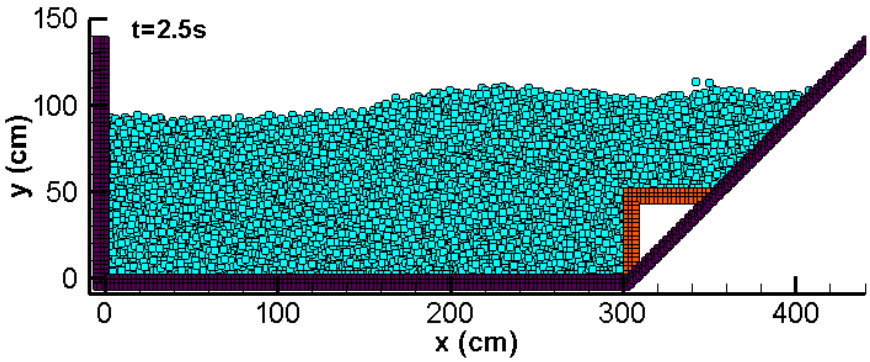

WC-MPS results for particle configuration at different times for the submarine landslide (continued).

Table 3- Information on water surface elevation at different times obtained by MPS, WC-MPS and I-SPH methods

Method	*Maximum water elevation at t=0.8s (cm)*	*Water elevation at t=1.5s adjacent to left vertical wall (cm)*
MPS	107.2	107.6
WC-MPS	109.7	106.9
I-SPH	107	106.6

Figure 20 shows the pressure field at different times calculated by the WC-MPS model. At t=0.1s, far from the landslide mass, it is expected to have nearly hydrostatic pressure distribution. This is achieved by the MPS model, but the WC-MPS model shows relatively higher pressure at this region. A pressure drop is visible in the results of WC-MPS model as the time proceeds from 0.1s to 0.8s, which is unphysical. The MPS method suffers from unphysical pressure fluctuation, which results in irregularity of the pressure field. This

irregularity is obvious at t=0.8s and t=0.9s. The pressure fluctuation may result in high pressure gradient at some regions of flow. This will cause some particles to obtain high unphysical velocity which reduced the accuracy of simulation as well as decreasing the time steps due to CFL stability condition. This unphysical pressure fluctuation and the associated pressure field irregularity are relatively lower in the WC-MPS results.

Figure 21 shows a comparison between the water surface profile calculated by MPS and WC-MPS models and the experimental data (Rzadkiewicz et al. 1997) at t=0.5s and t=1s. The overall agreement between the computational results and the experimental data is satisfactory and demonstrates the accuracy of the models. However, the MPS results are in closer agreement with experimental data than the WC-MPS results. The water surface elevation near the left vertical wall has an unphysical raise in the WC-MPS results due to the observed slight turbulence at this region.

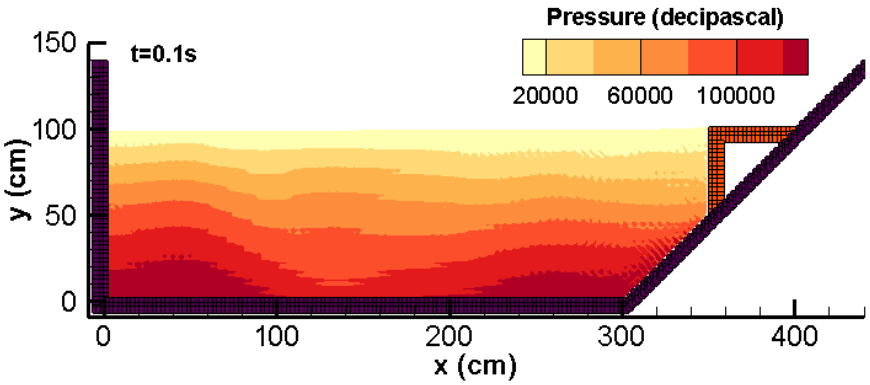

Figure 20- WC- MPS results for pressure field at different times for the submarine landslide.

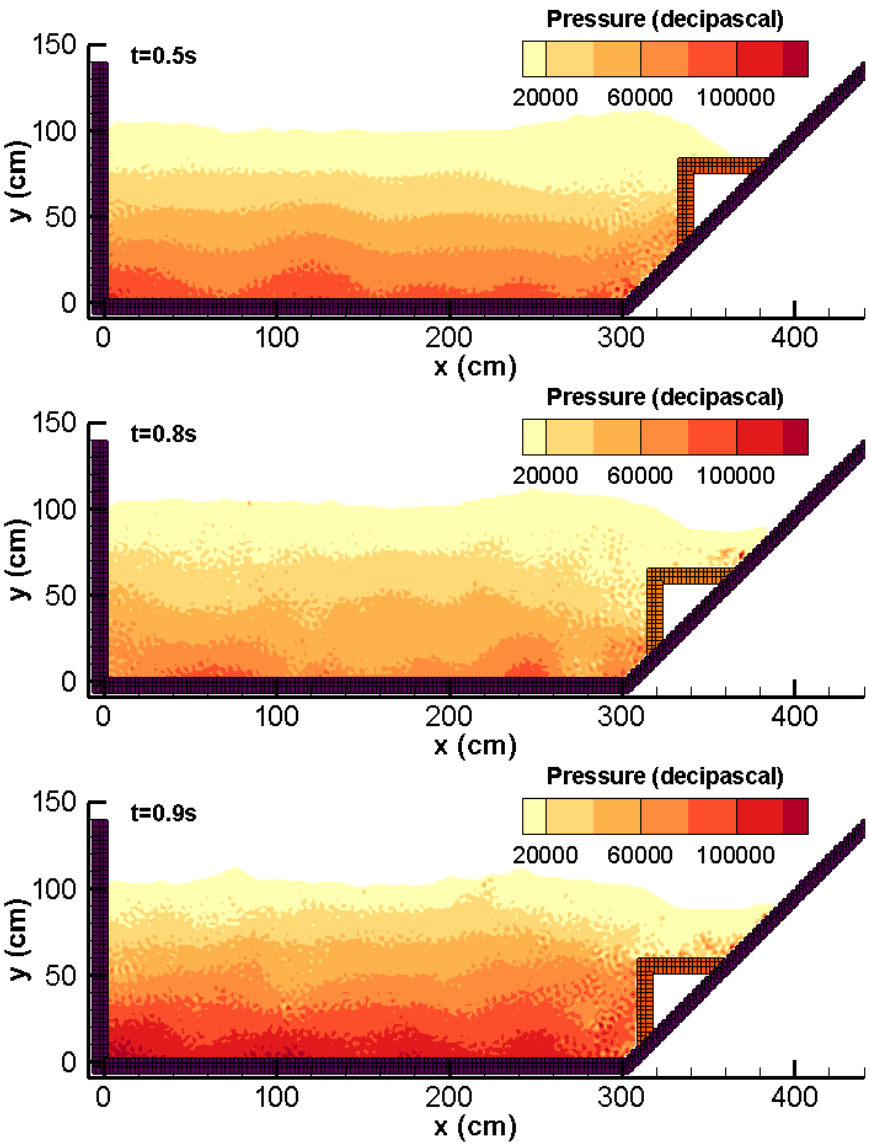

WC- MPS results for pressure field at different times for the submarine landslide (continued).

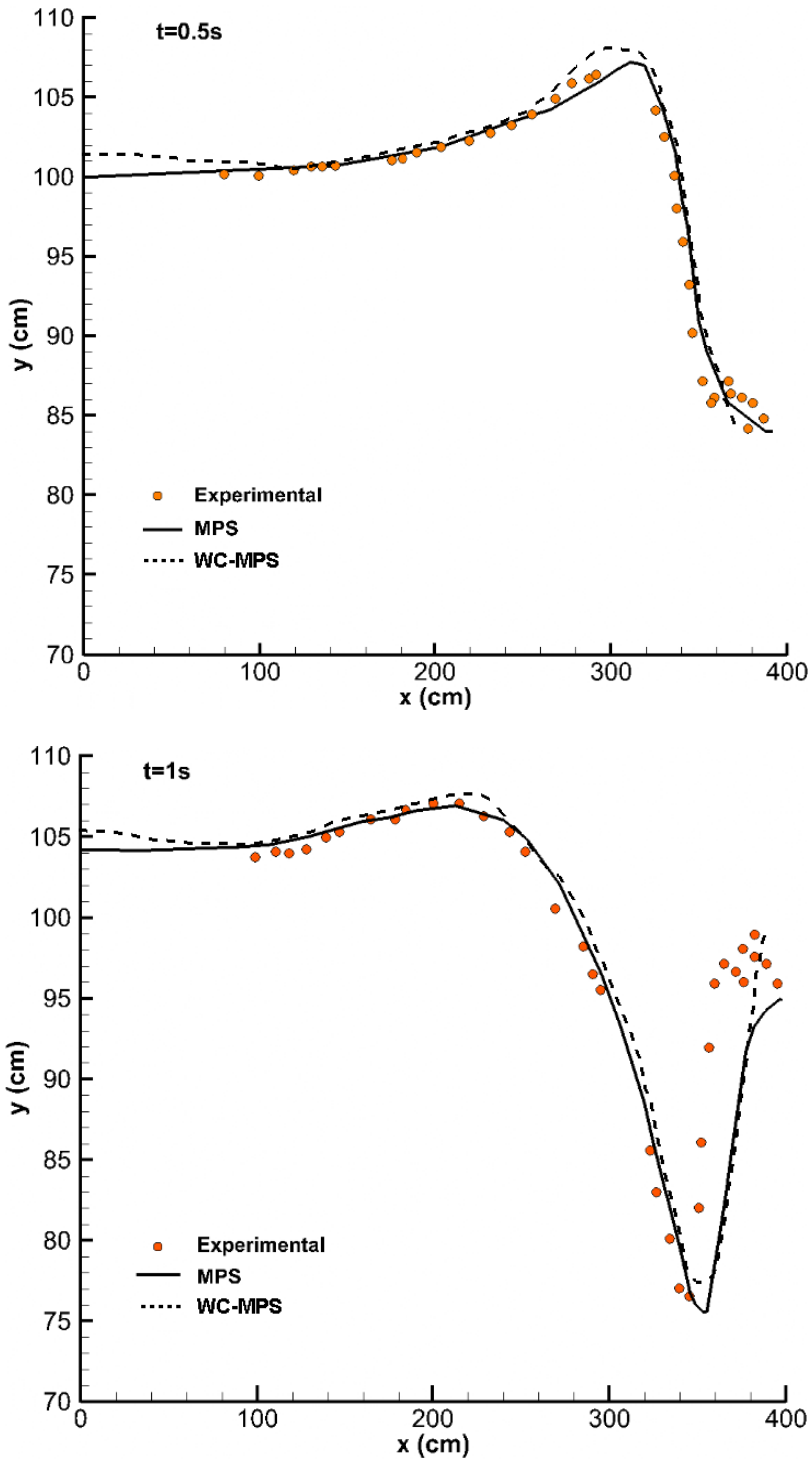

Figure 21- A comparison for the water surface profile between the MPS, WC-MPS, and experimental results.

The average CPU time per time step for the MPS and WC-MPS models are 117.15s and 3.03s, respectively. The computer is equipped with Intel® Core™ i7-2600 CPU 3.40 GHz and a system memory of 16.0 GB. In the present MPS model, a direct method of Gauss-elimination is used to solve the system of linear equations derived from Poisson equation of pressure, which is an expensive solver. Indeed, by implementing an iterative method such as conjugate gradient method in the code, the computational time will considerably decrease. There is no doubt that the most time consuming parts of the simulation is the solver of Poisson equation of pressure. As reported by Koshizuka et al. (1998), this part of simulation takes about 84% of the total CPU time, using the incomplete Cholesky decomposition conjugate gradient (ICCG) method to model the breaking waves on slopes represented by 2418 particles.

The advantage of the WC-MPS method is that it does not deal with the solution of Poisson equation of pressure and accordingly, the CPU time per each time step will considerably reduce. However, to satisfy CFL stability condition for explicit schemes, usually smaller time steps should be used in the simulation, depending on the choice of numerical value for sound speed in reference fluid and the Courant number. Usually, the MPS model needs smaller Courant number than WC-MPS model to remain stable. In general, in most cases, especially when the total number of particles is high, the WC-MPS has better CPU time performance (Shakibaeinia 2011).

3.3. Introduction to multiple-size particle technique

In the mesh-free particle methods, such as the MPS method, in order to have a high order of accuracy, the size of particles should be sufficiently small. However, fine

resolution is not necessary on the whole computational domain as we are mainly interested in particle configuration at specific regions of the computational domain, such as free surface. Using very small particle sizes for representing the entire domain makes the simulations computationally expensive and even impractical.

In this section, a number of fluid particles, initially located at a specific region of the computational domain are marked to further track their motion during the landslide. The dimensions of the marked region (white region in) are 292cm×60cm. The particle size is set to 4 cm, and the domain is represented with 2109 fluid particles. The number of marked particles is 1095, 52% of the fluid particles.

As shown in Figure 22, marked fluid particles (white particles) do not reach the free surface until t=3s. Therefore, by increasing the size of the fluid particles located at the initially marked region, we expect the free surface to be simulated with high resolution with no significant change in the shape of water surface profile.

In chapter 5, a new multiple-size particle algorithm is introduced, which allows the use of different particle sizes within a computational domain. This will considerably increase the efficiency of mesh-free particle methods in modeling free surface problems in large scales by significantly decreasing the computational time.

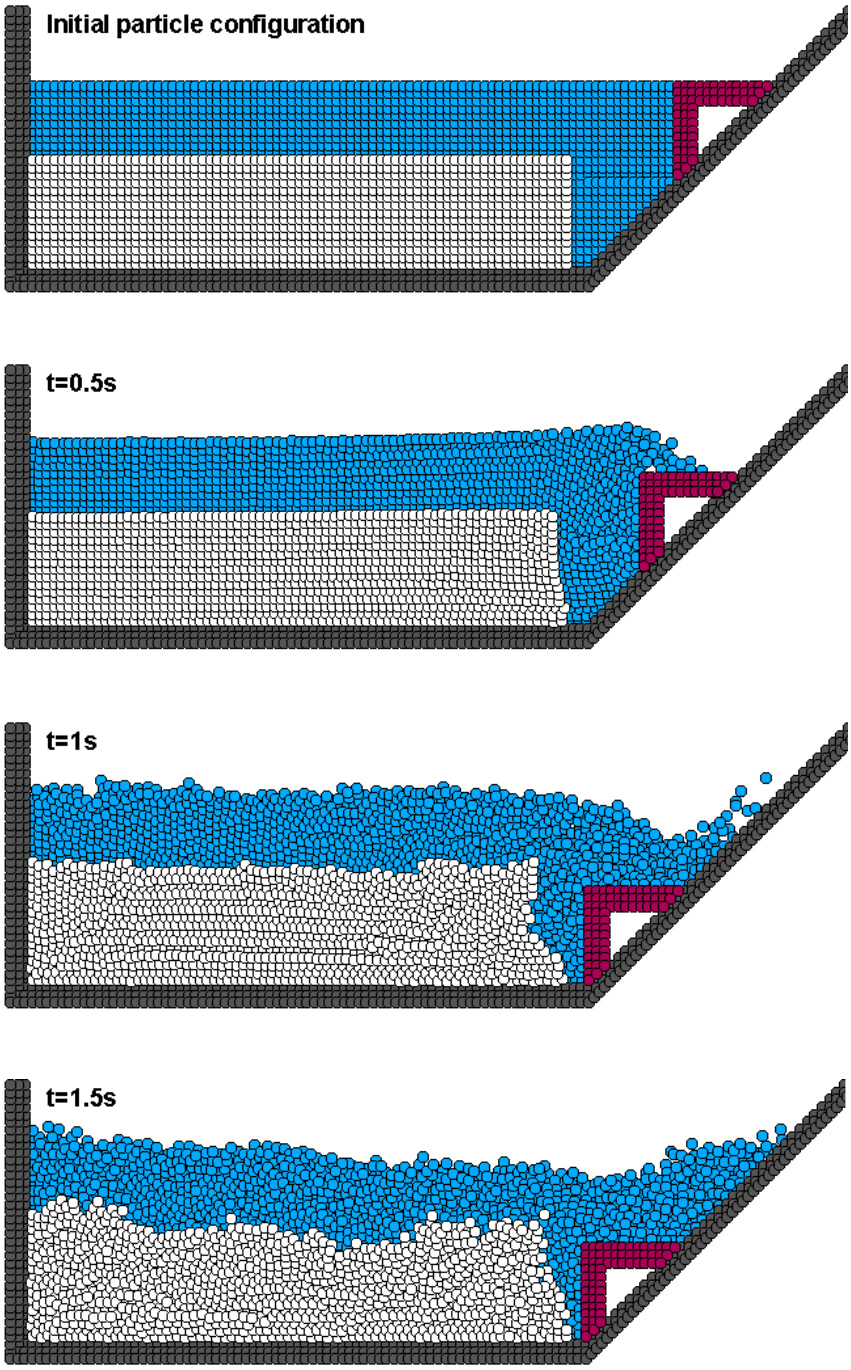

Figure 22- Tracking the motion of the marked particles (white particles) in the computational domain.

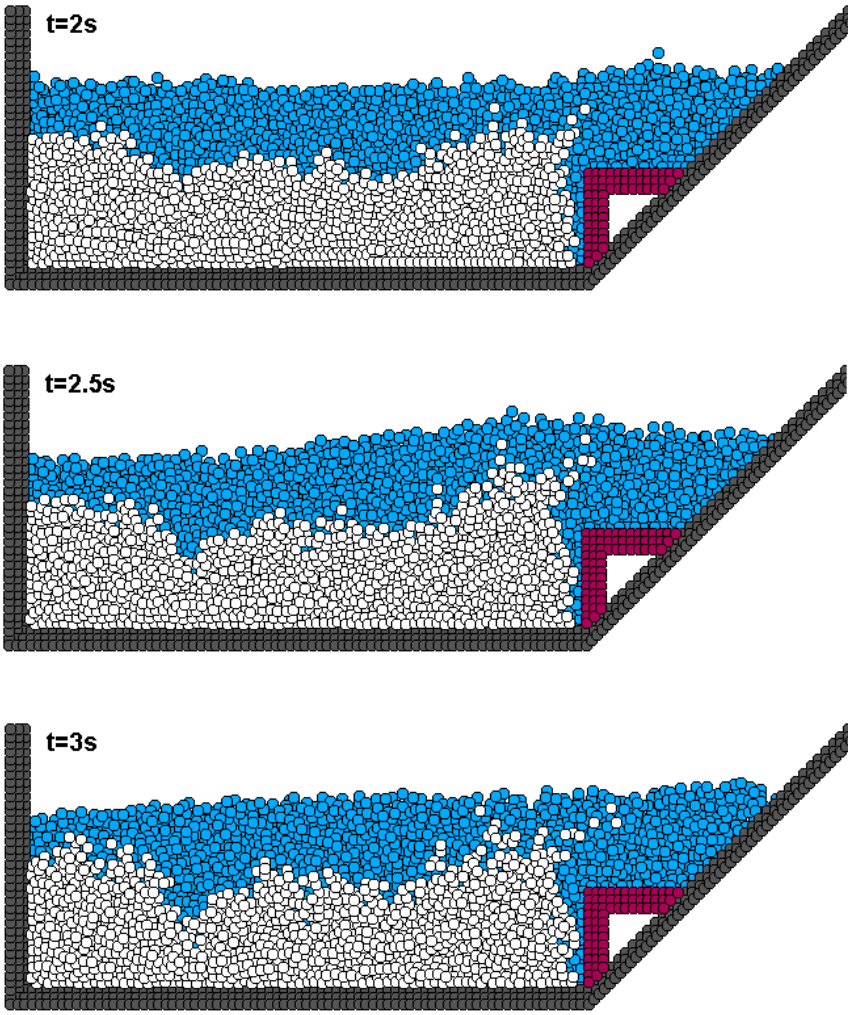

Tracking the motion of the marked particles (white particles) in the computational domain (continued).

3.4. Summary

Modeling of water waves generated by landslides is of significant importance in flood hazard assessment of coastal areas. Due to the complex motion of the submerged bodies and the wave interaction with the shore line which results in non-linearity of governing equations, numerical methods are often used to model the landslide–generated water

waves. Grid-based methods have difficulties dealing with such flows due to the high deformation of the free surface. Alternatively, mesh-free particle methods are often better suited to cope with the geometric changes of domain of interest. In this chapter, the MPS method, which is a mesh-free fully Lagrangian method, is used to model the water waves generated by vertical and submarine landslides. In both cases, a wave and a vortex are generated as a result of the landslide. The water surface profiles and velocity fields are presented at different times. Measurements of the wave characteristics are reported. By comparing the results with the available experimental data or analytical solutions, it is shown that the MPS method is capable of providing accurate prediction of the surface profile and amplitude of the landslide-generated water waves.

In this study the kernel function suggested by Ataie-Ashtiani and Farhadi (2006), to improve the stability of the MPS method, is applied to simulate vertical and submarine landslides. Analyses demonstrate the good stability of MPS method using this kernel function. Unlike the SPH (Monaghan and Kos 2000) and I-SPH (Ataie-Ashtiani and Shobeyri 2008) vertical landslide simulation results, which are presented only up to 0.7s, the MPS method could stably simulate the problem until 17s and up to when the water surface profile has become approximately horizontal.

Accurate prediction of water surface profile of vertical and submarine landslides using the MPS method demonstrates the utility of this method in simulating problems with irregular and complex free surfaces in hydraulic and coastal engineering, where accurate prediction of water surface profile and wave characteristics is of significant importance.

Chapter 4 : Multiphase MPS Method for Granular Flows

Free surface multiphase flows occur frequently in nature and in industry and are of significant practical and theoretical interests. Examples include sediment transport in rivers and estuaries, gravity currents, ocean-air coupling, and ship in stratified fluid flow. The unique challenges of free surface multiphase flow often make analytical solutions to the governing equations impossible and experimental investigations very difficult; therefore, numerical methods have gained a lot of interest in the area of scientific computation of free surface multiphase flows under very complicated conditions to disclose the detailed flow information.

Multiphase flows have been the subject of a few studies conducted using the mesh-free Lagrangian methods. For instance, the SPH method was used to model interfacial flows (Colagrossi and Landrini 2003), gravity currents (Shao 2011; Monaghan 1999), and oil spills (Violeau et al. 2007). Hu and Adams (2007; 2009) used the projection I-SPH approach to model multiphase flows under a wide range of density ratios. Shakibaeinia and Jin (2012) developed a WC-MPS multiphase model in which the multiphase system is treated as a multi-density multi-viscosity fluid.

In this chapter, an improved MPS method, named the multiphase MPS method, is proposed for incompressible flows. The multiphase system is treated as a multi-density multi viscosity fluid. A single set of governing equations is solved on the whole computational domain. A high-order accurate density smoothing scheme suggested by Khayyer and Gotoh (2013) is applied to the phase interfaces to avoid pressure

discontinuities. Similar to the approach of Shakibaeinia and Jin (2012), a viscosity arithmetic averaging formula is applied to smooth the shear stress discontinuities at the phase interfaces. An adaptive density algorithm is proposed and applied for modeling of rigid boundary particles. The cubic spline kernel function suggested by Ataie-Ashtiani and Farhadi (2006) is used to improve the stability of the simulations. The present algorithm can be applied to a wide range of multiphase flow simulations with relatively low density ratios.

The proposed multiphase MPS method is then is then implemented to simulate deformable submarine landslide and dam-break over an erodible bed. The granular media is assumed to behave as a non-Newtonian fluid and the Bingham plastic model is utilized to deal with the rheology of the system. Similar to the water phase, the granular phase is also represented with particles with the same size as of the particles representing the water phase. Results are presented and compared with the available experimental data and with other numerical results to evaluate the accuracy of the simulations.

4.1. Multiphase MPS Formulation

In the present formulation for modeling of multiphase flows, only one set of governing equations is considered and solved on the whole computational domain. However, this will produce significant pressure and shear stress discontinuities across the phase interfaces. To avoid the pressure discontinuity, a simple spatial averaging formula may be used to calculate the density of a fluid particle adjacent to the phase interface, as follows

$$\rho_i = \frac{1}{\sum w(|\mathbf{r}_i - \mathbf{r}_j|)} \sum \rho_j w(|\mathbf{r}_i - \mathbf{r}_j|) \tag{4.1}$$

The above formulation is applied to a variety of SPH-based simulations, (e.g. Hu and Adams 2007; Shao 2012), and to the WC-MPS simulation conducted by Shakibaeinia and Jin (2012). Note that unlike the calculation of the particle number density (equation (2.3)), the reference fluid particle should take part in the weighted averaging for a more accurate approximation of the density of that particle. If so, those kernel functions which are singular at the reference fluid particles $(r = 0)$ cannot be implemented in this formulation, such as the delta kernel function proposed by Koshizuka et al. (1996).

As reported by Khayyer and Gotoh (2013), equation (4.1) will result in numerical diffusion and accordingly, an unphysical density smoothing. Furthermore, application of this equation will lead to unphysical intrusions of the heavier phase into the lighter one (Colagrossi and Landrini 2003). Equation (4.1) corresponds to a zeroth-order accurate evaluation of the density without considering the spatial variations of density at a reference particle i. Using the Taylor series expansion, Khayyer and Gotoh (2013) provided a first-order accurate calculation of the density across the phase interfaces, expressed as:

$$\rho_i = \frac{1}{\sum w(\left|\mathbf{r}_i - \mathbf{r}_j\right|)} \sum \left(\rho_j - \frac{\partial \rho_i}{\partial x_{ij}} x_{ij} - \frac{\partial \rho_i}{\partial y_{ij}} y_{ij} \right) w(\left|\mathbf{r}_i - \mathbf{r}_j\right|) \tag{4.2}$$

This equation is implemented in the present multiphase MPS formulation.

Using the Laplacian model (equation (2.7)), the MPS approximation for the viscous term can be written as

$$\left\langle \upsilon \nabla^2 \phi \right\rangle_i = \frac{2d}{\lambda n^0} \sum_{i \neq j} [\upsilon_{ij} (\phi_j - \phi_i) \; w(|\mathbf{r}_j - \mathbf{r}_i|)] \tag{4.3}$$

υ_{ij} is the interaction kinematic viscosity. Far from the phase interfaces, it is equal to kinematic viscosity of each particle. To avoid the shear stress discontinuity across the phase interfaces of unlike fluids, similar to the approach of Shakibaeinia (2011), a simple arithmetic average of the particle viscosities is used across the phase interfaces. This approach will turn the MPS approximation of viscos term to the following expression

$$\left\langle \upsilon \nabla^2 \phi \right\rangle_i = \frac{d}{\lambda n^0} \sum_{i \neq j} [(\upsilon_i + \upsilon_j)(\phi_j - \phi_i)\ w(|\mathbf{r}_j - \mathbf{r}_i|)] \tag{4.4}$$

Using the DPD (Dissipative Particle Dynamics) method, Visser et al. (2006) showed that this approach will provide good approximations for the value of the interaction kinematic viscosity.

4.2. Granular Media Rheology

The granular media is treated as a non-Newtonian fluid. Particles (which are called *pseudo particles* in this paper) are representing the grains and they are having the same size as of the particles representing the water phase. Thus, depending on the average size of grains, each pseudo particle is representing a number of grains. Figure 23 shows a schematic of this assumption.

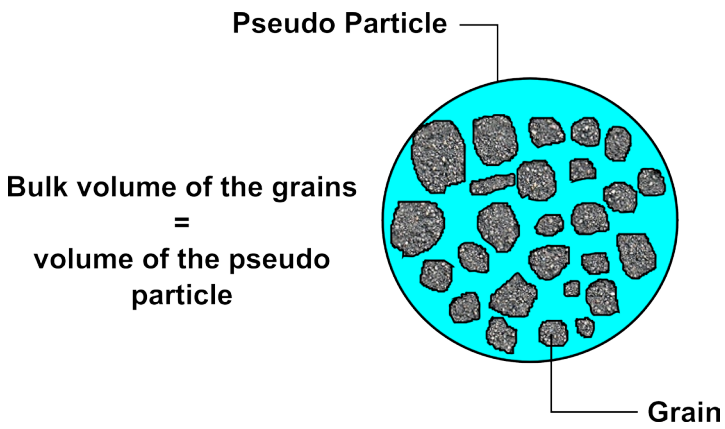

Figure 23- A schematic of the pseudo particles carrying a number of attached grains.

In Non-Newtonian fluids, viscosity is a function of the shear rate or shear rate history and unlike Newtonian fluid there is no linear relationship between shear stress and shear rate. Molten polymers, toothpaste, many salt solutions, and starch suspensions are some examples of the non-Newtonian fluids. For these types of fluids, a variety of rheological models relating the shear rate to viscosity exists. The simplest and most common rheology model is the Bingham plastic model (Bingham 1922). Some SPH studies have implemented the Bingham model for granular flow simulation (e.g. Huang et al. 2012; Pastor et al. 2009; Laigle et al. 2007; Shao and Lo 2003). The Bingham plastic model is expressed as:

$$\mu_{eff} = \begin{cases} \mu_B + \dfrac{\tau_B}{\dot{\gamma}} & \dot{\gamma} \geq \tau_B \\ \infty & \dot{\gamma} < \tau_B \end{cases} \tag{4.5}$$

μ_{eff}, μ_B, τ_B and $\dot{\gamma}$ are effective dynamic viscosity, Bingham plastic dynamic viscosity, Bingham yield stress and shear rate, respectively. The shear rate can be calculated as

$$\dot{\gamma} = \sqrt{2\left(\frac{\partial u}{\partial x}\right)^2 + 2\left(\frac{\partial v}{\partial y}\right)^2 + \left(\frac{\partial u}{\partial y} + \frac{\partial v}{\partial x}\right)^2} \tag{4.6}$$

u and v are the horizontal and vertical components of the velocity vector, respectively. Within this model, no deformation will take place until a specified shear stress (which is the yield stress) is applied to the system. The Bingham plastic model is implemented in this study for modeling non- Newtonian granular media.

4.3. Boundary Treatment

To allocate a density value to solid boundary particles, an adaptive algorithm is used. At each time step, density of the solid boundary particles is dynamically adjusted to the local weighted average of the density of neighboring fluid particles. Hence, each solid boundary particle may obtain different density values during the simulation time. To apply the no-slip boundary condition, a frozen high value of viscosity is assigned to the particles which are modeling no-slip walls.

4.4. Deformable Submarine Landslide

Deformable underwater landslide has been the object of a few studies. Didenkulova et al. (2010) studied the tsunami wave generation by deformable submarine landslides of a variable volume in a basin of variable depth using the shallow-water theory. Jiang and LeBlond (1992) developed a numerical model based on finite-difference method to study the coupling of an underwater landslide and the resulting surface waves. Rzadkiewicz et al. (1997) assumed a two-phase flow of sediment motion and simulated the underwater landslides using the VOF method. Ataie-Ashtiani and Shobeyri (2008) developed an I-SPH model to simulate water waves generated by rigid and deformable landslide masses.

Capone et al. (2010) conducted the same study for the deformable underwater landslide using the SPH method.

The experiment on the hydraulic effects of the submarine landslide carried out by Rzadkiewicz et al. (1997) is simulated herein using the multiphase MPS method. A rectangular cross sectional channel, 4m long, 0.3m wide and 2m high is used in the experiment. The channel consists of a left vertical and a right 45° inclined enclosing walls. A small tank is also connected to the right side of the main tank to model the shore line. The channel is filled with clean-water up to 1.6m.

A mass of sand, having a triangular vertical cross-section is held at rest by a vertical guillotine water gate on the inclined wall and 10cm below the water surface. The vertical cross-sectional dimensions of the mass are 0.65m×0.65m. The width of the sand and the channel are the same. Therefore, the experiment can be considered 2D in a vertical plane. Figure 24 shows the experimental setup. The model consists of generating water waves by sudden removal of the gate and allowing the mass to slide along the inclined wall of the channel. The mass consists of coarse gravel, having a mean apparent density of 1950 kg/m^3.

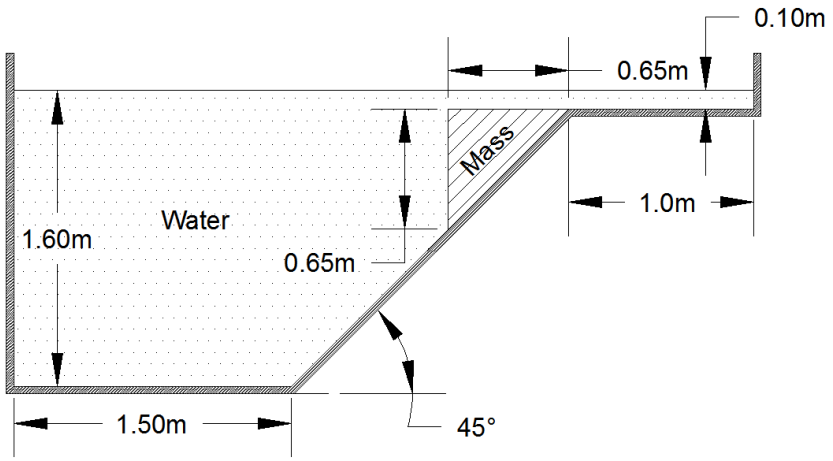

Figure 24- Experimental setup for the deformable underwater landslide experiment performed by Rzadkiewics et al. (1997).

In the present multiphase MPS model, initial particle spacing is 2.5cm, resulting a total number of 6789 particles (including water, sediment, wall, and ghost particles). The cubic spline kernel function which is suggested by Ataie-Ashtiani and Farhadi (2006) is used and the kernel size is set to twice the initial particle distance. The initial size of the time steps is set to 0.001s, controlled by the CFL stability condition (Courant et al. 1967). To satisfy the CFL stability condition, a Courant number of 0.4 is selected. The free surface parameter is set to 0.99. In addition to one layer of solid boundary particles, two layers of ghost particles are considered. The simulation is conducted for 1 second. It is assumed here that the gate is removed instantly.

The clean-water is a Newtonian fluid and its dynamic viscosity is 1.002×10^{-3} Pa.s (at 20℃). First, the landslide mass is considered as an ideal fluid, meaning that the viscosity term in the governing equations is neglected for both water and sand phases. Figure 25 shows the corresponding particle configuration.

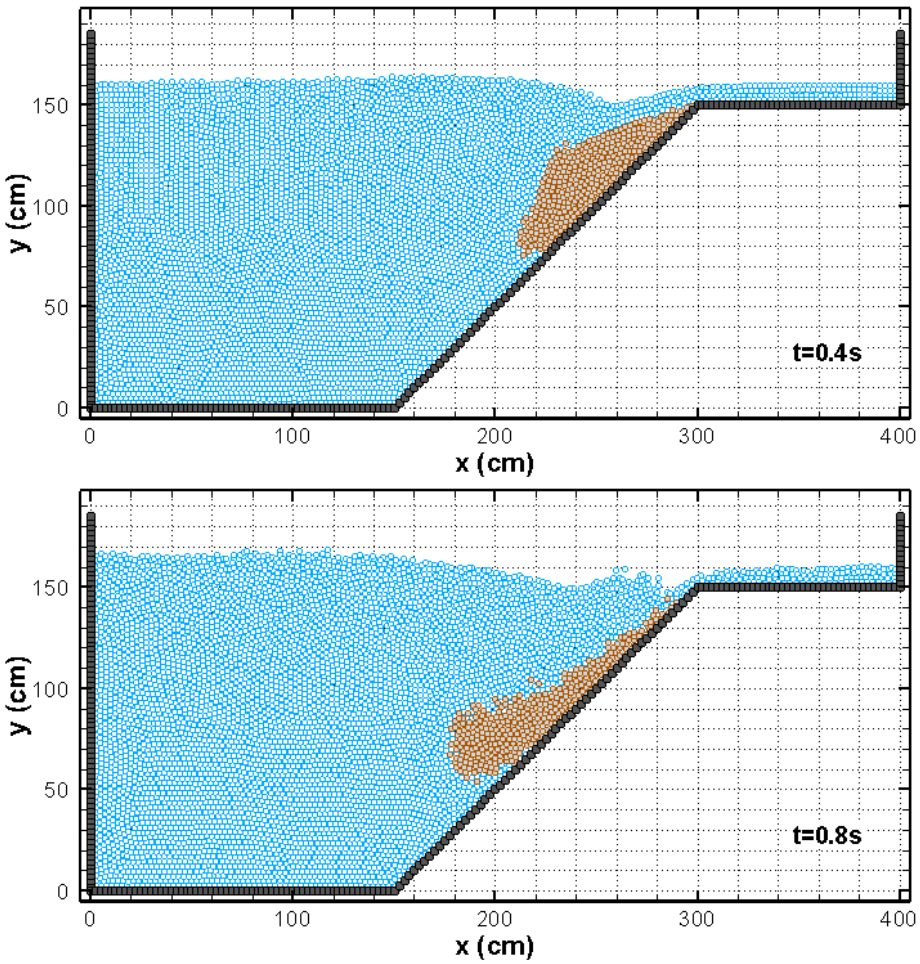

Figure 25- Particle configuration for the deformable submarine landslide at t=0.4s and 0.8s. The landslide mass is considered as an ideal fluid. x to y ratio is 1.

A comparison for the water surface profile at 0.4s and 0.8s is provided between the multiphase MPS results and experimental data in Figure 26. This comparison clearly shows that it is not accurate to assume the landslide mass as an ideal fluid, since the water surface profile predicted by the multiphase MPS method under this assumption does not match appropriately with the experimental data.

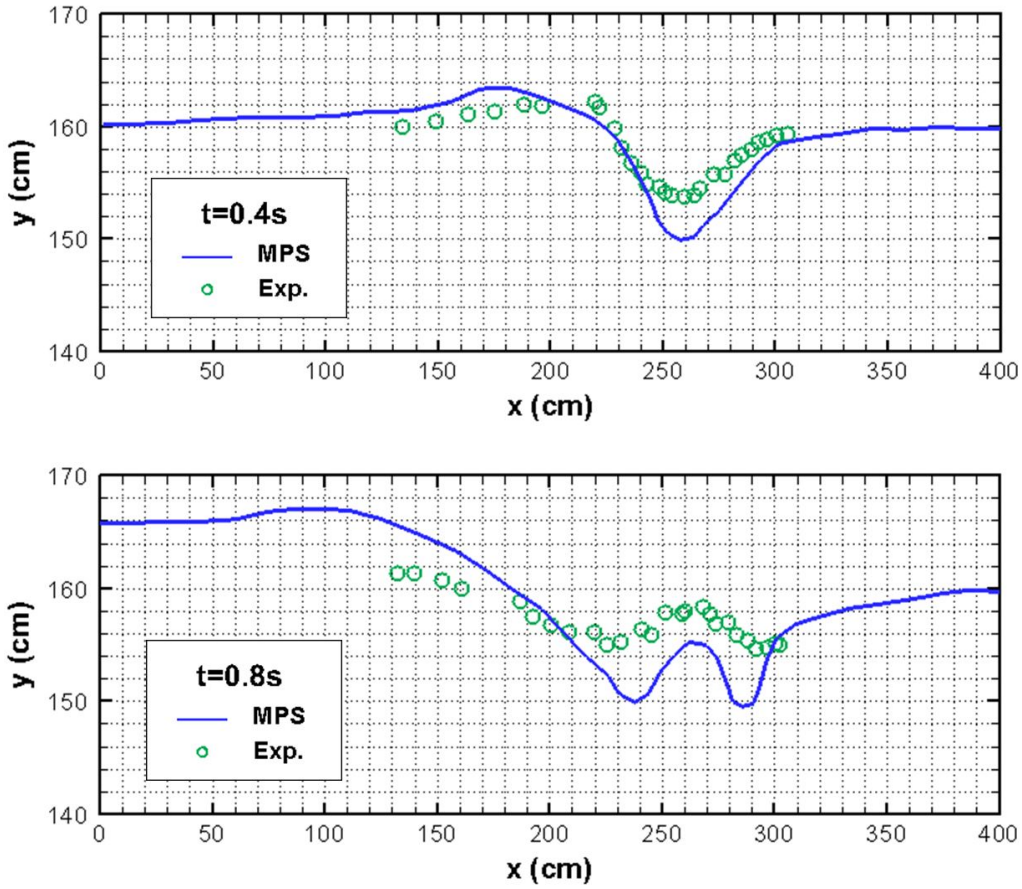

Figure 26- A comparison for the water surface profile at t=0.4s (top) and t=0.8s (bottom) between the MPS and experimental results. The mass is considered as an ideal fluid. x to y ratio is 0.2.

Next, the landslide mass is assumed as a Non-Newtonian fluid. No measurement is performed on the rheological parameters in the experiment. Nevertheless, these parameters are obtained by trials and errors studies conducted by Rzadkiewicz et al. (1997). Following these studies, Bingham plastic dynamic viscosity and the sand yield stress are set to 0Pa.s and 1000Pa, respectively. Results for the particle configuration are presented in Figure 27.

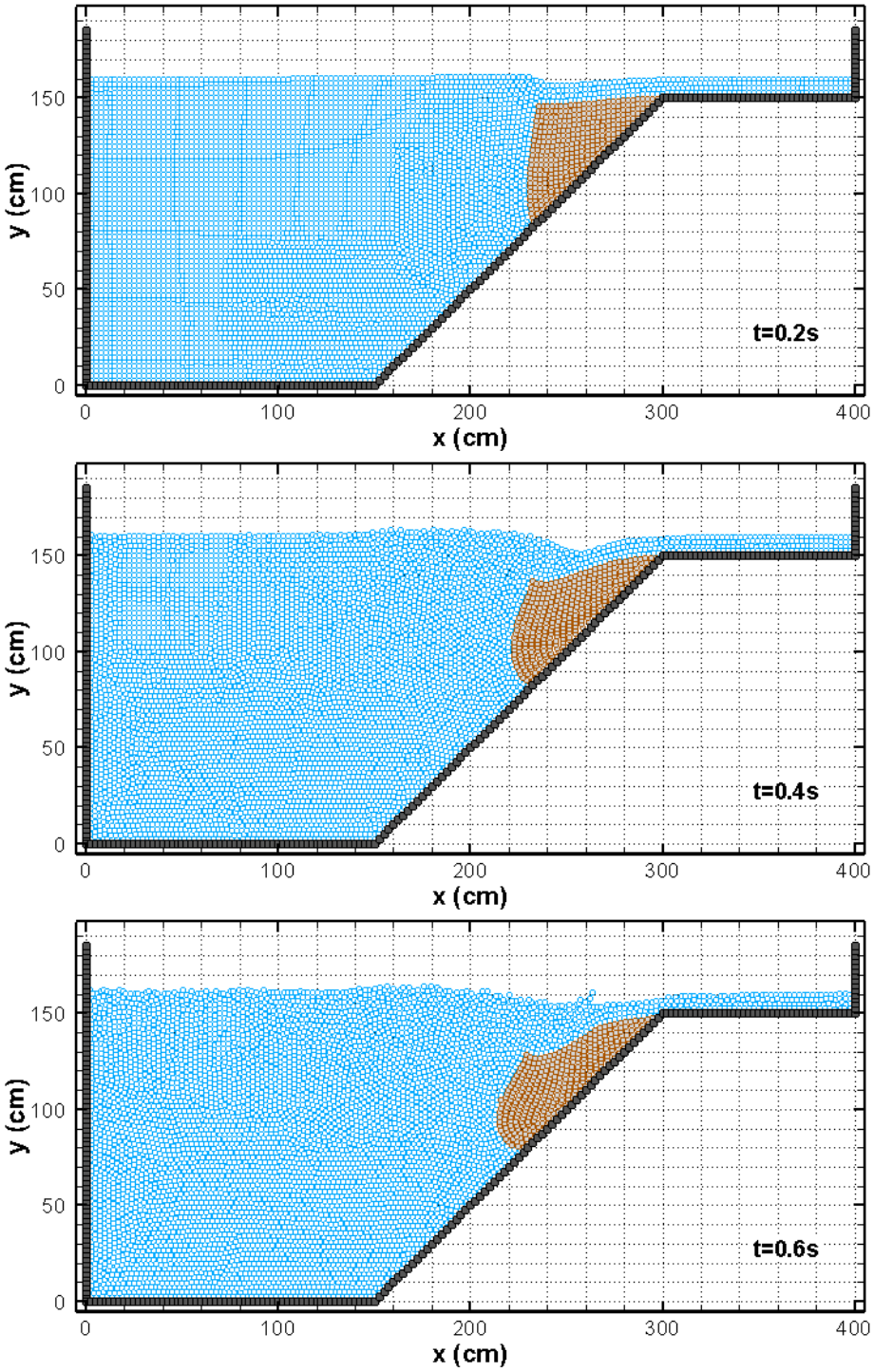

Figure 27- Particle configuration for the deformable submarine landslide problem at different times.

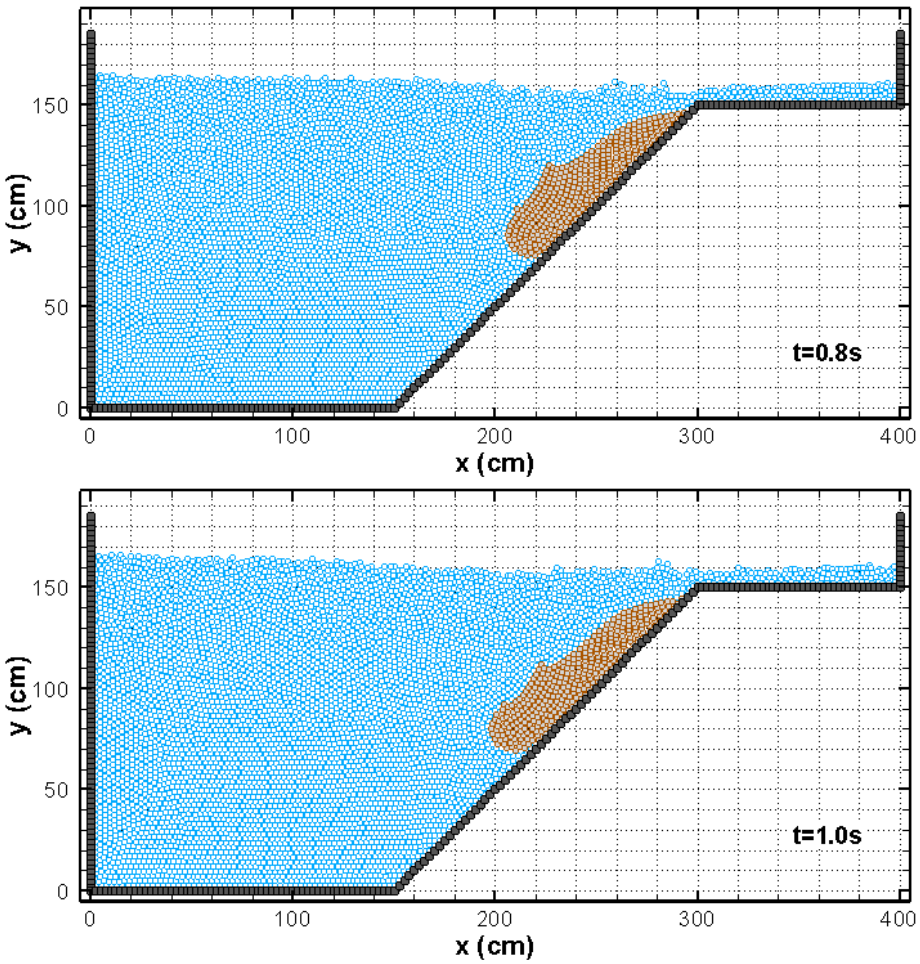

Particle configuration for the deformable submarine landslide problem at different times (continued).

Figure 28 shows the velocity field at 0.4s and 0.8s. As the landslide mass slides along the inclined wall, it generates a reverse plunging wave which creates a vortex. To show the accuracy of the model, a comparison for the water surface profile between the multiphase MPS results, the SPH results (Capone et al. 2010) and the experimental data (Rzadkiewicz et al. 1997) is provided in Figure 29. The good agreement between the multiphase MPS results and experimental data shows the applicability and accuracy of the present method to predict the water surface profile.

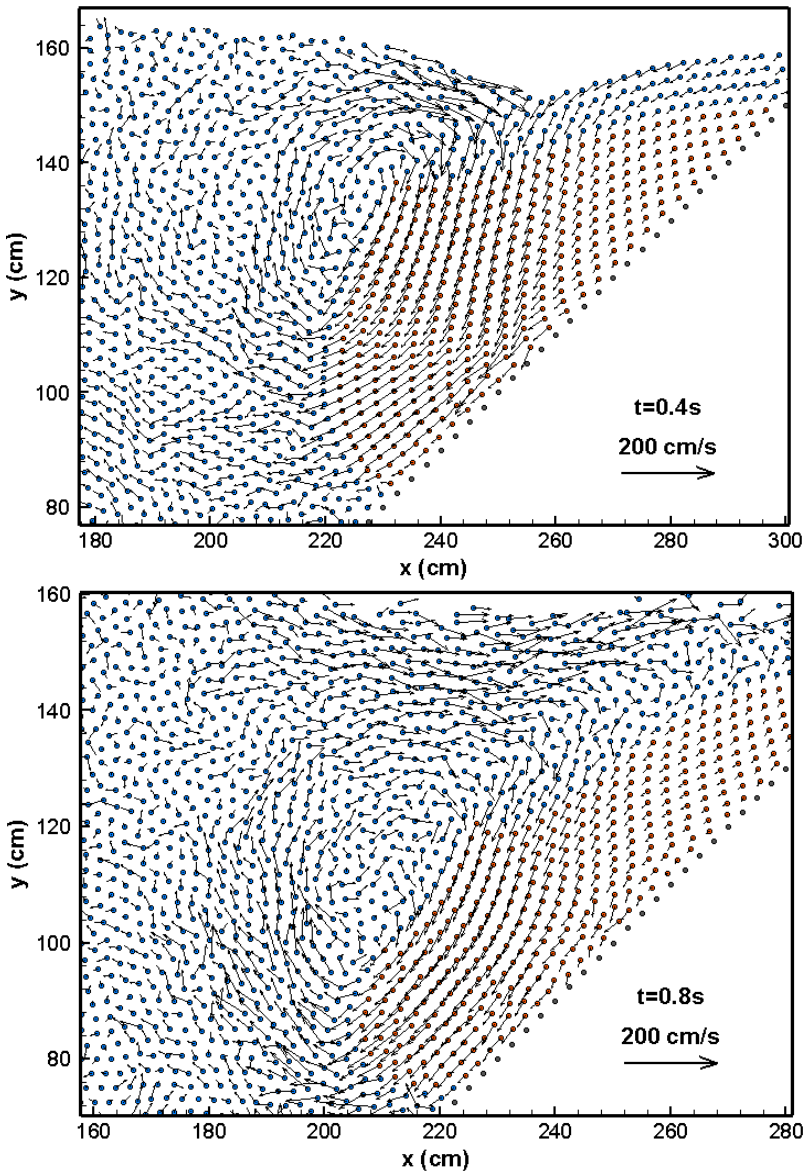

Figure 28- Velocity field for the deformable submarine landslide problem at t=0.4s and 0.8s. The landslide mass is considered as a non-Newtonian fluid. x to y ratio is 1.

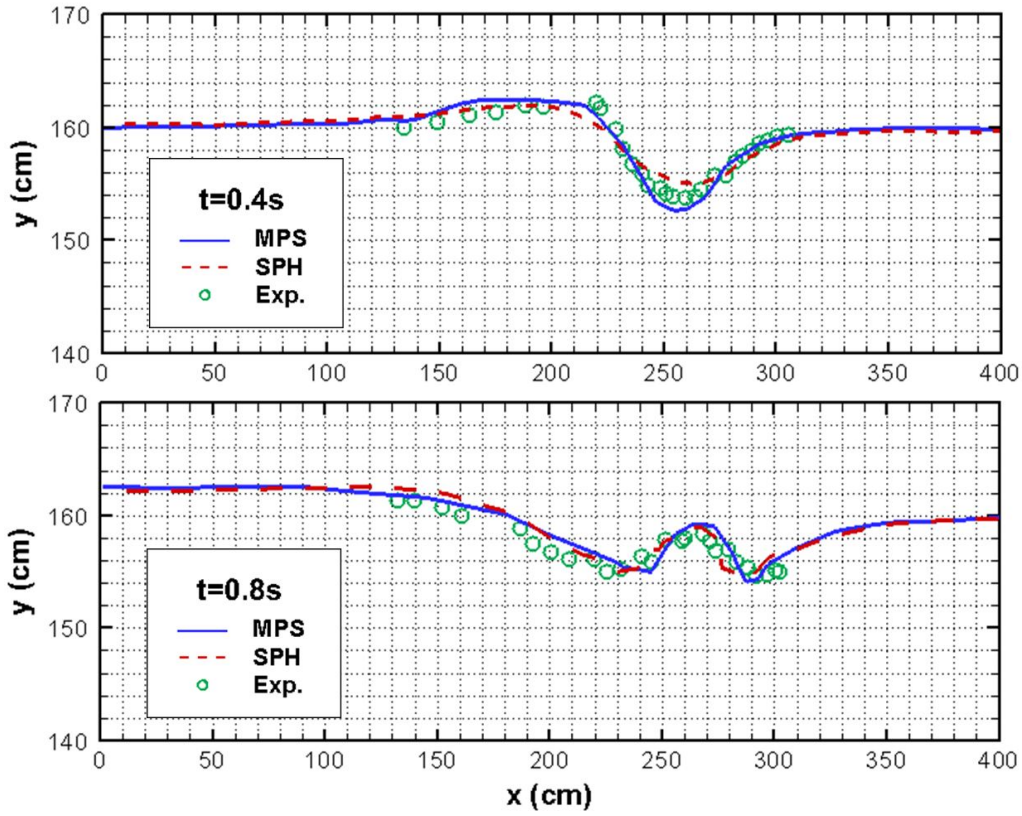

Figure 29- A comparison for the water surface profile at t=0.4s (top) and t=0.8s (bottom) between the MPS, SPH and experimental results. The mass is considered as a Non-Newtonian fluid. x to y ratio is 0.2.

Figure 30 shows a comparison for the landslide mass profile predicted by the MPS, SPH (Capone et al. 2010) and VOF (Rzadkiewicz et. al. 1997) methods. The agreement between the results is close and the small discrepancies are likely due to the difference in the boundary conditions and calculation parameters. There is no quantitative experimental result available for the landslide mass profile.

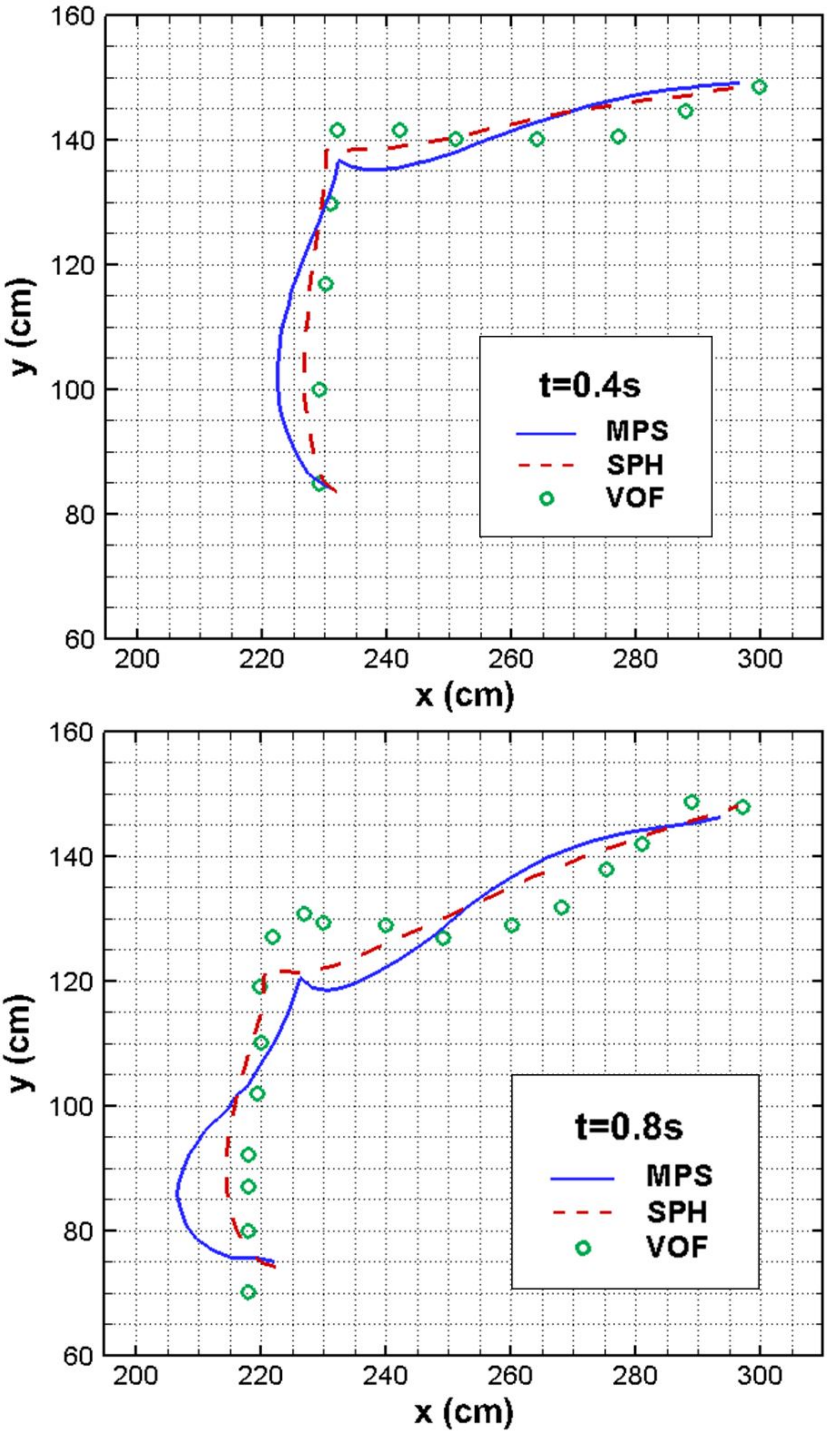

Figure 30- A comparison for the landslide mass profile at t=0.4s (top) and t=0.8s (bottom) between the MPS, SPH and VOF results. x to y ratio is 1.

4.5. Dam-Break over an Erodible Bed

The majority of the existing numerical models for the dam-break problem are applicable only for fixed beds. However, dam-break waves usually propagate along floodplains and rivers, in which the interaction between the dam-break flow and the bed sediments should be taken into account. The dam-break flow over the sediments is highly erosive, which results in a complicated interaction between the flood and the bed sediments. Therefore, implementing an efficient numerical method can improve our understanding of such flows.

Spinewine (2005) conducted several experiments on the dam-break flow over sediments, exploring different bed configurations and sediment densities. Shakibaeinia and Jin (2011) performed numerical studies on the Spinewine's experiments using the WC-MPS method. Cao et al. (2004) built a theoretical model for predicting dam-break flows over mobile beds upon the conservative laws of shallow water hydrodynamics. Xia et al. (2010) developed a 2D morphodynamic model by modifying shallow water equations to consider the effect of sediment concentrations and bed evolution on the flood wave propagation, and by using an unstructured finite volume algorithm.

An idealized dam-break laboratory experiment over loose granular beds conducted by Spinewine (2005) is simulated herein using the multiphase MPS method. A rectangular cross sectional flume, 6m long, 1.6m high and 0.10m wide, is used in the experiment. Fully saturated sediment of 10cm thickness is evenly distributed on the bottom of the flume. A narrow vertical gate separates the flume to two upstream and downstream sections with the

same length. The upstream section is filled by clear-water with density of 1000kg/m^3. The depth of water above the flume bed sediment is 35cm. The dam-break wave formation is initiated by sudden removal of the separating gate. The geometrical domain for the experiment is sketched in Figure 31.

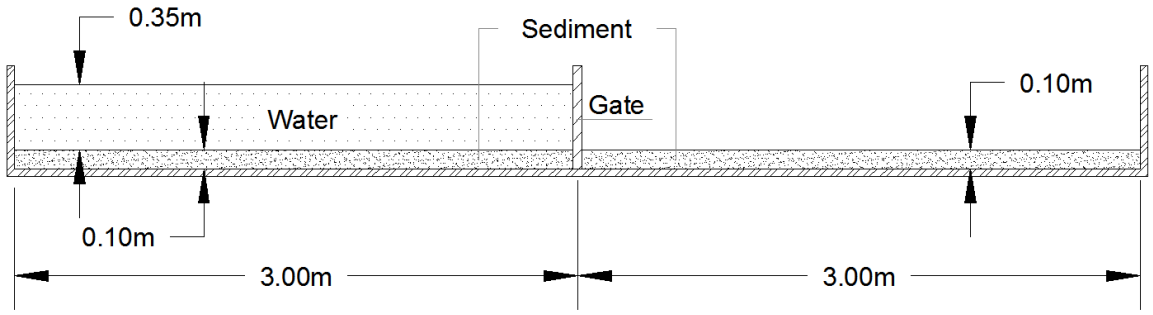

Figure 31- Experimental setup for the mobile bed dam-break experiment performed by Spinewine and Zech (2005).

Two distinct sediment materials were used in each set of experiment; coarse crushed sand and extruded PVC pellets. The coarse crushed sand sediment has the following properties: equivalent particle diameter of 1.82mm, a specific granular density of 2683kg/m^3, a bulk density of 1892kg/m^3, a friction angle of 30° and negligible cohesion. The extruded PVC pellets sediment has the following properties: equivalent particle diameter of 3.92mm, a specific density of 1580kg/m^3, a bulk density of 1336kg/m^3, a friction angle of 38° and no cohesion.

In the present multiphase MPS model, the simulation is performed with 7218 particles, which corresponds to an initial particle spacing of 1.67cm. The cubic spline kernel function suggested by Ataie-Ashtiani and Farhadi (2006) is used and the kernel size is set to twice the initial particle spacing. The initial size of the time steps is set to 0.001s, and a Courant

number of 0.4 is selected. The free surface parameter is set to 0.99. Two layers of ghost particles are considered in addition to the layer of solid boundary particles. The simulation is performed for 2 seconds. The removal speed of the separating gate is unknown in the experiment. Hence, it is assumed that the gate is removed instantly.

The clean-water is a Newtonian fluid and its dynamic viscosity is 1.002×10^{-3} Pa.s (at 20°C). The sediments are considered as a non-Newtonian fluid. The Bingham plastic model is used to calculate the viscosity of the sediment particles at each time step. No measurement of rheological parameters is performed in the experiment. Hence, the necessary rheological parameter, i.e. plastic dynamic viscosity, is calibrated based on the range offered by Chen and Ling (1996) and is set to 0.03 Pa.s for sand and to 0.02 Pa.s for PVC. The Mohr-Coulomb failure criterion is used for the calculation of the Bingham yield stress at each time step.

Having PVC as the bed sediment, the particle configurations at different times are presented in Figure 32. As soon as the gate is removed, a wave is formed and starts to propagate toward downstream while washing the sediments. It is observed that the maximum sediment displacement occurs almost under the wave front. At late stages, as the water wave energy decreases, the shear stress on the sediments will also decrease, making them to deposit gradually. The pressure field and the velocity field at different times are plotted in Figure 33 and Figure 34, respectively.

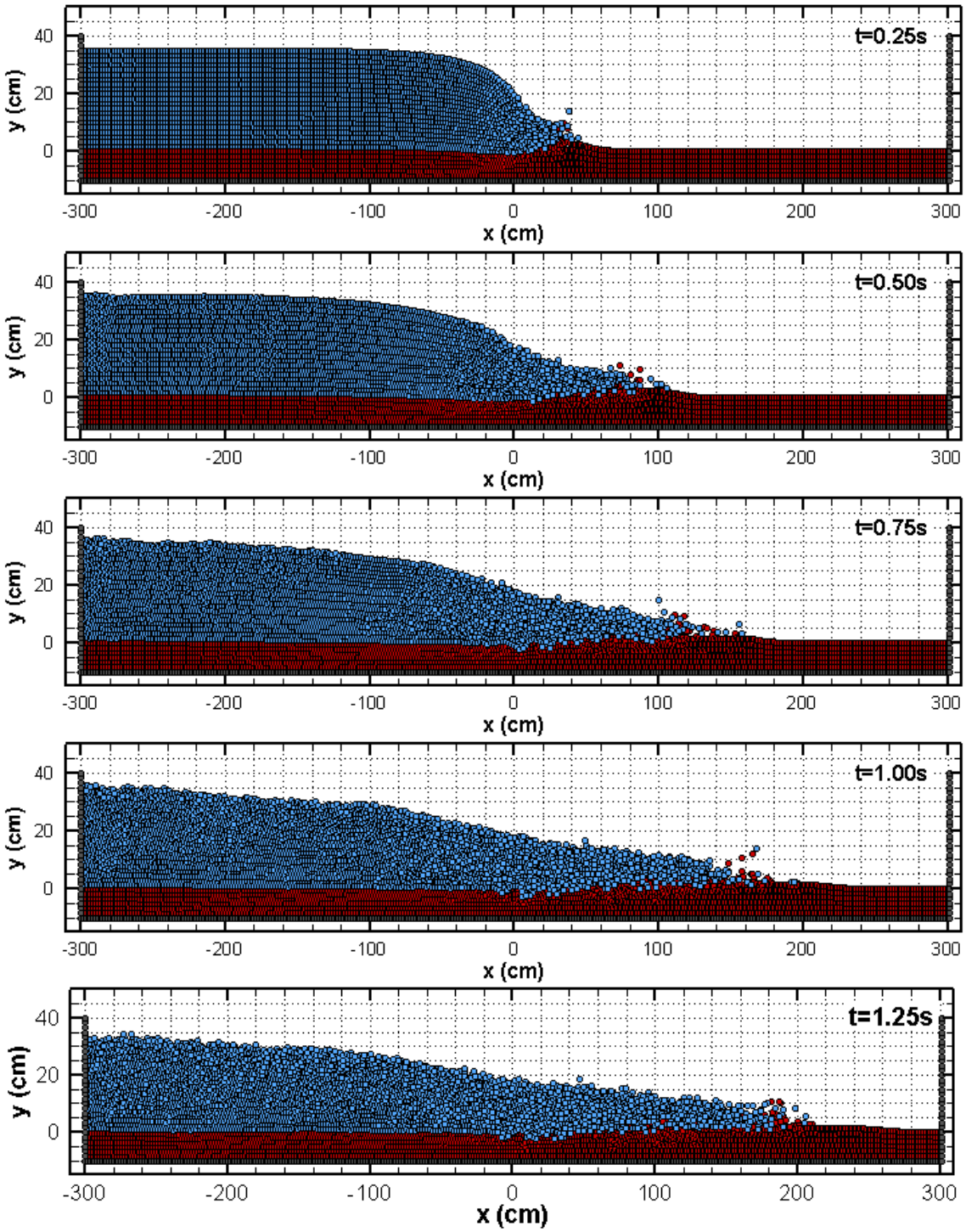

Figure 32- Particle configuration for the mobile-bed dam break problem at different times. The sediment material is PVC. x to y ratio is 0.5.

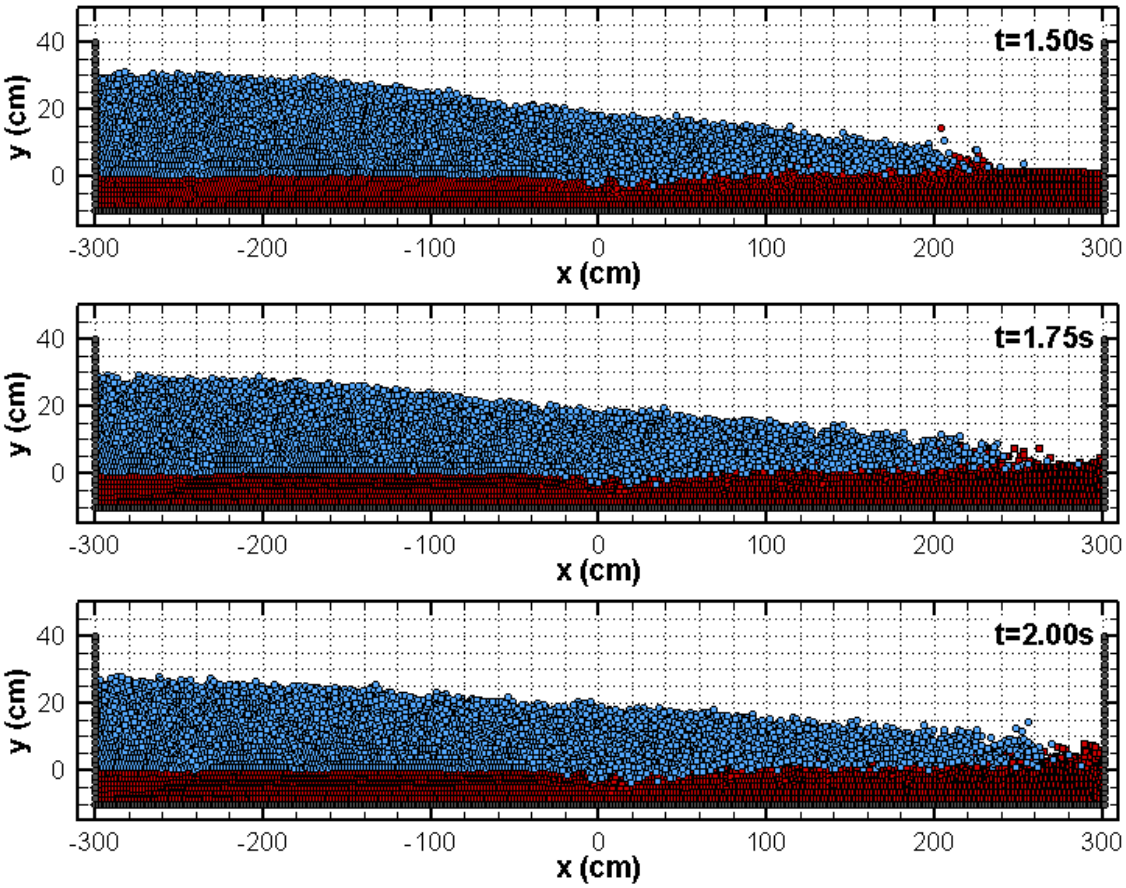

Particle configuration for the mobile-bed dam break problem at different times. The sediment material is PVC. x to y ratio is 0.5 (Continued).

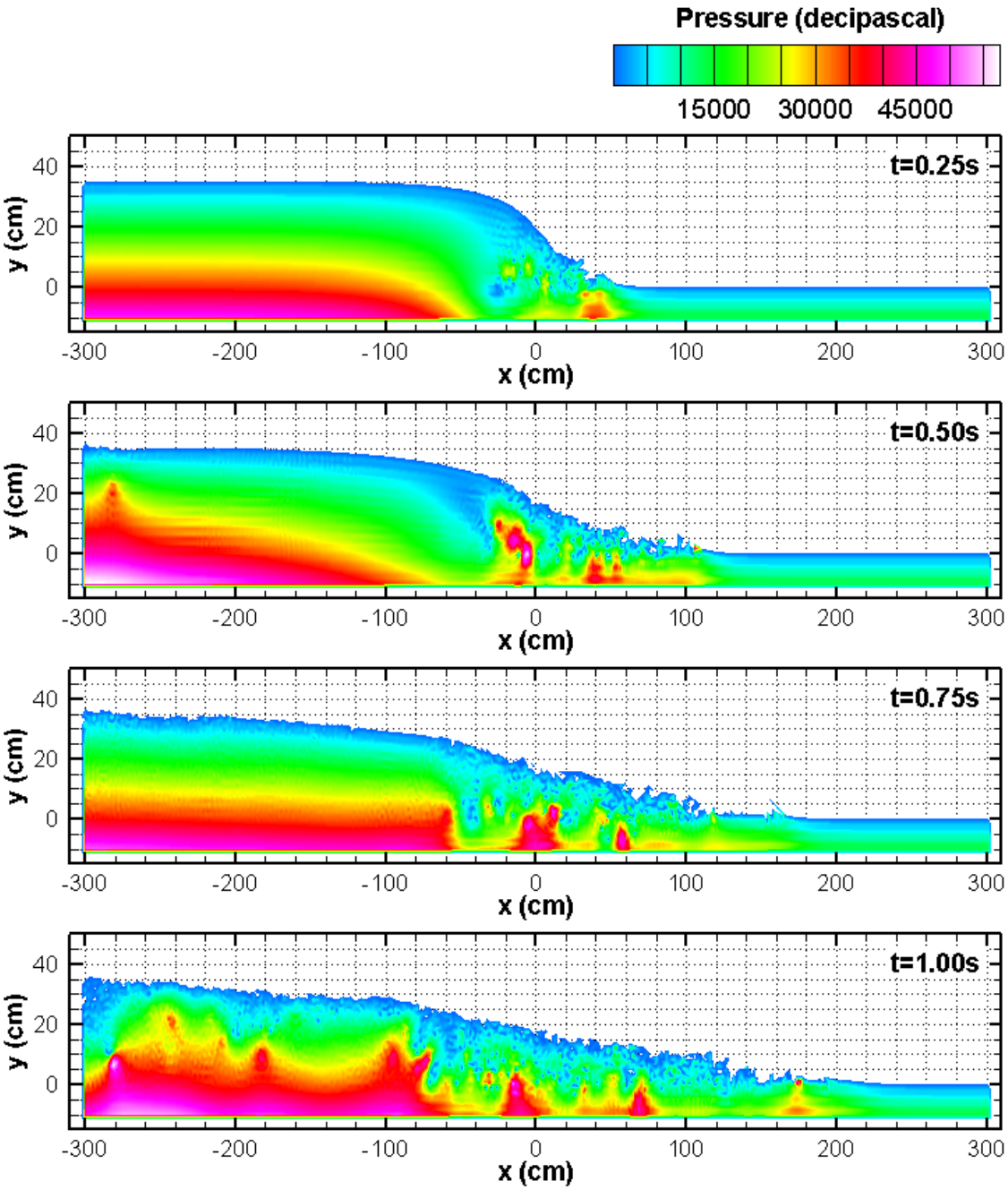

Figure 33- Pressure field for the mobile-bed dam break problem at different times. The sediment material is PVC. x to y ratio is 0.5.

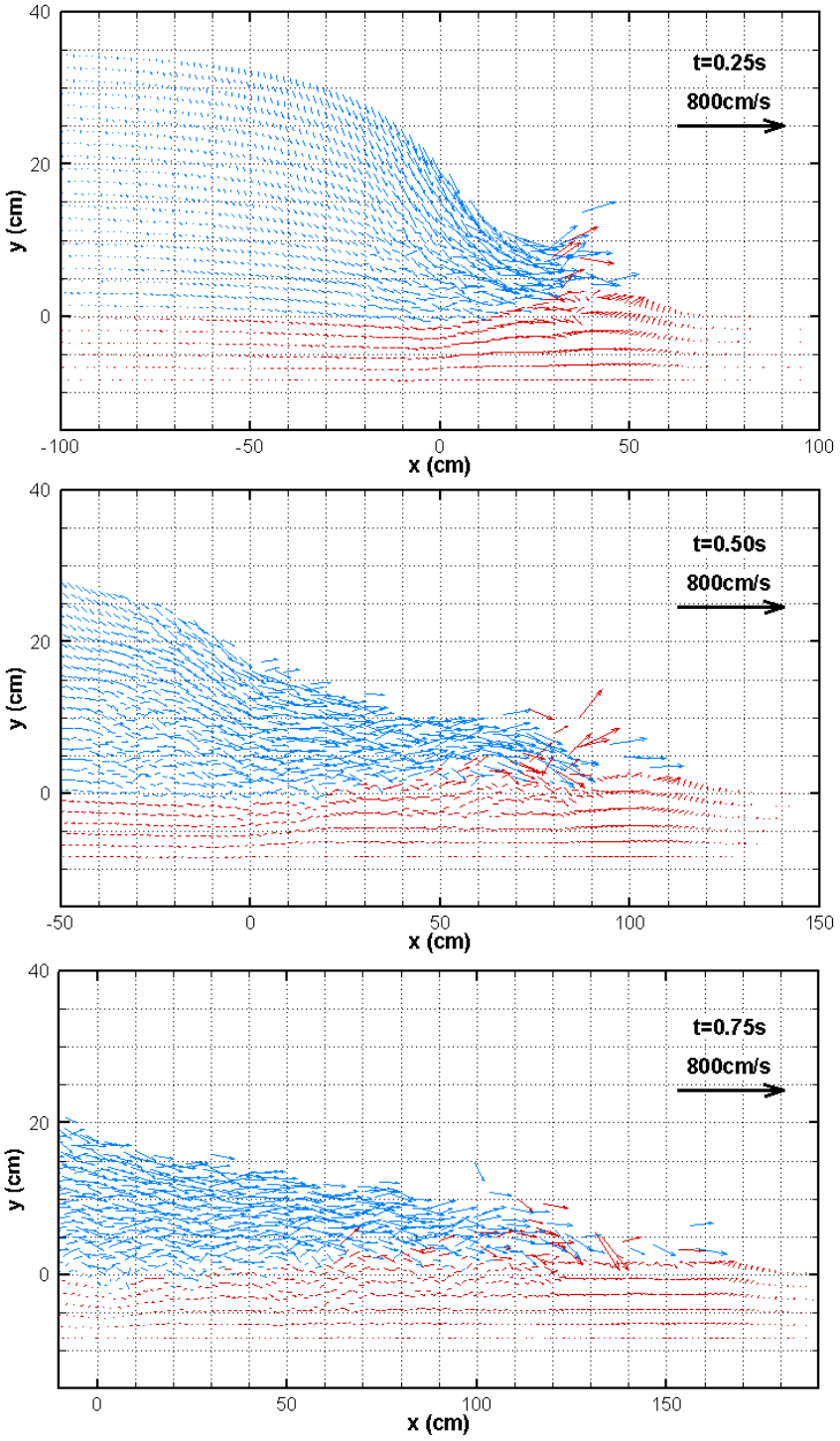

Figure 34- Velocity field for the mobile-bed dam break problem at different times. The sediment material is PVC. x to y ratio is 0.5.

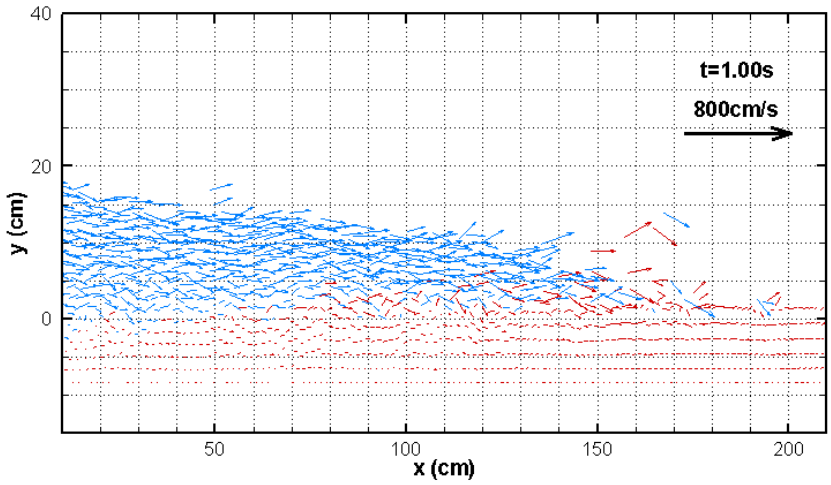

Velocity field for the mobile-bed dam break problem at different times. The sediment material is PVC. x to y ratio is 0.5 (continued).

Figure 35 shows a comparison between the present multiphase MPS results, experimental data (Spinewine 2005), and WC-MPS results (Shakibaeinia and Jin 2011) for the wave and sediment profiles. It is evident that the multiphase MPS results are predicting the water wave profile to a satisfactory extent. The position of the wave front at different times is almost the same in multiphase MPS and experimental results. The curvature of the water wave profile is predicted accurately by the multiphase MPS model. The multiphase MPS results do not perfectly match the experimental data for the sediment profile. Several factors are likely to contribute to these observed discrepancies such as (a) The assumption of treating the sediments as non-Newtonian fluid may not be valid or may have some deficiencies in predicting the accurate displacement of the sediments; (b) A number of assumptions and simplifications are associated with the Mohr-Coulomb criterion; (c) The Bingham plastic model is a simple model which may have some deficiencies in accurate prediction of the flow viscosity; moreover, no measurement is performed on the rheological

parameters and the values are estimated and calibrated. Yet the multiphase MPS results are accurately predicting some important features of the sediment motion. The peak sediment displacement in experimental and multiphase MPS results is almost the same at different times. The local peaks in sediment profile are almost accurately captured by the multiphase MPS model. The general fluctuation trend of the sediment profile at different times is predicted accurately by the multiphase MPS model.

Moreover, Figure 35 shows that the multiphase MPS performance surpass the WC-MPS simulations of the same problem. The WC-MPS model does not detect the accurate position of the wave front and the wave curvature. Results of the WC-MPS model show overestimation of the water wave height at the regions close to the wave front. This overestimation is not seen in the multiphase MPS results. Overall, the WC-MPS results are showing more bed erosion than the multiphase MPS and experimental results do. For instance, the WC-MPS overestimates the peak displacement of the sediments, especially at t=0.25s and t=0.5s. There are unphysical drops in sediment height in the WC-MPS results in range of $10cm \leq x \leq 60cm$ at t=0.5s and t=0.75s. Despite the multiphase MPS, the WC-MPS does not predict the local sediment profile peaks accurately. In general, the water wave profile and the sediment profile at different times predicted by the multiphase MPS model are in much better agreement with the experimental data than the WC-MPS results are. It should be noted that in the WC-MPS model, a general visco-plastic fluid model is used for the rheology of sediments, which is a more advanced model compared to the Bingham plastic model and is expected to perform better.

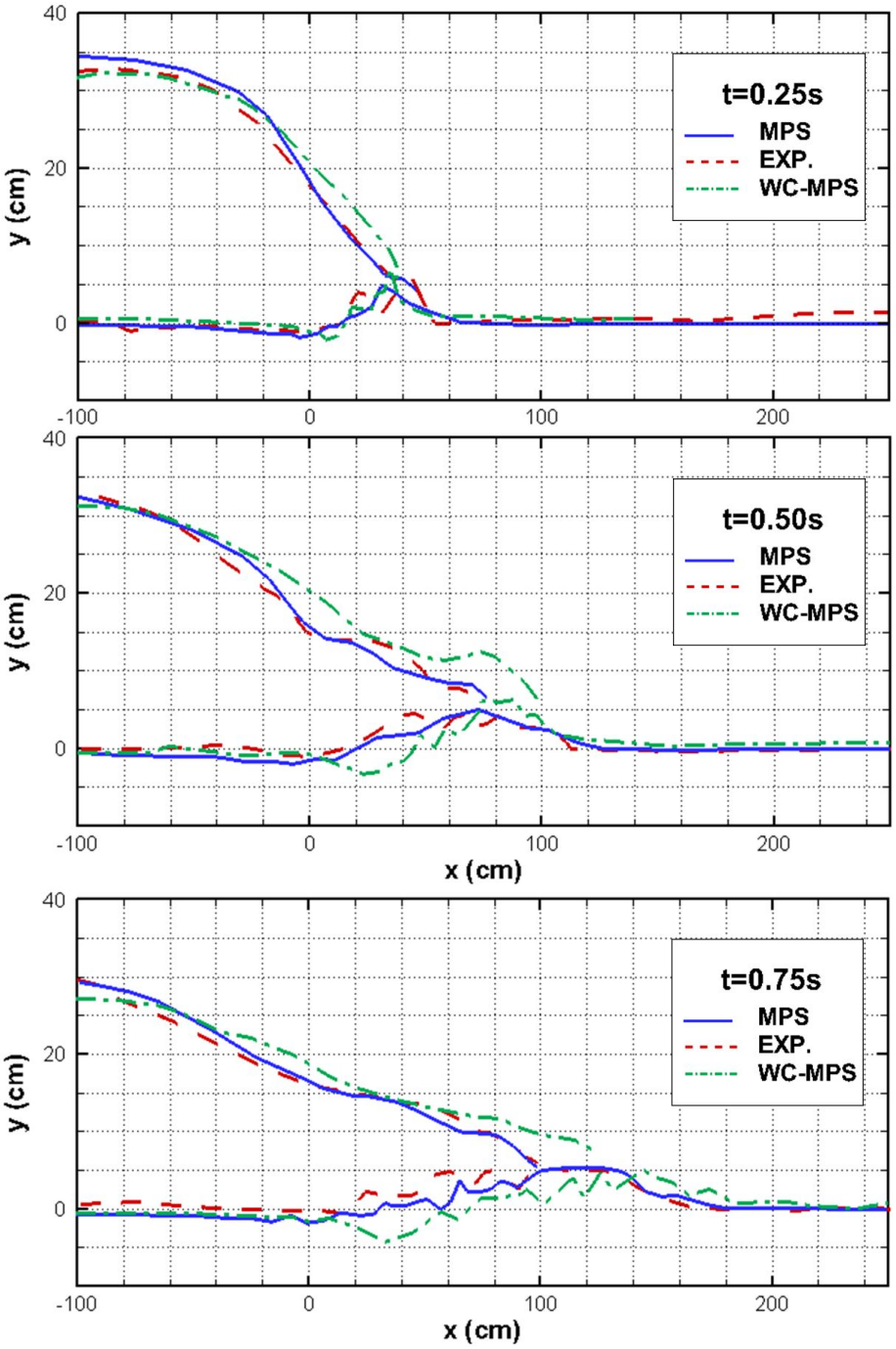

Figure 35- A comparison between the experimental data, MPS results, and the WC-MPS results for the water surface and sediment profiles at 0.25s (top), 0.50s (middle), and 0.75s (bottom). The sediment material is PVC. x to y ratio is 0.3.

Figure 36 shows the particle configuration at different times for the case of having sand as the bed sediment. The simulation is performed for 1 second. Compared to the PVC case, the bed erosion and displacement is less as the density of the sand is higher than the PVC and requires relatively more dynamic pressure for being displaced. Figure 37 represents a comparison between the multiphase MPS results, the WC-MPS results, and the experimental data for the sand profile and another comparison between the multiphase MPS results and the experimental data for the water wave profile. There is no quantified WC-MPS result available for the water wave profile in this case. The general discussion for the PVC case is also applicable here and is avoided to be elaborated again for the sake of briefness. The agreement between the multiphase MPS and experimental results for water wave profile is close. At t=0.25s, the wave front is predicted accurately by the multiphase MPS model. However, at t=0.5s and t=0.75s, the wave front is overestimated and the errors of the overestimations are 7.79% and 4.05%, respectively, compared to the experimental data. The water wave profile curvature in multiphase MPS results are the same as in the experimental results. Compared to the WC-MPS, results of the multiphase MPS model are in closer agreement with the experimental results for the peak sediment displacement. The local peaks in sediment profiles are also in better agreement with the experimental results in the multiphase MPS simulation, compared to the WC-MPS model. At t=0.5s, there is likely a lag time in the sediment peak displacement between the multiphase MPS and experimental results, meaning that the two peaks are happening at different positions. In comparison with the WC-MPS results, it is obvious that the WC-MPS simulation is showing very high and unphysical erosion and respectively high sediment deformation and

that the multiphase MPS simulation results surpass the WC-MPS simulation of the same problem.

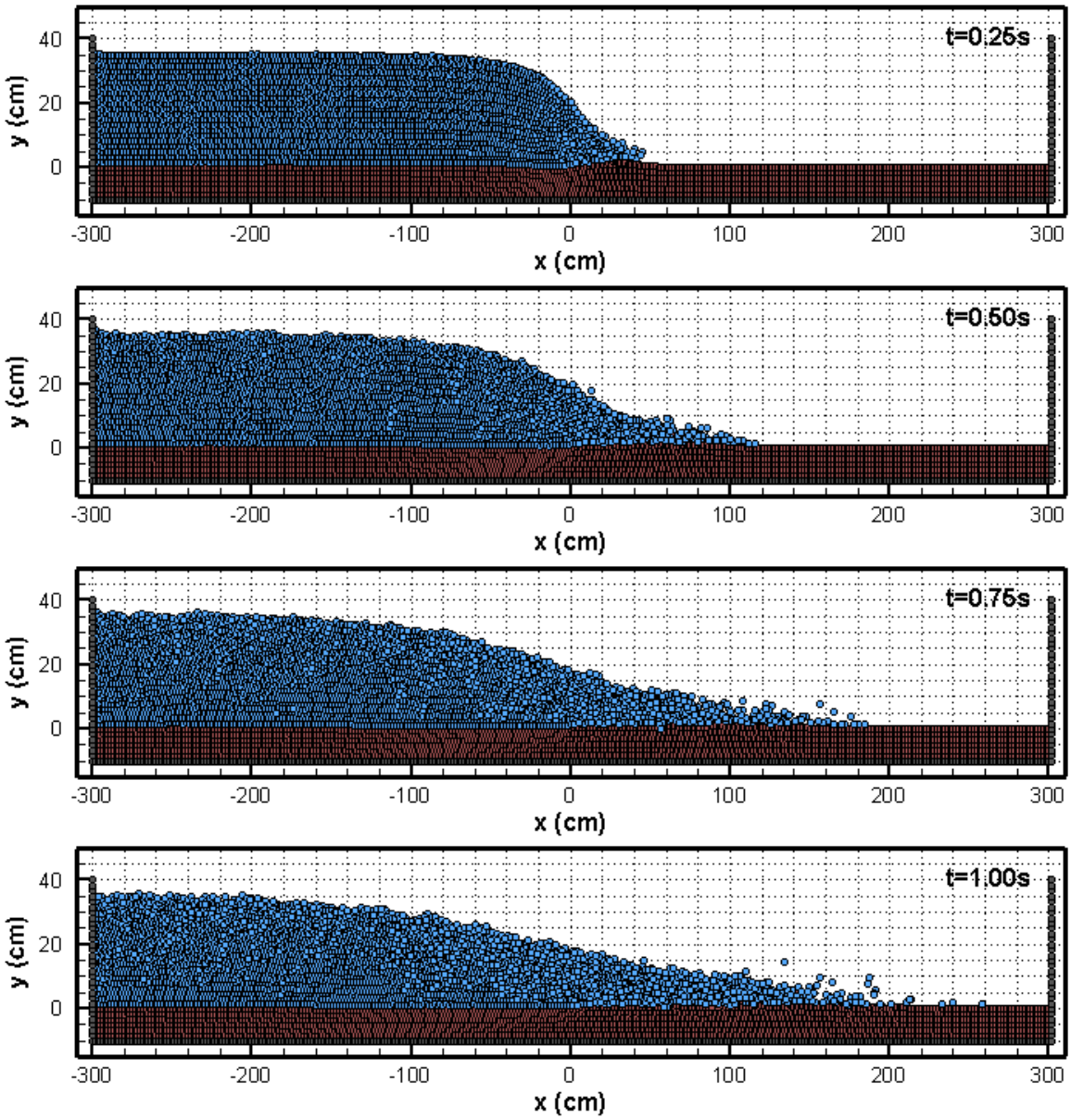

Figure 36- Particle configuration for the mobile-bed dam break problem at different times. The sediment material is sand. x to y ratio is 0.5.

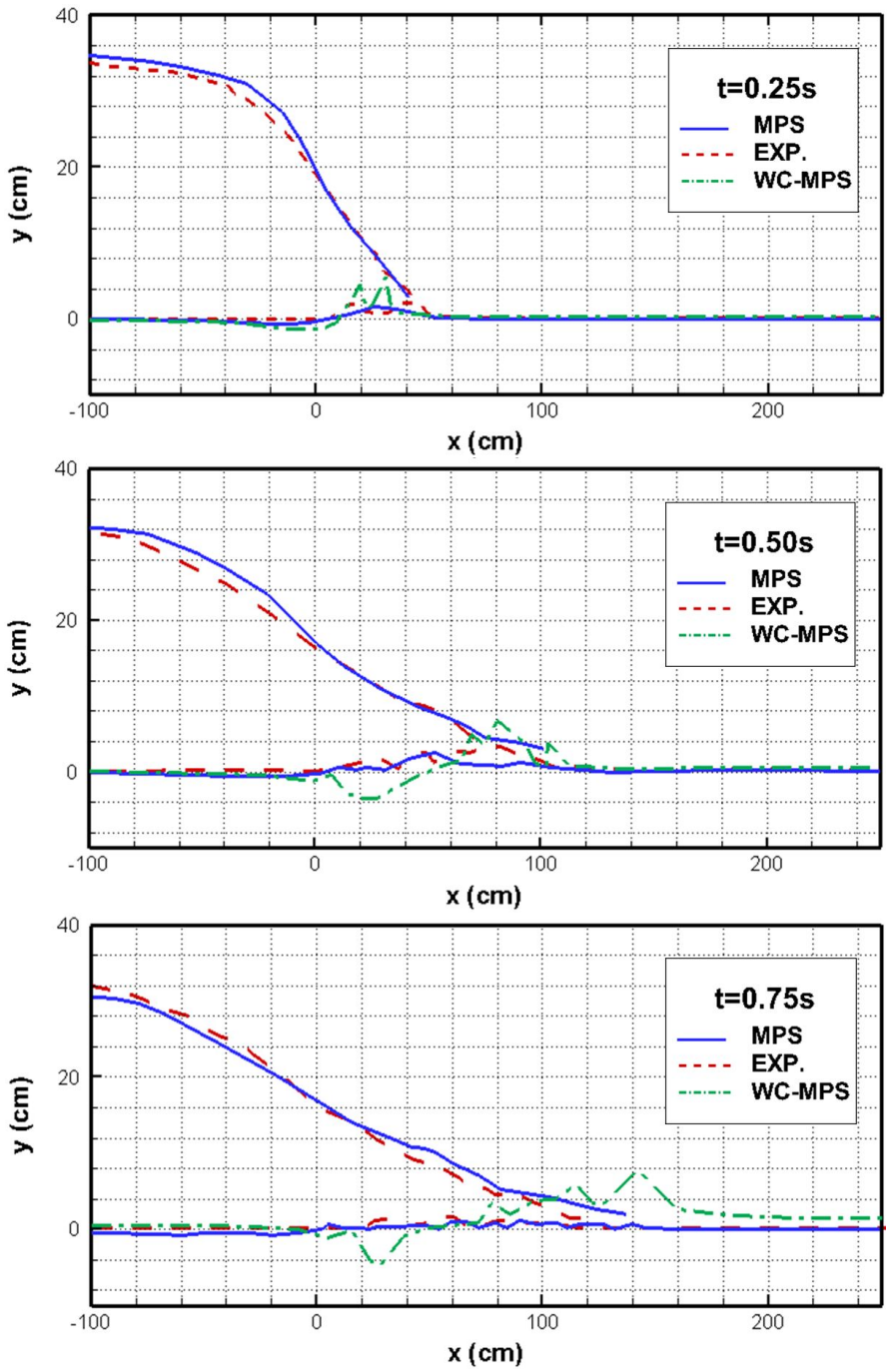

Figure 37- A comparison between the experimental data, MPS results, and the WC-MPS results for the water surface and sediment profiles at 0.25s (top), 0.50s (middle), and 0.75s (bottom). The sediment material is sand. x to y ratio is 0.3.

4.6. Summary

In this chapter, a multiphase mesh-free particle method is proposed based on the MPS formulation. The proposed multiphase MPS method treats the multiphase system as a multi-density multi viscosity fluid and solves one single set of governing equations on the whole computational domain. The pressure and shear stress discontinuities along the phase interfaces are smoothed by applying density and viscosity averaging algorithms. The granular media is represented by particles which have the same size as of the fluid particles and their behavior is assumed to be similar to non-Newtonian fluids. The Bingham plastic model is applied as the rheology model to calculate the viscosity of the granular phase at each time step.

The proposed method is then utilized in simulation of granular flow and sediment transport. Two problems, deformable submarine landslide and dam-break over an erodible bed, are simulated and the results are presented and discussed in detail.

Comparing the experimental results for the underwater landslide problem with the results of the present multiphase MPS model clearly shows that the multiphase MPS model can accurately predict different features of the flow and the water surface profile is in good agreement with the experimental data. The simulated landslide mass profile is also comparable with the results of other numerical methods and despite few discrepancies which are likely caused by the assumptions associated with the applied rheology model and rheological parameters and the boundary conditions, the results are in good agreement with each other.

The dam break over an erodible bed is modeled in two cases with different bed materials; PVC and sand. The particle configuration at different times is presented. The results for the water wave and sediment profiles are compared with the experimental data and the WC-MPS results. The general conclusion is that the present multiphase MPS model can satisfactorily predict the water wave profile. Also, despite few discrepancies between the experimental data and the multiphase MPS results for sediment profiles, the multiphase MPS model is successfully predicting some important features of the sediment flow. In addition, the results of the present multiphase MPS model are significantly in closer agreement with the experimental data than the WC-MPS results. This makes a significant enhancement in the application of this mesh-free particle method in simulating free surface multiphase flow systems.

Successful prediction of the free surface and sediment flow through the proposed multiphase MPS method, straightforward boundary and interphase treatment, ease of coding, and good stability of this method are factors suggesting the idealness of this technique for simulating complex free surface multiphase problems. This method can be used to simulate free surface and multiphase problems in hydraulics, river, coastal and ocean engineering where an accurate prediction of water surface profile is necessary.

Chapter 5 : Multiple-Size Particle Algorithm for Mesh-Free Methods

5.1. Problem Definition

In a typical numerical analysis of fluid flow by mesh-free methods, the number (distance) of particles representing the fluid is of importance. Decreasing the number of particles in favor of reducing the computational cost may adversely affect the accuracy of the simulations, while to keep the use of resources at an optimum level, the number of particles should not be unreasonably large.

It is well known that the complexity of free surface flows differ significantly depending on the flow region. Specifically, flow in regions close to free surface is usually much more complex than the flow deep below the surface. As shown in chapter 3 for simulation of landslide-induced water waves, it is not necessary to have fine distribution of particles everywhere in the computational domain. Alternatively, to increase the efficiency of the simulations while keeping the accuracy at a desired level, one can implement particles with different initial distances (or say particles with different sizes) to represent the fluid and boundaries. Those parts of the fluids that are associated with relatively less complexity may be represented by particles with large initial distances. On the other hand, particles that have a leading role in determination of important features of the flow such as free surface should have relatively smaller initial particle spacing in order to provide the desired accuracy.

Beside the efficiency of the multiple-resolution representation of fluid flow, there is sometimes a big need in CFD codes to be capable of representing the boundaries or external objects in a different resolution compared to the fluid flow resolution; for instance, in simulation of fluid-structure interaction, flow in vegetated channels, or flow on an airfoil (see Larroude and Oudart (2012)). There are sometimes restrictions in the thickness of the boundaries or external objects. Those codes that are not capable of dealing with multiple-resolution representation of computational domain have to simulate the whole domain in a relatively high resolution arising from the restrictions, making the computational time often dramatically large. The computational resources might not be available or affordable for simulation of problems in such high resolutions. By utilizing a multiple-resolution algorithm, the restrictions on the size of the objects or boundaries could be satisfied while the fluid flow is simulated in a desired resolution depending on the availability of computational resources and desired level of accuracy.

In this chapter, a new algorithm for the usage of particles with different sizes in one computational domain is proposed for mesh-free particle methods. The algorithm is applied to the WC-MPS method and results for simulations of dam-break and landslide-induced water waves are presented. It is preferred to apply the algorithm to the WC-MPS method rather than to the MPS method for the sake of simplicity to avoid unnecessary difficulties dealing with Poisson equation of pressure. Again for the sake of simplicity, the third-order spiky kernel function proposed by Shakibaeinia and Jin (2010) is utilized herein. The proposed multiple-size particle method applied to the WC-MPS formulation is abbreviated to MS-WC-MPS herein in this chapter.

5.2. Mechanism of fine-region coarse-region interaction

For a better presentation of the multiple-size particle algorithm, the case of having just two resolutions in one computational domain is discussed herein; a coarse region and a fine region. The same algorithm can be easily utilized and applied for simulation of fluid flow represented with more than two scales.

Particles representing the coarse and fine regions are called "large" and "small" particles and are labeled as "Ll" and "Ls" particles, respectively. The initial particle spacing between Ll particles is nl_0, and between Ls particles is l_0. The initial particle spacing between an Ll and an Ls particle would be $(n+1)/2 \times l_0$. Figure 38 shows a schematic of the corresponding particle configuration. In this configuration, the value of parameter *n* is set to 2, meaning that each Ll particle is occupying the space of four Ls particles.

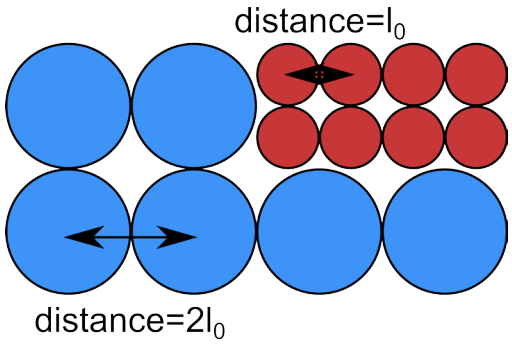

Figure 38- Schematic of a sample two-scale computational domain.

Assume the kernel size for particles representing the fine region is set to αl_0. For calculation of kernel function, consider four distinct scenarios:

- Scenario 1: when a reference Ll particle interacts with another particle of the same type ($Ll \rightarrow Ll$). The kernel size in this scenario is $\alpha n l_0$.

- Scenario 2: when a reference Ls particle interacts with another particle of the same type ($Ls \rightarrow Ls$). The kernel size in this scenario is αl_0 .
- Scenario 3: when a reference Ls particle interacts with a Ll particle ($Ls \rightarrow Ll$). We do not define any kernel size in this scenario.
- Scenario 4: when a reference Ll particle interacts with a Ls particle ($Ll \rightarrow Ls$). We do not define any kernel size in this scenario.

The calculation of kernel function in scenarios 1 and 2 is pretty straightforward as the kernel size is specified. The difficulties will be raised in calculation of kernel function in either scenario 3 or 4, in absence of a specified kernel size.

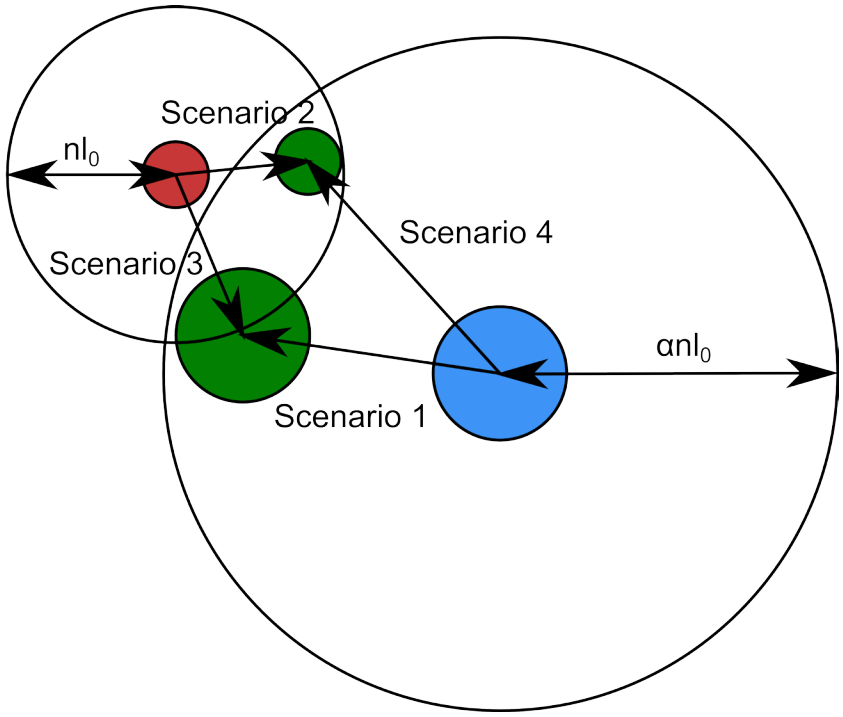

Figure 39- Definition of the four distinct scenarios of particle interaction.

The key point in the present multiple-size particle algorithm is large particle splitting, meaning that whenever a small particle is in interaction with a large particle, the large particle will be split to so-called *fictitious* particles. Therefore, an interaction between a Ll and a Ls particle is considered "possible" when the Ls particle can interact with at least one fictitious Ls particles. Assume dx and dy are respectively horizontal and vertical distances between a Ll and a Ls particle in a time step. For a case that *n* is equal to 2, we can write

$$\text{if} \quad \left[(dx+\frac{l_0}{2})^2+(dy+\frac{l_0}{2})^2\right]^{1/2} \le r_e \quad \xrightarrow{then} \quad \text{interaction}$$

$$\text{if} \quad \left[(dx+\frac{l_0}{2})^2+(dy-\frac{l_0}{2})^2\right]^{1/2} \le r_e \quad \xrightarrow{then} \quad \text{interaction}$$

$$\text{if} \quad \left[(dx-\frac{l_0}{2})^2+(dy+\frac{l_0}{2})^2\right]^{1/2} \le r_e \quad \xrightarrow{then} \quad \text{interaction}$$

$$\text{if} \quad \left[(dx-\frac{l_0}{2})^2+(dy-\frac{l_0}{2})^2\right]^{1/2} \le r_e \quad \xrightarrow{then} \quad \text{interaction}$$

In scenario 3, when a reference Ls particle interacts with a neighboring Ll particle, the neighboring Ll particle will be split into fictitious particles of the same size as of the Ls particles. Therefore, the kernel function in this scenario is calculated as

$$w(Ls \to Ll) = \sum_{i=1}^{n^2} w(Ls \to Lf_{ni}) \tag{5.1}$$

Lf_n is a label for fictitious small particles corresponded to a neighboring particle, and n^2 is the number of fictitious small particles when a large particle is being split.

Scenario 4 is a little more complicated. Two cases are considered in this scenario. The first case happens when a large particle interacts with only small particles in one time step. The kernel function in this case is calculated as the arithmetic average of the interaction between each fictitious small particle and the neighboring small particle, written as

$$w(Ll \to Ls) = \frac{\sum_{i=1}^{n^2} w(Lf_{ri} \to Ls)}{n^2} \tag{5.2}$$

Lf_r is a label for fictitious small particles corresponded to a reference particle.

In this scenario, the second case happens if the reference large particles interact with both small and large neighboring particles in one time step. In this case, the two large particles do not interact according to the first scenario. Instead, both will be split to fictitious small particles and the kernel function (w') for interaction of two large particles in this case is calculated as

$$w'(Ll \to Ll) = \frac{\sum_{j=1}^{n^2}\sum_{i=1}^{n^2} w(Lf_{rj} \to Lf_{ni})}{n^2} \tag{5.3}$$

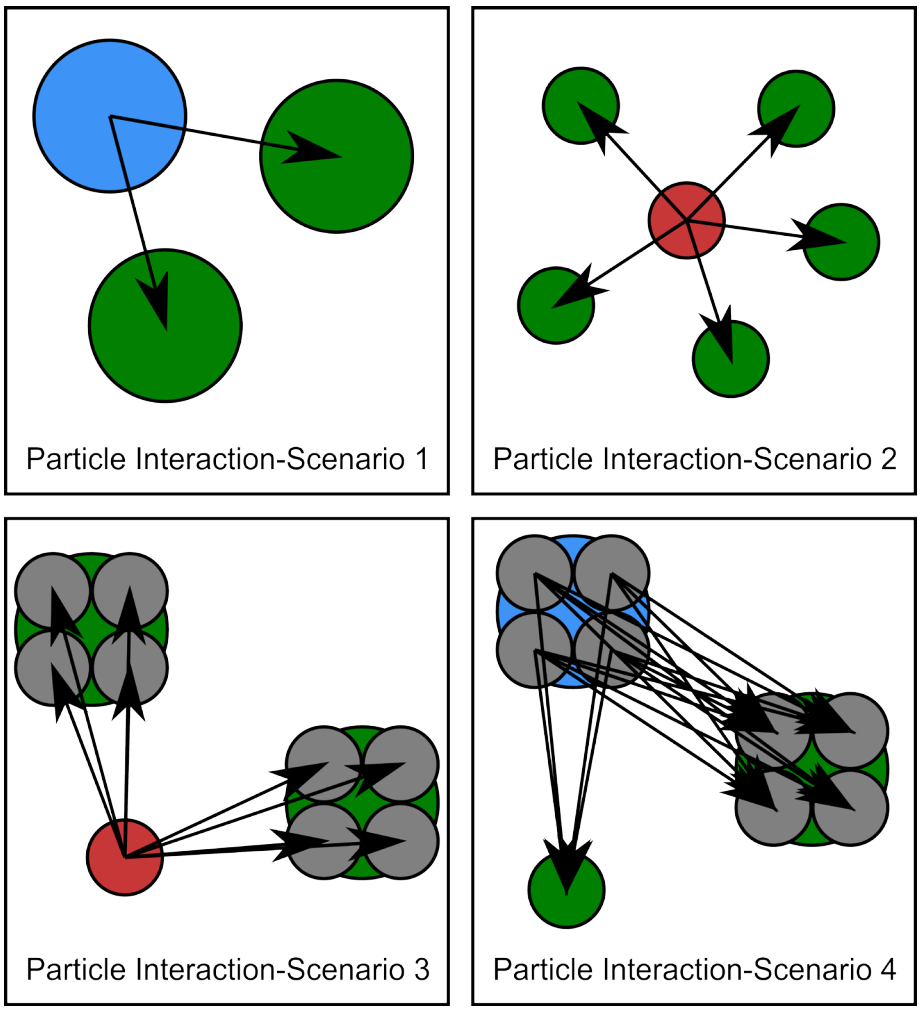

Figure 40- The particle interaction mechanism in each of the four scenarios.

5.3. Calculation of the particle number density

If a reference Ls particle interacts with both neighboring Ls and Ll particles in one time step, particle number density for the particle p, $\langle n \rangle_p$,is written as

$$\langle n \rangle_p = \sum_{q \neq p} w(Ls_p \rightarrow Ls_q) + \sum_{s \neq p} w(Ls_p \rightarrow Ll_s) \tag{5.4}$$

If the reference Ls particle interacts with only either Ls or Ll particles in one time step, the first or second term in right hand side of the above equation will vanish, respectively.

If a reference Ll particle interacts only with neighboring Ll particles in a time step, the particle number density for the particle p is equal to

$$\langle n \rangle_p = \sum_{q \neq p} w(Ll_p \rightarrow Ll_q) \tag{5.5}$$

If a reference Ll particle interacts with both neighboring Ll and Ls particles in a time step, the particle number density for the particle p is calculated as

$$\langle n \rangle_p = \sum_{q \neq p} w(Ll_p \rightarrow Ls_q) + \sum_{s \neq p} w'(Ll_p \rightarrow Ll_s) + w(\text{inner particle}) \tag{5.6}$$

The term w(inner particle) is considering the interaction between the fictitious small particles corresponding to one large particle (see Figure 41):

$$w(\text{inner particle}) = \frac{\sum_{j=1}^{n^2} \sum_{k \in I} w(Lf_{rj} \rightarrow Lf_k)}{n^2}; I = \{[k = (1, \ldots, j-1)] \cup [k = (j+1, \ldots, n)]\} \tag{5.7}$$

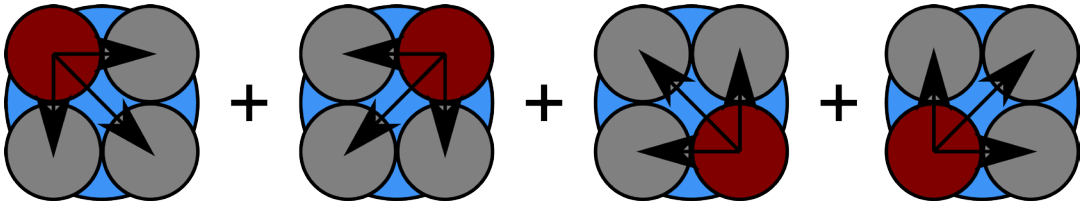

Figure 41- Calculation of the kernel function for inner particle interaction.

Calculation of the pressure gradient term in the MPS formulation is very similar to the calculation of the particle number density discussed herein. The pressure of the large particle will be assigned to the corresponding fictitious small particles.

Note that the fictitious particles do not carry any physical variables. Instead, the corresponding Ls particles will carry the physical variables. The size of the time steps are calculated using the CFL stability condition for the small particles. In this algorithm, the constant particle number density (n^0) remains the same in both fine and coarse regions. Similar to the most of the common kernel functions in particle methods, the third-order spiky kernel function used herein in simulations of this chapter is a sole function of the ratio of initial particle spacing to kernel size. In both coarse and fine regions, as this ratio is kept the same in this algorithm, the constant particle number density will be the same in all regions.

5.4. Dam-break induced water waves

Dam-break-induced flows are among the important problems in civil engineering and their prediction is now a required element in design of a dam and analysis of dam downstream. The idealized 2D problem of the instantaneous removal of a barrier holding a water column at rest in a water tank with fixed beds is known as the "dam-break" problem. This problem has been widely used as a verification problem of the codes for the free surface flows and it is considered a bench-mark problem.

In this part, the experimental results for dam-break-induced water waves (Martin and Moyce1952; Koshizuka and Oka 1996) are reproduced numerically using the WC-MPS method. Then, to verify the accuracy and efficiency of the proposed multiple-size particle method, results of the MS-WC-MPS simulation are compared with the experimental data and the WC-MPS results. Figure 42 shows the experimental setup.

In the present WC-MPS simulation, the initial distance between two adjacent particles is 0.1825 cm, corresponding to 14734 particles including fluid, wall and ghost particles. Free surface parameter and kernel size are set to 0.99 and 0.365cm, respectively. The fluid is considered non-viscid. The Courant number is set to 0.5. Two layers of ghost particles are modeled adjacent to actual particle layer of solid boundaries. It is assumed that the barrier holding the water column at rest is removed instantly. Figure 43 shows the particle configuration at different times computed using the WC-MPS method.

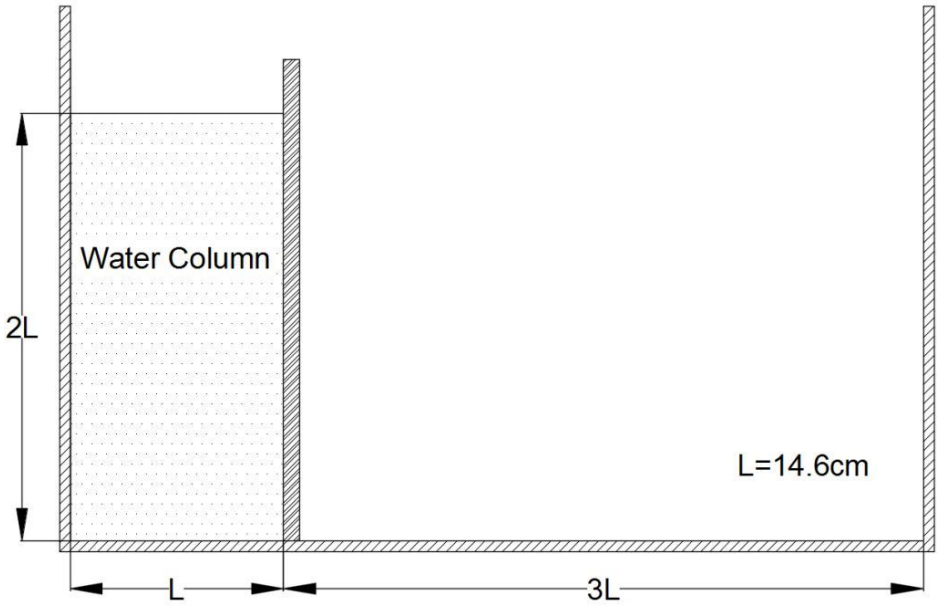

Figure 42- Geometry of the dam-break experiment.

In simulation of the similar dam-break problem using the proposed multiple-size particle method (MS-WC-MPS method), calculation parameters are kept similar to those of the WC-MPS simulation. The only difference in model configuration between the two simulations is that in the MS-WC-MPS simulation, part of the computational region is represented with relatively larger particles and the initial distance between two adjacent large particles is 0.365cm (n=2), reducing the total number of particles to 8975 particles. Figure 44 shows the configuration of the coarse and fine regions in the computational domain. A rectangular region relatively far from the free surface is selected to be represented in coarse resolution as the fluid in this region is expected to have less complex behavior compared to the near free surface region. Figure 45 shows the particle configuration at different times calculated by the MS-WC-MPS method.

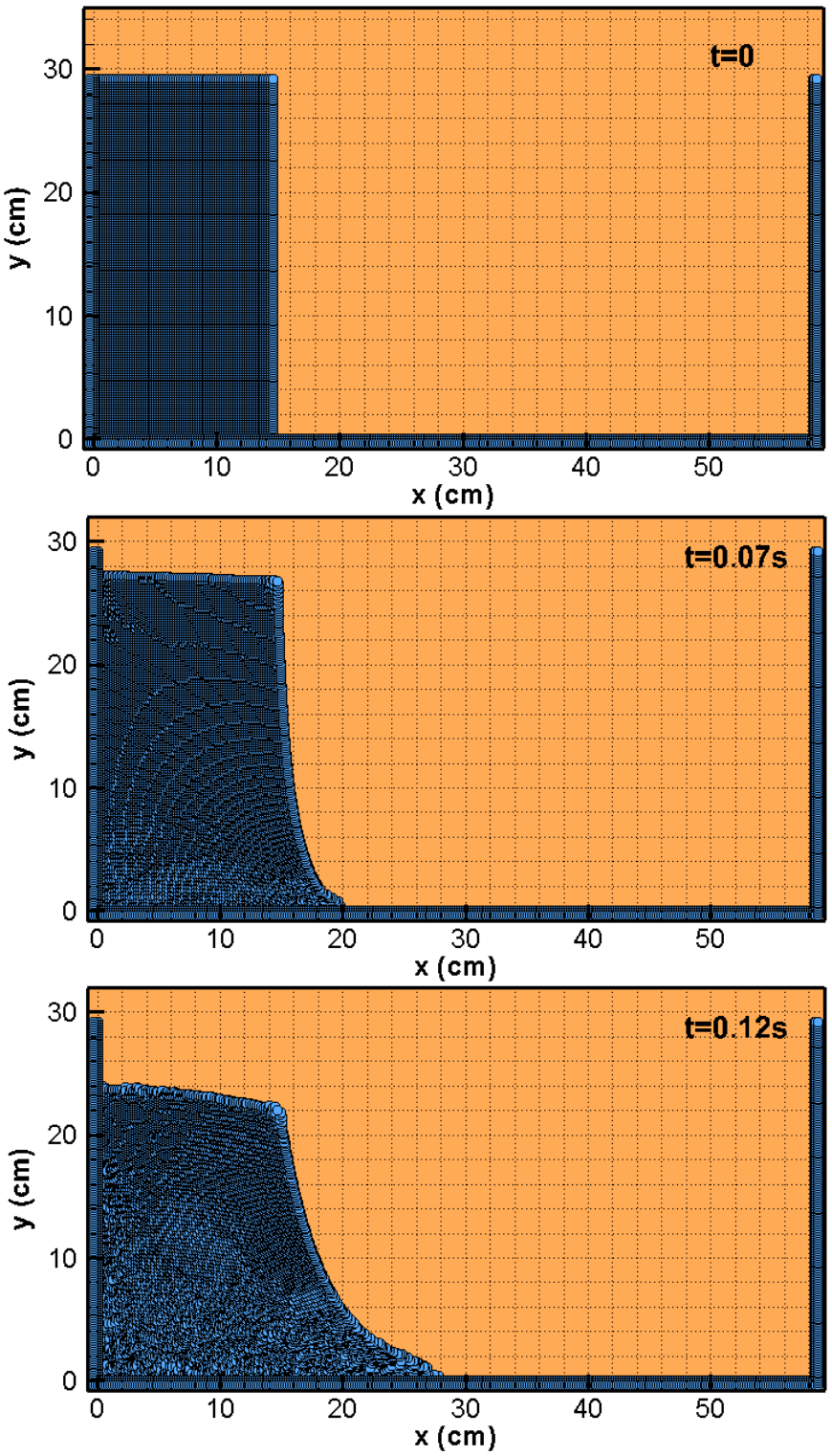

Figure 43- Particle configuration for dam-break problem computed by the WC-MPS method.

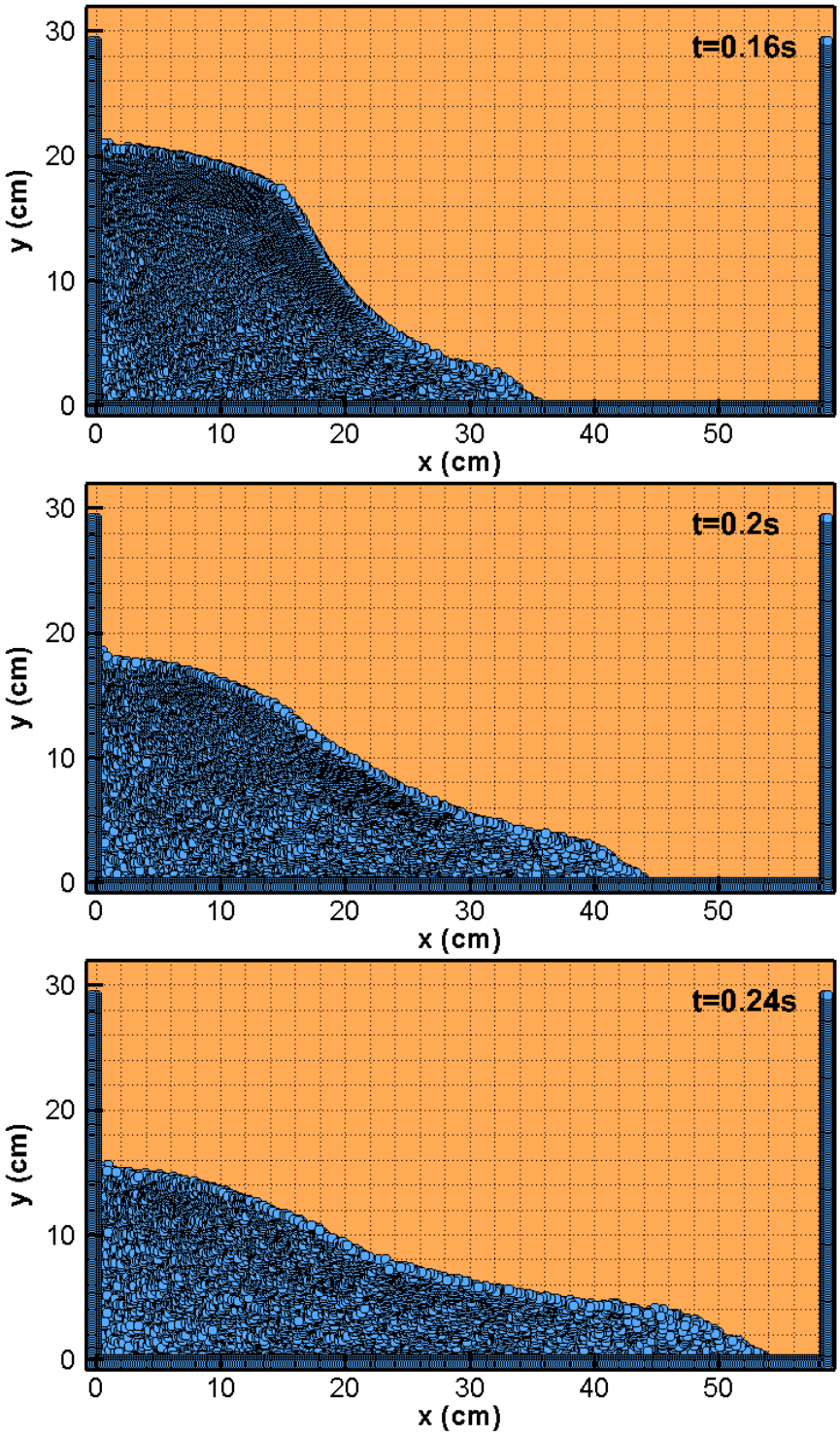

Particle configuration for dam-break problem computed by the WC-MPS method (continued).

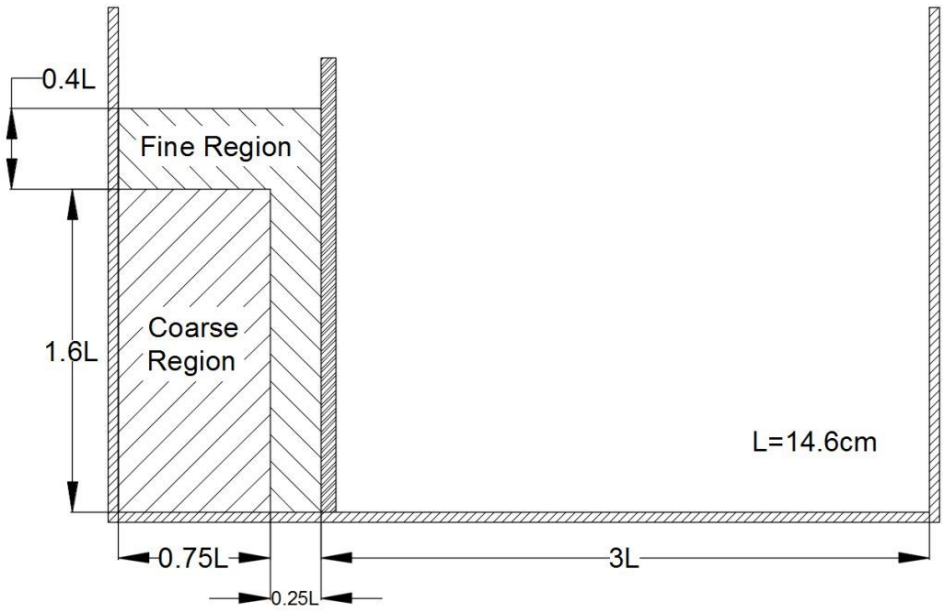

Figure 44- configuration of the coarse and fine regions in computational domain of the dam-break problem.

Figure 46 shows a comparison between the experimental, MPS, WC-MPS, and MS-WC-MPS results for the position of dam-break wave front at different times. At early times, numerical results are in good agreement with the experimental results. At relatively later times, small discrepancies are observed between the experimental data and numerical results. It is evident that the experimental results show relatively lower wave front speed than the numerical results, which is due to the friction between the fluid and the tank boundary in the experiment. Results of the MPS and WC-MPS simulations are in good agreement with each other and few discrepancies is results can be due to the use of different boundary conditions and calculation parameters. Results of the MS-WC-MPS and WC-MPS simulations are in great agreement with each other, showing the accuracy of the proposed multiple-size particle method.

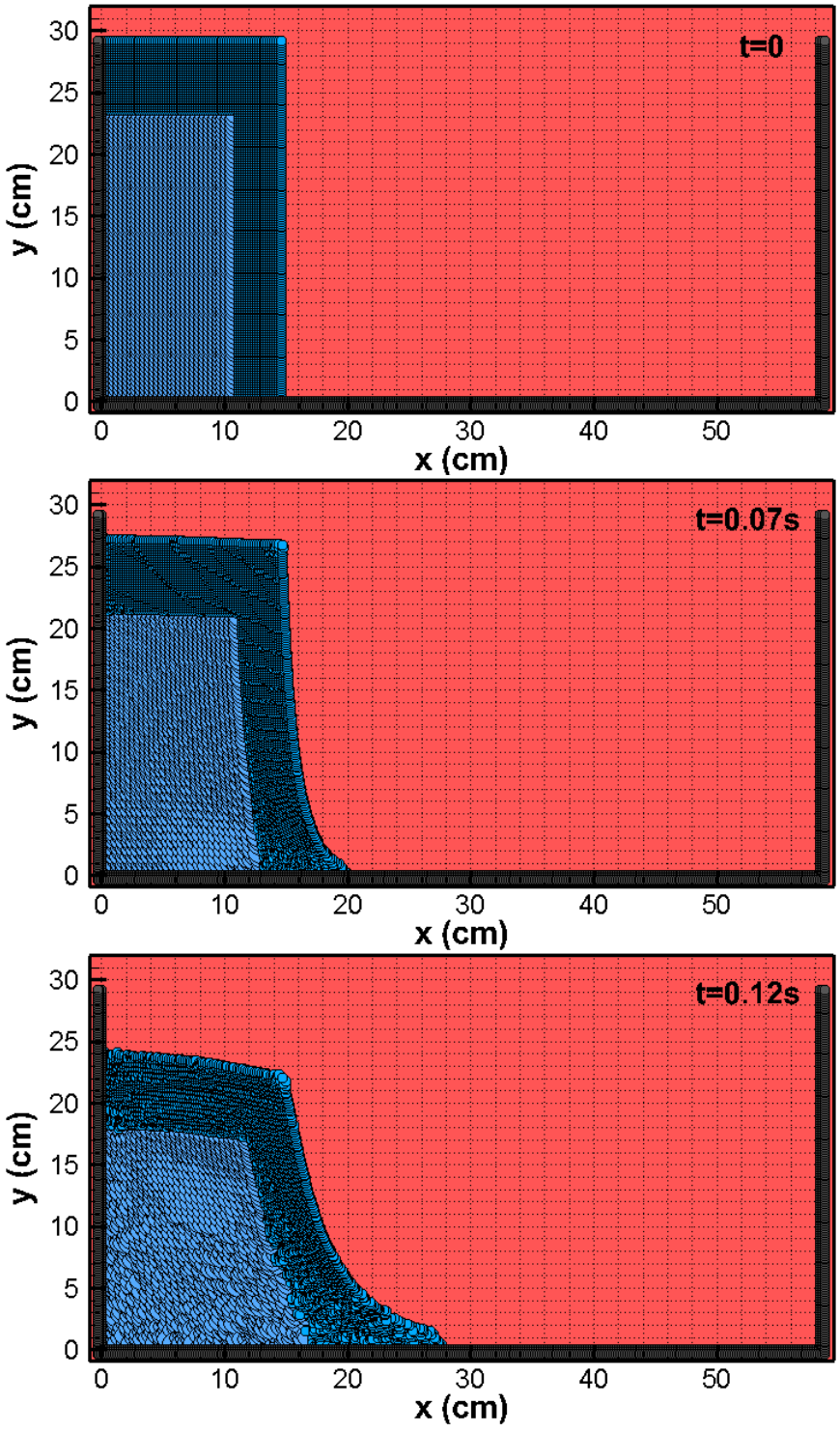

Figure 45- Particle configuration for dam-break problem computed by the proposed MS-WC-MPS method.

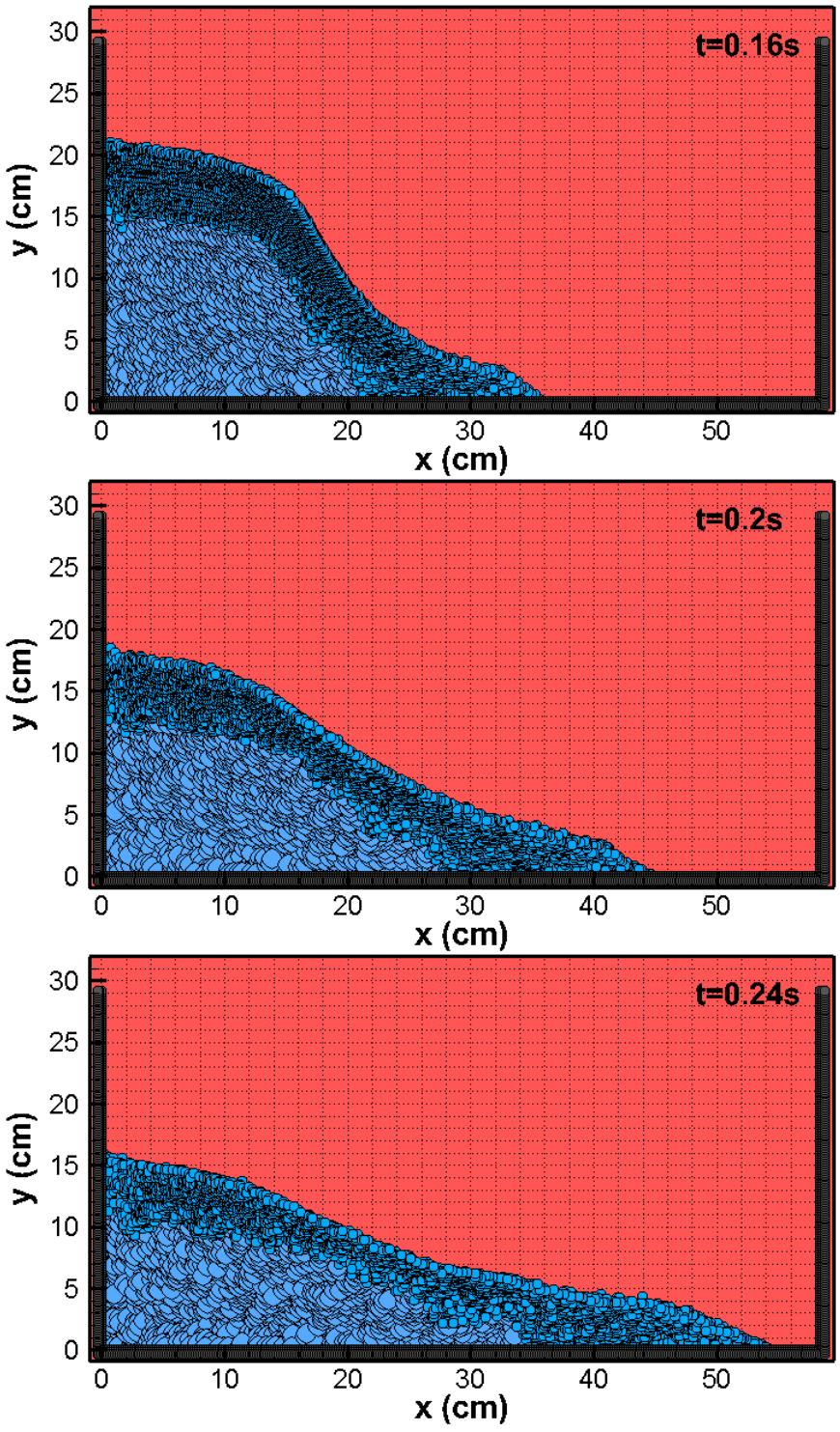

Particle configuration for dam-break problem computed by the proposed MS-WC-MPS method (continued).

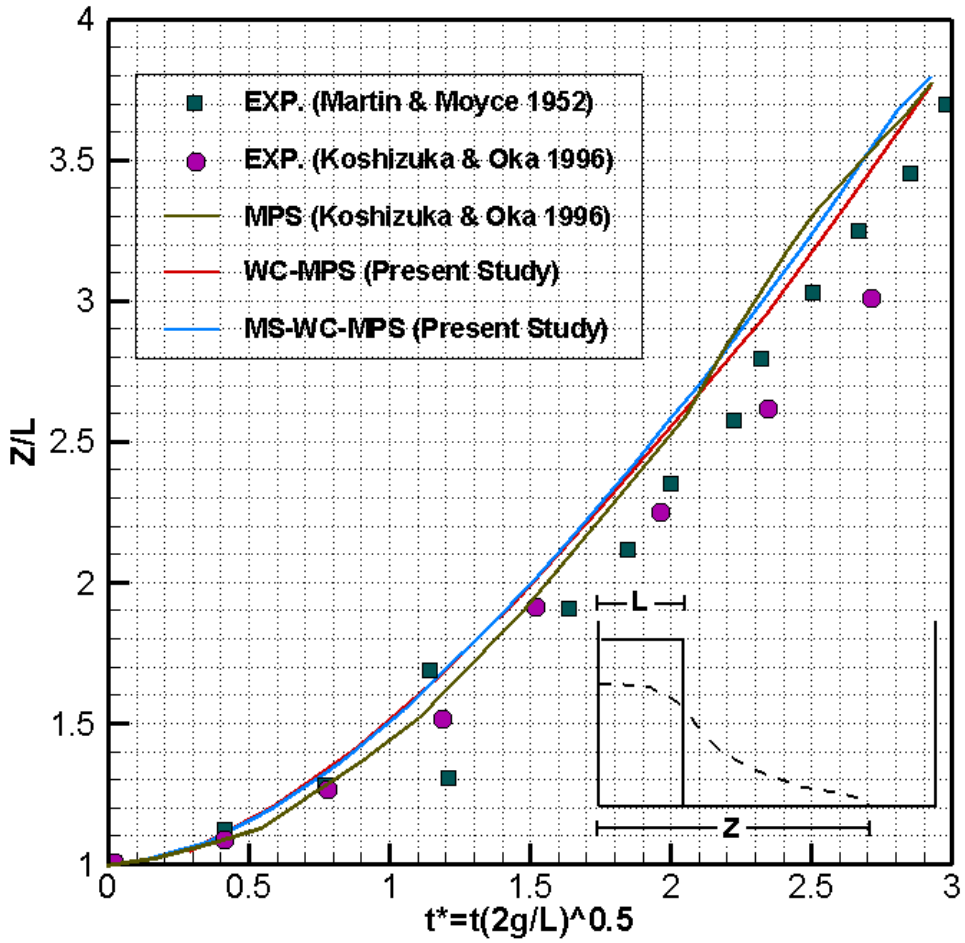

Figure 46- Comparison for the dam-break wave front position between the experimental, MPS, WC-MPS, and MS-WC-MPS results.

The total computational time for the WC-MPS simulation is 373.8 minutes, while it is 321.0 minutes (14.13% less) for the MS-WC-MPS simulation. The computer is equipped with Intel® Core™ i7-2600 CPU 3.40 GHz and a system memory of 16.0 GB. Although the calculation of the interactions between large and small particles at the spatial resolution interfaces will add up some time to the total computational time of the multiple-resolution simulations, the total computational time compared to the similar simulations performed by

single-resolution models is decreased due to the savings in the computer memory and the amount of computation process.

The difference between the total computational time of the WC-MPS and the MS-WC-MPS simulations might not be very significant in the present simulations; however, the computational time savings of this multiple-size particle method will be bolded once the dam-break problem (or any other problem of interest) is simulated either in higher resolution, or in larger scales. This means that by utilizing larger number of particles in simulation of a problem, the difference between the total number of particles in single-resolution and multiple-resolution simulations will increase, meaning more savings in the total computational time.

Moreover, the present multiple-size particle algorithm will indeed perform better in terms of efficiency if applied to semi-implicit or fully-implicit schemes, as the size of the arrays (or identically the number of particle) in these schemes play a relatively more significant role in total computational time due to higher computational time sensitivity of these schemes to the size of arrays. This higher computational time sensitivity is because of the solution process of the system of linear equations (Poisson-type equations).

5.5. Landslide-induced water waves

The results reported earlier in chapter 3 for the water waves generated by rigid underwater landslide are reproduced herein using the present multiple-size particle algorithm. In chapter 3, a number of particles initially located at a specific region of the computational domain are marked and their motion is tracked throughout the landslide and associated water wave propagation. It is shown that the marked particles do not reach the

free surface during the simulation time (2.5sec). In this part, the same region marked in chapter 3 is represented with large particles, and the rest of the computational domain is represented with small particles, having the same size as of those used for the simulations of chapter 3. The proposed MS-WC-MPS method is used herein. The simulation is performed with 4242 particles, which corresponds to an initial particle spacing of 2.5cm for fine region and 5 cm for coarse region. The fluid is considered non-viscid. A Courant number of 0.5 is selected. A value of 1800 cm/s is selected for the numerical sound speed. The free surface parameter is set to 0.99. Two layers of ghost particles are considered in addition to the layer of solid boundary particles. The simulation is performed for 2.5 seconds. Figure 47 shows the corresponding particle configuration at different times.

The computational time for the simulation performed in chapter 3 using the WC-MPS method is 176.97 minutes, while the computational time of the present simulation using the MS-WC-MPS method is 150.33 minutes (15.05% less). Figure 48 shows a comparison for the water surface profile between the present MS-WC-MPS method, WC-MPS method, and the experimental results. It is evident that the discrepancies between the MS-WC-MPS and the WC-MPS results are minor and probably negligible. Therefore, by keeping the accuracy at the same level, the computational time is decreased.

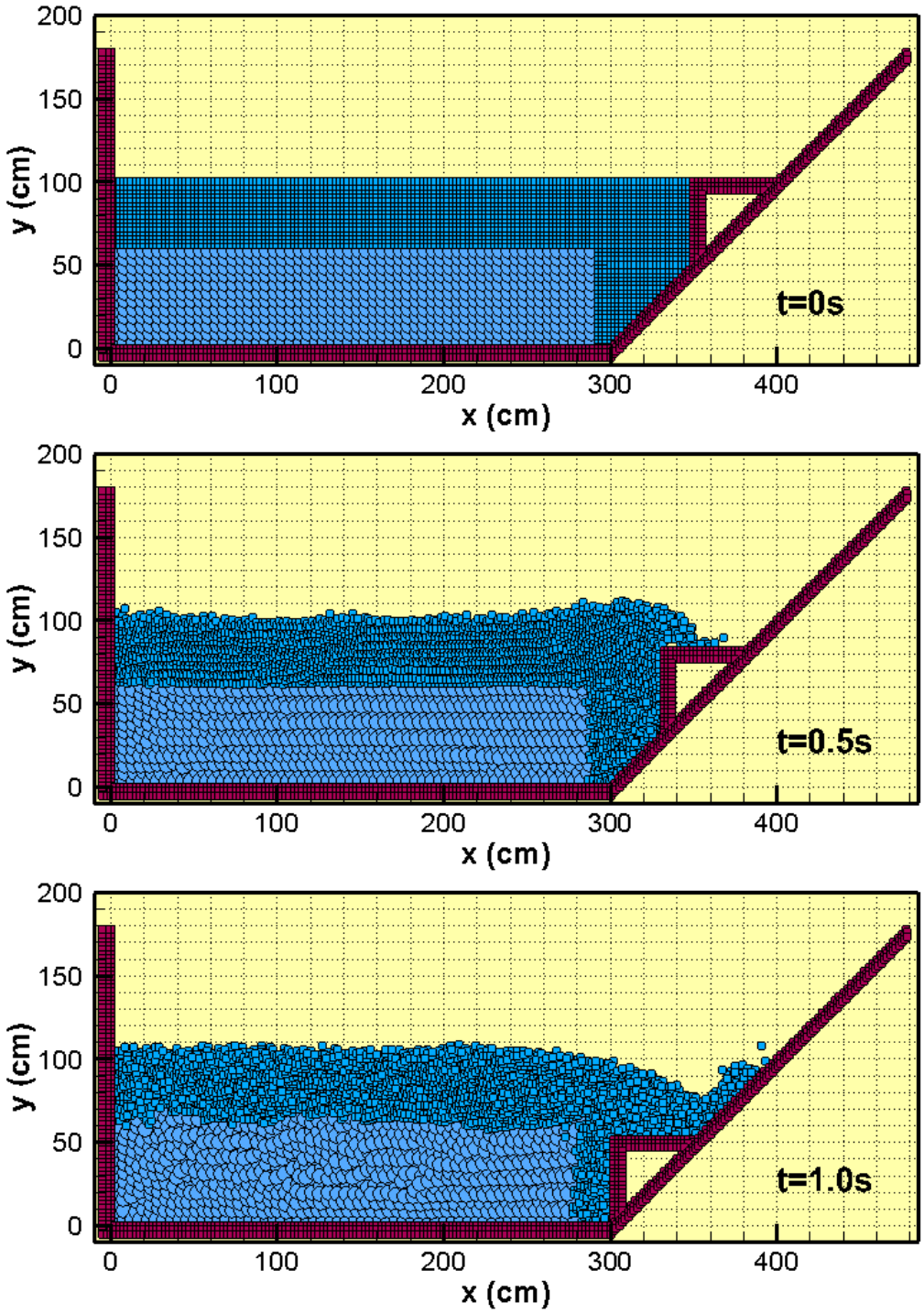

Figure 47- Particle configuration at different times for the submarine landslide problem using the multiple-size particle algorithm.

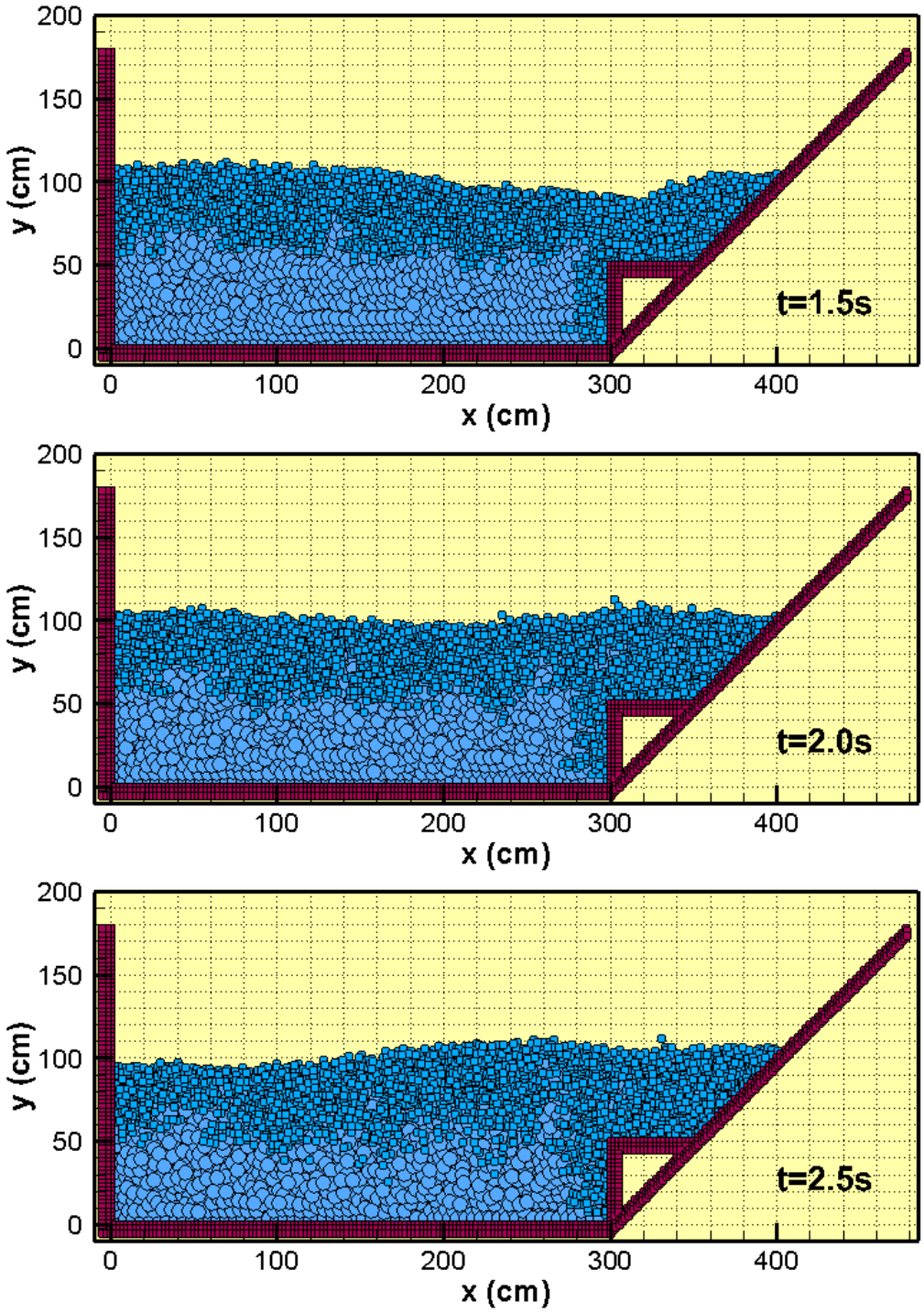

Particle configuration at different times for the submarine landslide problem using the multiple-size particle algorithm (continued).

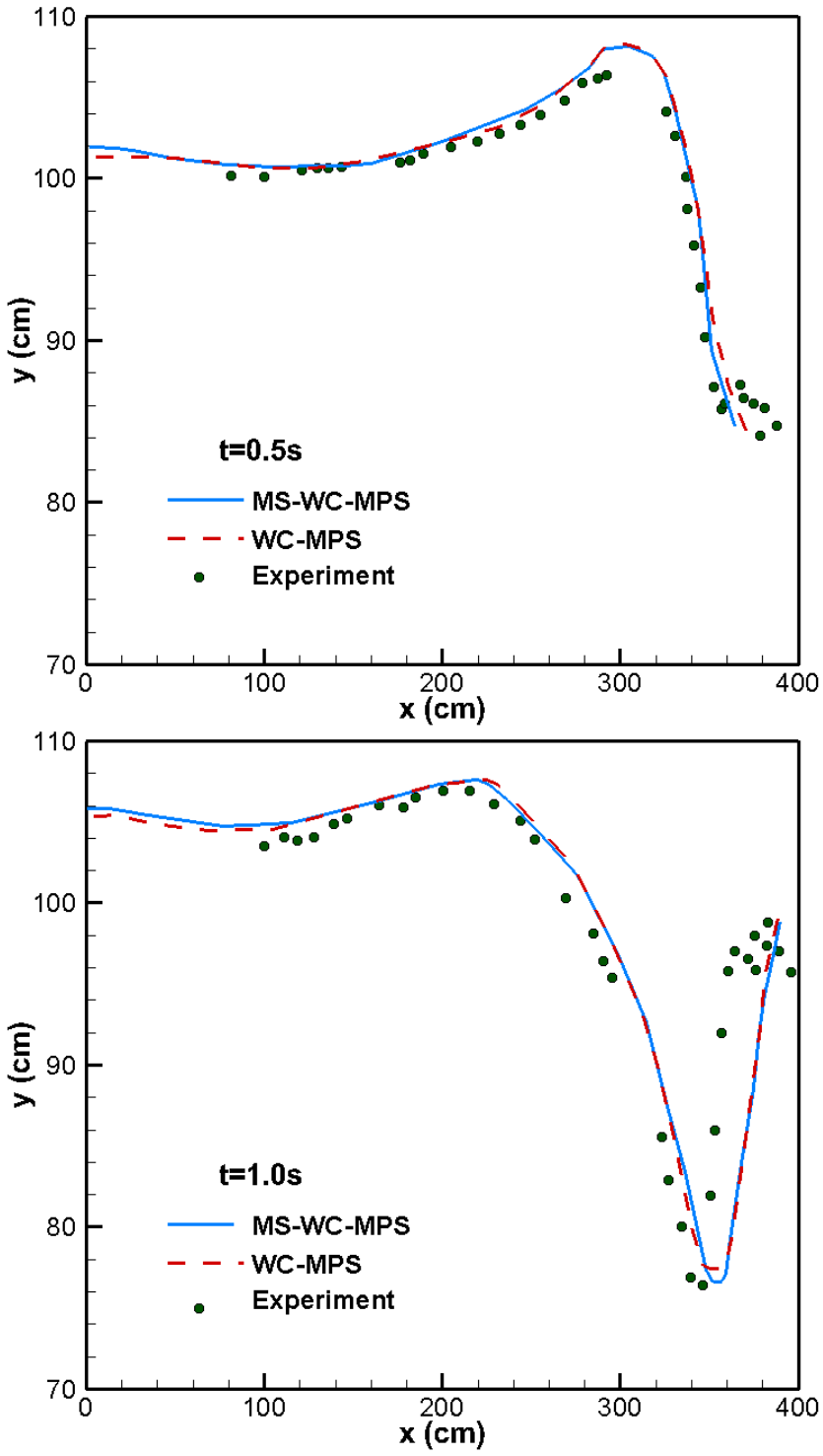

Figure 48- A comparison for the water surface profile between the MS-WC-MPS, WC-MPS, and experimental results.

5.6. Summary

In this chapter, a new multiple-size particle algorithm is introduced. This algorithm enables the multi-resolution simulation in one computational domain to save computer time and memory. Those parts of the fluid flow and boundaries associated with relatively high complexity can be simulated in high resolution, while the simulation of less complex regions may be performed in relatively lower resolution to reduce the overall computational time.

The general idea behind the present algorithm is particle splitting; whenever a small particle is in interaction with a large particle, the large particle with be split to a number of so-called *fictitious* particles, and then the interaction occur between the reference small particle and target fictitious small particles. The fictitious particles do not carry any physical variables; the position of these particles can be calculated based on the position of the corresponding large particle, and the velocity, density, and pressure of the factious particles may be set to those of the corresponding large particle. Therefore, there will be significant savings in computer memory and CPU time by reducing the size of arrays.

The proposed algorithm is then applied to a bench-mark problem for model verification. Results for the simulation of the dam-break-induced water waves are shown using the proposed algorithm and then compared with the available experimental data and with the results of other mesh-free methods using single-size particle representation of domain. Results for the landslide-induced water waves are also reproduced in this chapter using the proposed algorithm and compared with the available experimental data and single-size numerical simulation of this phenomenon. The general conclusion is that using

the present algorithm, the overall computational time is reduced while the accuracy of free surface profile prediction is kept almost at the same level.

The present algorithm will indeed make a great contribution in significant reduction of computational time in large scale simulations when a considerable portion of the computational domain can be represented in relatively low resolution. Although the present multiple-size particle algorithm is applied to the WC-MPS method, it can be easily modified and applied to similar mesh-free particle methods such as the SPH method.

Chapter 6 : Conclusion and Recommendation

This research introduces some improvements to a mesh-free particle method (MPS method) for efficient and stable simulations of free surface and multiphase flows. The MPS method is a fully Lagrangian method which provides approximations to the strong form of partial differential equations on the basis of integral interpolants. In this method, the governing equations for incompressible viscous flows (Navier-Stokes equations) are solved in a fully Lagrangian form using a fractional step method which consists of splitting each time step in two steps. The fluid is represented with particles. The motion of each particle is calculated through interactions with neighboring particles by means of a kernel function.

The suggested improvements are focused on the stability, applicability, and efficiency of this method. The stability of the simulations is improved by the use of a newly-introduced kernel function. The applicability of this method is extended by introducing a new model for simulation of multiphase flows, granular flows, and sediment transport. The efficiency of this method is improved by introducing a new multiple-size particle algorithm which allows the use of particles with different sizes to represent one computational domain. Each one of the improvements is verified in terms of accuracy and stability by successful simulation of a number of sample free surface problems.

6.1. Major contributions

In general, the contributions of this research can be categorized into three distinct parts:

1. Application of the MPS method is shown through the successful simulation of two sample complex free surface flows; the generation of water waves by rockslide and underwater landslide. Compared to the similar former studies focused on the application of this method, this research implements a newly-introduced kernel function. It is shown that by utilizing this new kernel function the stability of the simulations is significantly enhanced.
2. A multiphase MPS method is proposed for incompressible flows. The multiphase system is treated as a multi-density multi-viscosity fluid. A single set of governing equations is solved on the whole computational domain, and high-order accurate density and viscosity schemes are applied to stabilize the fluid pressure and shear stress fields. The proposed method is utilized for modeling of granular flows and sediment transport. The numerical results are verified with the available experimental results for the landslide-induced water waves and sediment transport via dam-break.
3. A new algorithm is introduced to enhance the efficiency of the mesh-free particle methods. This algorithm enables the implementation of a set of particles with different sizes in one computational domain. This algorithm is applied to a simplified explicit form of the MPS method, and it is verified by accurate and efficient modeling of dam-break-induced water waves and landslide-induced water waves.

This research aims to contribute to enhancement of the stability, applicability, and efficiency of the mesh-free particle methods. Although the present studies are focused on the MPS method, the proposed improvements are easily applicable to other mesh-free

particle methods. Having the proposed improvements applied to the MPS method makes it a very useful utility for solving problems in hydraulic, hydrodynamic, coastal, ocean, and river engineering that an accurate prediction of free water surface is required.

6.2. Recommendations for future work

Recommendations for future work in this area are presented in three categories; efficiency, accuracy and stability, and applicability:

6.2.1. Efficiency

1. **Adaptive Particle Refinement:** The multiple-size particle algorithm proposed in chapter 5 can be easily extended for adaptive refinement of particles. Considering two criteria, closeness to free surface and the Reynolds number, each big particle may dynamically be split to small particles and likely, a set of small particles may turn to a big particle. This technique will increase the efficiency of simulations even more.
2. **Multiple-Size Particles Multiple Time-Scale Simulation:** The approach used in this research (chapter 5) in coupling sub-domains is to use the integration method (explicit or implicit) with the same time-step over the entire computational domain. However, this approach restricts the simulation to use a single time-step that meets the stability and accuracy criteria for the entire computational domain. In case of large scale problems this is not desirable as different regions can very well represent significantly different stability and accuracy requirements. Therefore, in order to increase the efficiency of the simulations, it is recommended to use different time-stepping algorithms in

different regions of the flow represented with different resolutions. The integration algorithm on the computational domain can be performed in a procedure in which coarse regions are advanced in time, while fine regions are advanced multiple steps to reach the same time as the coarse grids and the data at different levels are then synchronized. For more information, readers are referred to Almgren et al. (1998) and Ruparel et al. (2012), which have applied this approach to grid-based methods and have shown applications in fluid and structural dynamics.

3. **Concurrent Simulation:** The MPS method has the capability to be broken into discrete parts that can be solved concurrently. Most significantly, the solution to large sparse matrix equations (Poisson-type equations) in the MPS formulation is the most time-consuming part of the simulation (as aforementioned in chapter 3). Therefore, by using a parallel iterative solver, the computational time for MPS simulations will indeed dramatically decrease. Moreover, by applying the multiple-size particles multiple time-scale approach, the time advancement of each of the flow regions can be calculated in parallel which indeed will have a great contribution in reducing the overall computational time.

6.2.2. Accuracy and Stability

4. **Pressure Field Instabilities:** As shown earlier in chapter 3, the MPS method is still suffering from high pressure fluctuations in a fixed arbitrary point in the computational domain, and from high pressure irregularities in the flow pressure field. In the past few years, researchers have proposed a number of

modifications to the MPS formulation to solve the pressure field instabilities. Not all these modifications have yield successful simulation results. For example, Khayyer and Gotoh (2009) proposed a modified formulation for the calculation of pressure gradient for exact conservation of linear momentum. However, as shown by Shakibaeinia (2011), although this modified pressure gradient formulation will result is relatively accurate calculation of pressure field, it may not yield exact calculation of the pressure gradient between two particles, which is necessary for the accurate estimation of instantaneous motion of the fluid particles. Further studies are recommended to overcome the pressure field instability issue.

5. **Discretization Schemes:** The order of accuracy of the MPS method increases by including more terms in the Taylor series expression. There are different methods for providing more accuracy by including more terms in the expansion; for instance, the Runge-Kutta (RK) methods (e.g. Moin 2010). The additional function evaluations will indeed results in higher computational time; but the accuracy will increase, and as it turns out, better stability properties will be also obtained. It is recommended to use more advance discretization schemes in the MPS method with higher order of accuracy compared to the original MPS scheme. The use of high order accurate schemes will also make the pressure calculations more stable.

6.2.3. Applicability

6. **Fluid-Structure Interaction:** The grid-based methods have difficulties in analyzing the moving interfaces in fluid-structure interaction problems when the displacement of the interfaces is large, as the mesh will be distorted near the interfaces. Moreover, grid generation for complex geometries in grid-based methods may require very large computational time, often more time than the fluid and structure analysis. Mesh-free methods are free from difficulties arising from moving boundaries and interfaces, and complex grid generation process is much easier in mesh-free methods. The MPS method can be utilized to analyze complex fluid-structure interaction problems. Although this method is originally proposed for modeling of free surface incompressible flows, but it is possible to solve the governing equations of the structures using the approach of the MPS. Using the multiple-size particle formulation presented in this research (chapter 5), one can easily model the fluids and structures in different resolutions, depending on the desired accuracy. In simulation of fluid-structure interaction problems using the MPS, it is important to ensure the pressure field is calculated correctly in order to calculate accurate forces exerted to the structures by the fluids. This shows the need to apply more improvements to the MPS method to have accurate calculation of the flow pressure field.
7. **Flow in Vegetated Channels:** There is no trivial expression for the quantification of wave energy dissipation over plants. Numerical modeling of wave-vegetation interaction is tricky since the movement of the vegetation under waves and the stiffness parameters are difficult to define within a

mathematical model. It can be assumed in some cases that plants will behave as an elastic or visco-plastic structure (e.g. Larroude and Oudart 2012). By developing a model for fluid-structure interaction based on the MPS formulation, it is possible to deal with the flow in vegetated channel problems. Using the approach presented in chapter 5 for multiple-size particle representation of the computational domain, one can represent the thin plants with small particles while representing the fluid with relatively larger particles to keep the efficiency of the simulations at an acceptable level.

References

Almgren, A. S., Bell, J. B., Colella, P., Howell, L. H., and Welcome, M. L. (1998). "A conservative adaptive projection method for the variable density incompressible Navier–Stokes equations." Journal of computational Physics, 142(1), 1-46.

Arefmanesh, A., Najafi, M., and Abdi, H. (2005). "A meshless local Petrov-Galerkin method for fluid dynamics and heat transfer applications." Journal of fluids Engineering, 127(4), 647-655.

Ataie-Ashtiani, B., and Farhadi, L. (2006). "A stable moving-particle semi-implicit method for free surface flows." Fluid Dynamics Research, 38(4), 241-256.

Ataie-Ashtiani, B., and Najafi-Jilani, A. (2006). "Prediction of submerged landslide generated waves in dam reservoirs: an applied approach." Dam Engineering, 17(3), 135-155.

Ataie-Ashtiani, B., and Najafi Jilani, A. (2007). "A higher-order Boussinesq-type model with moving bottom boundary: Applications to submarine landslide tsunami waves." International journal for numerical methods in fluids, 53(6), 1019-1048.

Ataie-Ashtiani, B., and Shobeyri, G. (2008). "Numerical simulation of landslide impulsive waves by incompressible smoothed particle hydrodynamics." International Journal for numerical methods in fluids, 56(2), 209-232.

Atluri, S. N., Liu, H. T., and Han, Z. D. (2006). "Meshless local Petrov-Galerkin (MLPG) mixed finite difference method for solid mechanics." Computer modeling in engineering and sciences, 15(1), 1.

Atluri, S. N., and Zhu, T. (1998). "A new meshless local Petrov-Galerkin (MLPG) approach in computational mechanics." Computational mechanics, 22(2), 117-127.

Batchelor, G. K. (1973). "An introduction to fluid dynamics." Cambridge university press, UK.

Belytschko, T., Krongauz, Y., Organ, D., Fleming, M., and Krysl, P. (1996). "Meshless Methods: an Overview and Recent Developments." Computer methods in applied mechanics and engineering, 139(1), 3-47.

Belytschko, T., Lu, Y. Y., and Gu, L. (1994). "Element-free Galerkin methods." International journal for numerical methods in engineering, 37(2), 229-256.

Bingham, E. C. (1922). "Fluidity and plasticity." McGraw-Hill Book Co., Inc., New York, N.Y.

Cao, Z., Pender, G., Wallis, S., and Carling, P. (2004). "Computational dam-break hydraulics over erodible sediment bed." Journal of hydraulic engineering, 130(7), 689-703.

Capone, T., Panizzo, A. and Monaghan, J. (2010). "SPH modelling of water waves generated by submarine landslides." Journal of hydraulic research, 48(1), 80-84.

Chen, l. (2014). "Navier-Stokes equations for fluid dynamics." University of California, Irvine.

Chen, W. H., and Guo, X. M. (2001). "Element free Galerkin method for three-dimensional structural analysis." Computer modeling in engineering and sciences, 2(4), 497-508.

Chikazawa, Y., Koshizuka, S., and Oka, Y., 2001. "A particle method for elastic and visco-plastic structures and fluid-structure interactions." Computational Mechanics, 27(2), 97-106.

Colagrossi, A., and Landrini, M. (2003). "Numerical simulation of interfacial flows by smoothed particle hydrodynamics." Journal of Computational Physics, 191(2), 448-475.

Courant, R., Friedrichs, K., and Lewy, H. (1967). "On the partial difference equations of mathematical physics." IBM journal of Research and Development, 11(2), 215-234.

Cummins, S. J., and Rudman, M. (1999). "An SPH projection method." Journal of computational physics, 152(2), 584-607.

Dalrymple, R. A., and Rogers, B. D. (2006). "Numerical modeling of water waves with the SPH method." Coastal engineering, 53(2), 141-147.

Didenkulova, I., Nikolkina, I., Pelinovsky, E., and Zahibo, N. (2010). "Tsunami waves generated by submarine landslides of variable volume: Analytical solutions for a basin of variable depth." Natural Hazards and Earth System Science, 10(11), 2407-2419.

Enet, F., and Grilli, S. T. (2007). "Experimental study of tsunami generation by three-dimensional rigid underwater landslides." Journal of Waterway, Port, Coastal, and Ocean Engineering, 133(6), 442-454.

Gingold, R. A., and Monaghan, J. J. (1977). "Smoothed particle hydrodynamics: theory and application to non-spherical stars." Monthly notices of the royal astronomical society, 181(3), 375-389.

Gotoh, H., Ikari, H., Memita, T., and Sakai, T. (2005). "Lagrangian particle method for simulation of wave overtopping on a vertical seawall," Coastal Engineering Journal, 47(02n03), 157-181.

Farhadi, L. (2003). "Numerical Modeling of Irregular Free Surface Flow Using a Fully Lagrangian Method." Master Thesis, Sharif University of Technology, Tehran, Iran.

Grilli, S. T., and Watts, P. (1999). "Modeling of waves generated by a moving submerged body. Applications to underwater landslides." Engineering Analysis with Boundary Elements, 23(8), 645-656.

Heinrich, P. (1992). "Nonlinear water waves generated by submarine and aerial landslides." Journal of Waterway, Port, Coastal, and Ocean Engineering, 118(3), 249-266.

Heo, S., Koshizuka, S., and Oka, Y. (2002). "Numerical analysis of boiling on high heat-flux and high subcooling condition using MPS-MAFL," International Journal of Heat and Mass Transfer, 45(13), 2633-2642.

Hirt, C. W., and Nichols, B. D. (1981). "Volume of fluid (VOF) method for the dynamics of free boundaries." *Journal of computational physics*, 39(1), 201-225.

Hu, X. Y., and Adams, N. A. (2007). "An incompressible multi-phase SPH method." Journal of Computational Physics, 227(1), 264-278.

Hu, X. Y., and Adams, N. A. (2009). "A constant-density approach for incompressible multi-phase SPH." Journal of Computational Physics, 228(6), 2082-2091.

Huang, Y., Zhang, W., Xu, Q., Xie, P., and Hao, L. (2012). "Run-out analysis of flow-like landslides triggered by the Ms 8.0 2008 Wenchuan earthquake using smoothed particle hydrodynamics." Landslides, 9(2), 275-283.

Idelsohn, S. R., Onate, E., Del Pin, F., and Calvo, N. (2002). "Lagrangian formulations: the only way to solve some free-surface fluid mechanics problems," Fifth World Congress on Computational Mechanics, H. A. Mang, F. G. Rammerstorfer, J. Eberhardsteiner, eds., Viena.

Iwasaki, S. I. (1982). "Experimental study of a tsunami generated by a horizontal motion of a sloping bottom." Bulletin of the Earthquake Research Institute, 57, 239-262.

Iwasaki, S. (1997). "The wave forms and directivity of a tsunami generated by an earthquake and a landslide." Science of Tsunami Hazards, 15(1), 23-40.

Jiang, L., and LeBlond, P. H. (1992). "The coupling of a submarine slide and the surface waves which it generates." Journal of Geophysical Research: Oceans (1978–2012), 97(C8), 12731-12744.

Khayyer, A., and Gotoh, H. (2009). "Modified moving particle semi-implicit methods for the prediction of 2D wave impact pressure." Coastal Engineering, 56(4), 419-440.

Khayyer, A., and Gotoh, H. (2011). "Enhancement of stability and accuracy of the moving particle semi-implicit method." Journal of Computational Physics, 230 (8), 3093-3118.

Khayyer, A., and Gotoh, H. (2013). "Enhancement of performance and stability of MPS mesh-free particle method for multiphase flows characterized by high density ratios." Journal of Computational Physics, 242, 211-233.

Kondo, M., and Koshizuka, S. (2010). "Improvement of stability in moving particle semi-implicit method." International Journal for Numerical Methods in Fluids, 65(6), 638-654.

Koshizuka, S., Nobe, A., and Oka, Y. (1998). "Numerical analysis of breaking waves using the moving particle semi-implicit method." International Journal for Numerical Methods in Fluids, 26(7), 751-769.

Koshizuka, S., and Oka, Y. (1996). "Moving-particle semi-implicit method for fragmentation of incompressible fluid." Nuclear science and engineering, 123(3), 421-434.

Koshizuka, S., Shibata, K., Tanaka, M., and Suzuki, Y. (2007). "Numerical analysis of fluid-structure and fluid-rigid body interactions using a particle method." In ASME/JSME 2007 5th Joint Fluids Engineering Conference, 177-182.

Laigle, D., Lachamp, P., and Naaim, M. (2007). "SPH-based numerical investigation of mudflow and other complex fluid flow interactions with structures." Computational Geosciences, 11(4), 297-306.

Lancaster, P., and Salkauskas, K. (1986). Curve and surface fitting. Academic press.

Larroude, P., and Oudart, T. (2012). "SPH model to simulate movement of grass meadow of Posidonia under waves." Coastal Engineering Proceedings, 1(33), waves-56.

Lee, E. S., Moulinec, C., Xu, R., Violeau, D., Laurence, D., and Stansby, P. (2008). "Comparisons of weakly compressible and truly incompressible algorithms for the SPH mesh free particle method." Journal of computational physics, 227(18), 8417-8436.

Lee, J. J., Skjelbreia, J. E., and Raichlen, F. (1982). "Measurement of velocities in solitary waves." Journal of the Waterway Port Coastal and Ocean Division, 108(2), 200-218.

Li, S., and Liu, W. K., (2002). "Meshfree and particle methods and their applications." Applied Mechanics Reviews, 55(1), 1-34.

Lin, H., and Atluri, S. N. (2001). "The meshless local Petrov-Galerkin (MLPG) method for solving incompressible Navier-Stokes equations." CMES- Computer Modeling in Engineering and Sciences, 2(2), 117-142.

Liu, G. R. (2010). "Meshfree methods: moving beyond the finite element method." CRC press.

Liu, G. R., and Gu, Y. T. (2005). "An introduction to meshfree methods and their programming." Springer.

Liu, Y. N., Liu, Y., and Cen, Z. (2008). Daubechies wavelet meshless method for 2-D elastic problems. Tsinghua Science & Technology, 13(5), 605-608.

Löhner, R., Sacco, C., Onate, E., and Idelsohn, S. (2002). "A finite point method for compressible flow." International Journal for Numerical Methods in Engineering, 53(8), 1765-1779.

Lucy, L. B. (1977). "A numerical approach to the testing of the fission hypothesis." The astronomical journal, 82, 1013-1024.

Martin, J. C., and Moyce, W. J. (1952). "Part IV. An experimental study of the collapse of liquid columns on a rigid horizontal plane." Philosophical Transactions of the Royal Society of London. Series A, Mathematical and Physical Sciences, 244(882), 312-324.

Moin, P. (2010). "Fundamentals of engineering numerical analysis." Cambridge University Press.

Monaghan, J. J. (1988). "An introduction to SPH." Computer physics communications, 48(1), 89-96.

Monaghan, J. J. (1994). "Simulating free surface flows with SPH." Journal of computational physics, 110(2), 399-406.

Monaghan, J. J. (2005). "Smoothed particle hydrodynamics. Reports on progress in physics." 68(8), 1703.

Monaghan, J. J., Cas, R. A. F., Kos, A. M., and Hallworth, M. (1999). "Gravity currents descending a ramp in a stratified tank." Journal of Fluid Mechanics, 379, 39-69.

Monaghan, J. J., and Kos, A. (2000). "Scott Russell's wave generator." Physics of Fluids, 12(3), 622-630.

Nabian, M. A., and Farhadi, L. (2014a). "Numerical Simulation of Solitary Wave Using the Fully Lagrangian Method of Moving Particle Semi Implicit." In Proceedings of the ASME 2014 4th Joint US-European Fluids Engineering Division Summer Meeting, V01DT30A006-V01DT30A017, American Society of Mechanical Engineers.

Nabian, M. A., and Farhadi, L. (2014b). "Stable Moving Particle Semi Implicit Method for Modeling Waves Generated by Submarine Landslides." In Proceedings of the ASME 2014 International Mechanical Engineering Congress & Exposition, V007T09A019-V007T09A028, American Society of Mechanical Engineers.

Nabian, M. A., and Farhadi, L. (2014c). "Simulating water waves generated by underwater landslide with MPS and WC-MPS." Proceedings of the 11th International Conference on Hydrodynamics, ICHD, Singapore, 859-866.

Nayroles, B., Touzot, G., and Villon, P. (1992). "Generalizing the finite element method: diffuse approximation and diffuse elements." Computational mechanics, 10(5), 307-318.

Nguyen, V. P., Rabczuk, T., Bordas, S., and Duflot, M. (2008). "Meshless methods: a review and computer implementation aspects." Mathematics and computers in simulation, 79(3), 763-813.

Noda, E. (1970). "Water waves generated by landslides." Journal of the Waterways, Harbors and Coastal Engineering Division, 96(4), 835-855.

Onate, E., and Idelsohn, S. (1998). "A mesh-free finite point method for advective-diffusive transport and fluid flow problems." Computational Mechanics, 21(4-5), 283-292.

Onate, E., Idelsohn, S., Zienkiewicz, O. C., Taylor, R. L., and Sacco, C. (1996). "A stabilized finite point method for analysis of fluid mechanics problems". Computer Methods in Applied Mechanics and Engineering, 139(1), 315-346.

Onate, E., Sacco, C., and Idelsohn, S. (2000). A finite point method for incompressible flow problems. Computing and visualization in science, 3(1-2), 67-75.

Pastor, M., Haddad, B., Sorbino, G., Cuomo, S., and Drempetic, V. (2009). "A depth-integrated, coupled SPH model for flow-like landslides and related phenomena." International Journal for numerical and analytical methods in geomechanics, 33(2), 143-172.

Rzadkiewicz, S. A., Mariotti, C., and Heinrich, P. (1997). "Numerical simulation of submarine landslides and their hydraulic effects." Journal of Waterway, Port, Coastal, and Ocean Engineering, 123(4), 149-157.

Robortella, M. S., Kazuo, N. and Cheng, L. Y. (2009). "Dynamic analyzes of elastic structures by using moving particle semi-implicit method (MPS)." 20th International Congress of Mechanical Engineering, Gramado, RS, Brazil.

Ruparel, T., Eskandarian, A., and Lee, J. (2012, November). "Multiple Grid and Multiple Time-Scale (MGMT) Simulations in Continuum Mechanics." In ASME 2012 International Mechanical Engineering Congress and Exposition, 515-527, American Society of Mechanical Engineers.

Shakibaeinia, A. (2011). "A Mesh-Free Lagrangian Method for Free Surface and Interfacial Flows." University of Regina, Regina.

Shakibaeinia, A., and Jin, Y. C. (2010). "A weakly compressible MPS method for modeling of open-boundary free-surface flow." International journal for numerical methods in fluids, 63(10), 1208-1232.

Shakibaeinia, A., and Jin, Y. C. (2011). "A mesh-free particle model for simulation of mobile-bed dam break." Advances in Water Resources, 34(6), 794-807.

Shakibaeinia, A., and Jin, Y. C. (2012). "MPS mesh-free particle method for multiphase flows." Computer Methods in Applied Mechanics and Engineering, 229, 13-26.

Shao, S. (2012). "Incompressible smoothed particle hydrodynamics simulation of multifluid flows." International Journal for Numerical Methods in Fluids, 69(11), 1715-1735.

Shao, S., and Lo, E. Y. (2003). "Incompressible SPH method for simulating Newtonian and non-Newtonian flows with a free surface." Advances in Water Resources, 26(7), 787-800.

Shibata, K., and Koshizuka, S. (2007). "Numerical analysis of shipping water impact on a deck using a particle method," Ocean Engineering, 34(3), 585-593.

Shobeyri, G., and Afshar, M. H. (2010). Simulating free surface problems using discrete least squares meshless method. Computers & Fluids, 39(3), 461-470.

Singh, A., Singh, I. V., and Prakash, R. (2007). "Meshless element free Galerkin method for unsteady nonlinear heat transfer problems." International Journal of Heat and Mass Transfer, 50(5), 1212-1219.

Spinewine, B. (2005). "Two-layer flow behaviour and the effects of granular dilatancy in dam-break induced sheet-flow." Ph.D. Thesis, Université catholique de Louvain, Belgium.

Sturm, T. W. (2010). "Open channel hydraulics." McGraw-Hill Higher Education.

Sun, Z., Xi, G., and Chen, X. (2009). "A numerical study of stir mixing of liquids with particle method," Chemical Engineering Science, 64(2), 341-350.

Tsubota, K. I., Wada, S., Kamada, H., Kitagawa, Y., Lima, R., and Yamaguchi, T. (2006). "A particle method for blood flow simulation: application to flowing red blood cells and platelets," Journal of Earth Simulator, 5, 2-7.

Violeau, D., Buvat, C., Abed-Meraïm, K., and De Nanteuil, E. (2007). "Numerical modelling of boom and oil spill with SPH." Coastal Engineering, 54(12), 895-913.

Visser, D. C., Hoefsloot, H. C., and Iedema, P. D. (2006). "Modelling multi-viscosity systems with dissipative particle dynamics." Journal of computational Physics, 214(2), 491-504.

Wahba, G. (1979). "How to Smooth Curves and Surfaces with Splines and Cross-Validation." 24th conference on the design of experiments, US army research office, North Carolina, 167-192.

Watts, P. (1997). "Water waves generated by underwater landslides." Ph.D. Thesis, California Institute of Technology, Pasadena, CA.

Wiegel, R. L. (1955). "Laboratory studies of gravity waves generated by the movement of a submerged body." Transactions of the American Geophysical Union, 36(5), 759-774.

Xia, J., Lin, B., Falconer, R. A., and Wang, G. (2010). "Modelling dam-break flows over mobile beds using a 2D coupled approach." Advances in Water Resources, 33(2), 171-183.

Young Yoon, H., Koshizuka, S., and Oka, Y. (1999). "A particle–gridless hybrid method for incompressible flows." International Journal for Numerical Methods in Fluids, 30(4), 407-424.

Zienkiewicz, O. C., and Codina, R. (1995). "A general algorithm for compressible and incompressible flow—Part I. the split, characteristic-based scheme." International Journal for Numerical Methods in Fluids, 20(8-9), 869-885.

Appendix

Associated Publications

1. Nabian, M. A., and Farhadi, L. "Mesh-Free Lagrangian Modeling of Water Waves Generated by Landslides." In preparation.
2. Nabian, M. A., and Farhadi, L., "Multiphase Mesh-Free Particle Method for Simulation of Granular Flows and Sediment Transport." In preparation.
3. Nabian, M. A., and Farhadi, L., "Multiple-Resolution Simulation of Free Surface Flows by MPS." In preparation.
4. Nabian, M. A., and Farhadi, L. (2014). "Numerical Simulation of Solitary Wave Using the Fully Lagrangian Method of Moving Particle Semi Implicit." In Proceedings of the ASME 2014 4th Joint US-European Fluids Engineering Division Summer Meeting, V01DT30A006-V01DT30A017, American Society of Mechanical Engineers. doi:10.1115/fedsm2014-22237.
5. Nabian, M. A., and Farhadi, L. (2014). "Stable Moving Particle Semi Implicit Method for Modeling Waves Generated by Submarine Landslides." In Proceedings of the ASME 2014 International Mechanical Engineering Congress & Exposition, V007T09A019-V007T09A028, American Society of Mechanical Engineers. doi:10.1115/IMECE2014-22237.
6. Nabian, M. A., and Farhadi, L., (2014). "Simulating Water Waves Generated by Underwater Landslide with MPS and WC-MPS." In Proceedings of the 11th

International Conference on Hydrodynamics, ICHD, Singapore, 859-866. ISBN 978-981-09-2175-0.

7. Nabian, M. A., and Farhadi, L. (2015). "A multiphase mesh-free particle method for modeling sediment transport via dam-break." In Proceedings of the 2015 ASME-JSME-KSME Joint Fluid Engineering Conference, In Press.